GEND-061
Distribution Category: UC-78
TMI Supplement

GEND--061

DE87 010696

LESSONS LEARNED FROM HYDROGEN GENERATION AND BURNING DURING THE TMI-2 EVENT

J.O. Henrie
A.K. Postma
Rockwell Hanford Operations

Published May 1987

Prepared for the
U.S. Department of Energy
Hanford Operations Office
Under DOE Contract No. DE-AC06-77RL01030

ABSTRACT

This document summarizes what has been learned from generation of hydrogen in the reactor core and the hydrogen burn that occurred in the containment building of the Three Mile Island Unit No. 2 (TMI-2) nuclear power plant on March 28, 1979. During the TMI-2 loss-of-coolant accident (LOCA), a large quantity of hydrogen was generated by a zirconium-water reaction.

The hydrogen burn that occurred 9 h and 50 min after the initiation of the TMI-2 accident went essentially unnoticed for the first few days. Even though the burn increased the containment gas temperature and pressure to 1,200 °F (650 °C) and 29 lb/in^2 (200 kPa) gage, there was no serious threat to the containment building.

The processes, rates, and quantities of hydrogen gas generated and removed during and following the LOCA are described in this report. In addition, the methods which were used to define the conditions that existed in the containment building before, during, and after the hydrogen burn are described. The results of data evaluations and engineering calculations are presented to show the pressure and temperature histories of the atmosphere in various containment segments during and after the burn.

Material and equipment in reactor containment buildings can be protected from burn damage by the use of relatively simple enclosures or insulation.

ACKNOWLEDGMENTS

The authors gratefully acknowledge the following individuals who provided helpful information and advice, or reviewed drafts and made valuable comments and improvements to this document: G. R. Eidam, K. L. Imhof, and M. Saigusa, General Public Utilities Nuclear Corporation; L. J. Ball, J. E. Flaherty, P. Kuan, H. Reno, and J. Saunders, EG&G Idaho, Inc.; P. K. De, Burns and Roe, Inc.; R. D. Schilz, Joy Industrial Equipment Company; J. Sears, Foxboro Company; and R. G. Zalosh, Factory Mutual Research Corporation.

Sincere appreciation is also extended to the many authors and contributors to the reference documents listed in section 7.0. The majority of the work that has resulted from the TMI-2 hydrogen burn was performed by them.

Special thanks is expressed to those who authorized and so proficiently administratively controlled this work: R. Schmitt, EG&G Idaho, Inc.; W. W. Bixby and W. R. Young, DOE-TMI.

CONTENTS

1.0 Purpose and Objectives 1-1

2.0 Summary and Conclusions 2-1

3.0 Background 3-1
  3.1 Loss-of-Coolant Accident 3-1
  3.2 Previous Studies 3-1
  3.3 Previously Unresolved Technical Questions 3-4

4.0 Hydrogen Generation and Removal 4-1
  4.1 Reactor Cooling System and Containment Building Features 4-1
  4.2 Data Sources 4-1
  4.3 Hydrogen Evolution and Storage in the Reactor Cooling System 4-8
  4.4 Hydrogen Release and Mixing in Containment 4-14
  4.5 Preburn Conditions 4-19
  4.6 Engineering Analysis of Key Burn Parameters 4-19
  4.7 Characteristics of the Hydrogen Burn 4-27
  4.8 Postburn Hydrogen 4-37

5.0 Predicted Heatup of Equipment Exposed to a Hydrogen Burn in a Containment Building 5-1
  5.1 Basis for Predicted Temperature Transients 5-1
  5.2 Design Guidelines for Protecting Equipment 5-3

6.0 Equipment that Survived the TMI-2 Hydrogen Burn 6-1

7.0 References 7-1

Appendixes:
  A. Measured Time/Pressure Lag in Once-Through Steam Generator-B A-1
  B. Calculated Pressure Differences Between Compartments B-1
  C. Description of Containment Gas-Heat Transfer Processes and Parameters C-1
  D. Parametric Analysis of Component Heating Following a Postulated Hydrogen Burn D-1

Figures:
  3-1 Reactor Building Pressure Versus Time 3-2
  4-1 Cross Section of the TMI-2 Reactor Containment Building 4-2
  4-2 Floor Plan View of Elevation 282 4-3
  4-3 Floor Plan of Elevation 305 4-4
  4-4 Floor Plan of Elevation 347 4-5

Figures: (cont.)

4-5 Floor Plan at Elevation 450 Showing the Position of the Polar Crane at the Time of the Accident 4-6
4-6 Simplified Diagram of the Reactor Cooling System 4-7
4-7 Comparison of Zirconium-Water Reaction Correlations 4-9
4-8 Calculated TMI-2 Hydrogen Production from the Zirconium-Water Reaction 4-12
4-9 Calculated Hydrogen Concentration Versus Time Near the Water Interface in Once-Through Steam Generators -A and -B 4-16
4-10 Calculated Mass of Hydrogen Versus Time in Hot Legs and Once-Through Steam Generators -A and -B 4-17
4-11 Composition Diagram Showing Hydrogen Concentrations in Mixing Zone 4-22
4-12 Predicted Containment Temperature for an Adiabatic Isochoric Hydrogen Burn 4-25
4-13 Composite TMI-2 Containment Average Temperature and Pressure Versus Time 4-28
4-14 Comparison of Pressure Histories During the Burning of Hydrogen in Three Vessels Having Greatly Different Sizes 4-34
4-15 Thermal Effects of Burning, Compression Heating, and Cooling on Unit Volumes of TMI-2 Containment Gas, Which Burned at the Times Shown 4-36
5-1 Predicted Average Gas Temperature in Upper Containment Versus Time Following a Postulated Instantaneous Hydrogen Burn 5-2
5-2 Comparison of Wire-Surface Temperatures for Different Protective Conduits 5-6

Tables:

4-1 Total Pressure in the Reactor Cooling System and Steam Pressure in the Once-Through Steam Generators in lb/in^2, During the Principal Hydrogen Generation Period 4-15
4-2 Preburn Conditions 4-20
4-3 Containment Hydrogen Balance 4-38

1.0 PURPOSE AND OBJECTIVES

The purpose of this report is to summarize the many lessons that have been learned as a result of the hydrogen burn which occurred in the Three Mile Island Unit No. 2 (TMI-2) nuclear power plant containment building. Information was collected using the following methods:

- Analysis and evaluation of recorded data and evidence of damage
- Related test programs at other facilities
- Theoretical and empirical analyses of the accident, hydrogen generation, hydrogen-air reactions under various containment conditions, and heating of various types of receptors from exposure to the burn transient
- Comparative design analyses that provide protective measures to ensure that equipment will not be thermally damaged by a containment hydrogen burn.

The objectives of this report are to:

- Document, primarily by direct references, the related work that has been performed
- Evaluate and resolve to the extent practicable the areas where unresolved technical questions persist
- Determine and document the temperature and pressure histories of various segments of the containment atmosphere for use in predicting damage potential from postulated similar hydrogen burns
- Provide guidance that will be useful in the design of temperature-sensitive, in-containment equipment, to ensure that it would not be damaged from a postulated hydrogen burn.

2.0 SUMMARY AND CONCLUSIONS

The analysis of data available from the TMI-2 accident indicates that the hydrogen generation rate peaked at more than 20 kg/min (8,000 ft^3/min standard) shortly after 0654 when the hot reactor core was quenched. Just prior to that period, the zirconium-water reaction may have been steam-limited. Approximately 400 kg of hydrogen gas was generated between 0612 and 0700, and approximately 460 kg of hydrogen gas had been generated by 0748.

The hydrogen was released to containment from the reactor cooling system through the pressurizer and reactor coolant drain tank at a vent located on the west side, below the floor at Elevation 305. The hydrogen concentration was high in that area just prior to the burn. Based on accurately timed pressure data, it is likely that the burn originated in that area. It is also likely that the last regions to burn were the enclosed stairwell and elevator hoistway where, coincidentally, the hydrogen concentrations were lowest. The hydrogen had become well-mixed throughout containment except in the enclosed stairway and elevator hoistway areas, and probably averaged just below 8%. The burn moved primarily up the open stairway on the west side and laterally toward the east, below the reactor dome and the floors at Elevations 305 and 347.

The hydrogen burn occurred throughout essentially all of the 2,033,000 ft^3 (57,600 m^3) containment during a period of approximately 12 s. Less than 5% of the burning took place in the first 6 s, less than 40% during the next 3 s, and more than half of the burning occurred during the last 3 s. There was no detonation. The hottest gas was the gas that burned at approximately 6 s prior to the end of the burn. Even though the gas was losing heat to the unburned gas and surrounding surfaces after it burned, compression heating was dominant and significantly increased its temperature until the pressure peaked. The atmosphere in the upper dome of the containment became hotter and stayed hotter longer than in smaller, more congested compartments primarily because of its high volume-to-surface-area ratio, which resulted in lower cooling rates. This hotter condition was also a result of the more complete burning that would have occurred in that large open region. Burn damage to receptors was therefore highest in that region.

The predominant path of the hot steam and gas leaving the reactor coolant drain tank vent was determined to be up through the stairway opening at Elevation 305 then to the air coolers at Elevation 330. Steam condensation caused everything in the region of that path to become very wet and significantly minimized burn damage to receptors located there. The water spray, which started 32 s after the burn, rapidly cooled the hot gases in the region above Elevation 347 and quenched the objects that were charring and burning. Therefore, many objects were preserved in their partially burned state, which allowed relatively complete evaluations. Typically, the burn damage (and lack of burn damage) is explainable with little or no speculation.

A comparison of the burning rates, peak pressures, and cooling rates show the effects of scale during the burning of mixtures of approximately 8% hydrogen in air in vessels with greatly different sizes. Peak pressures are lower and cooldown rates are faster in smaller vessels because of the smaller volume-to-surface-area ratios. However, the total time for this particular gas mixture (approximately 8% hydrogen in air, which is just below the limit where downward flame propagation can occur in quiescent hydrogen-air mixtures) to burn was similar in each vessel; therefore (as a result of buoyancy effects) burn velocities are much higher in large vessels than in small vessels. The burn velocities in these tests were reasonably proportional to a characteristic length such as diameter, or the cube root of the volume. Typical burning velocities in the TMI-2 containment during the last few seconds of the burn were probably up to approximately 50 ft/s (15 m/s). Velocities of gases moving through openings in a partially enclosed compartment (room A) apparently reached approximately 250 ft/s (75 m/s).

Approximately 460 kg of hydrogen gas was accounted for; approximately 320 kg was converted to water vapor during the hydrogen burn; approximately 110 kg was removed by a hydrogen recombiner; and approximately 30 kg was eventually vented to the outside atmosphere.

Design analyses show that enclosures such as standard electrical panels and conduit are sufficient to protect most types of wiring and electronic equipment from overheating during a hydrogen burn, even if the burn occurs in the enclosure. It is concluded that equipment which has been qualified to withstand a typical loss-of-coolant-accident (LOCA) environment would likely also withstand the effects of a hydrogen burn; this would surely be the case if the results of a thermal analysis similar to that demonstrated in this document were appropriately considered during the design of the equipment.

3.0 BACKGROUND

3.1 LOSS-OF-COOLANT ACCIDENT

The LOCA that occurred at TMI-2 began at 0400 on March 28, 1979. There were many contributing causes to the accident: design, maintenance, operation, communication, and training errors.

The only significant load applied to the containment building was the hydrogen burn that occurred 9 h and 50 min after the initiation of the LOCA. The steam release from the relatively slow blowdown of the reactor cooling system had increased the containment pressure to a peak of less than 5 lb/in^2 or 34 kPa (gage) while the peak pressure rose to almost 30 lb/in^2 or 206 kPa (gage) during the hydrogen burn. The pressure pulse was recorded as a single sharp spike on the reactor building pressure stripchart recorder (fig. 3-1). This recorded spike was first considered a false electrical noise signal such as might be caused by a ground fault (Rogovin 1980). However, a careful analysis of other recorded temperature and pressure data showed conclusively that a hydrogen burn had occurred in the containment building. The containment building was designed to safely withstand an internal pressure of 65 lb/in^2 or 450 kPa (gage) and studies show that it would withstand much higher pressures; therefore, the hydrogen burn was not a serious threat to the containment building.

The probability of such an accident occurring was very low, but because of the increased awareness and improvements to correct potential problems and errors resulting from this accident, the probability of nuclear accidents of any kind has been reduced. Also, the consequence of the TMI-2 LOCA in terms of health effects was very low because of the performance of the containment building. However, because of the potential threat, the TMI-2 hydrogen burn and hydrogen technology in general have received considerable study and attention since the accident. Interest in hydrogen control was further enhanced as a result of the Chernobyl Unit 4 nuclear reactor accident on April 26, 1986.

3.2 PREVIOUS STUDIES

Studies conducted as a result of the TMI-2 hydrogen burn can be categorized as follows:

- Analysis of hydrogen generation, release, and mixing
- Analyses of the TMI-2 hydrogen burn
- Analysis of damage resulting from the TMI-2 hydrogen burn
- Experimental studies of hydrogen burn characteristics and damage
- Prevention and mitigation studies.

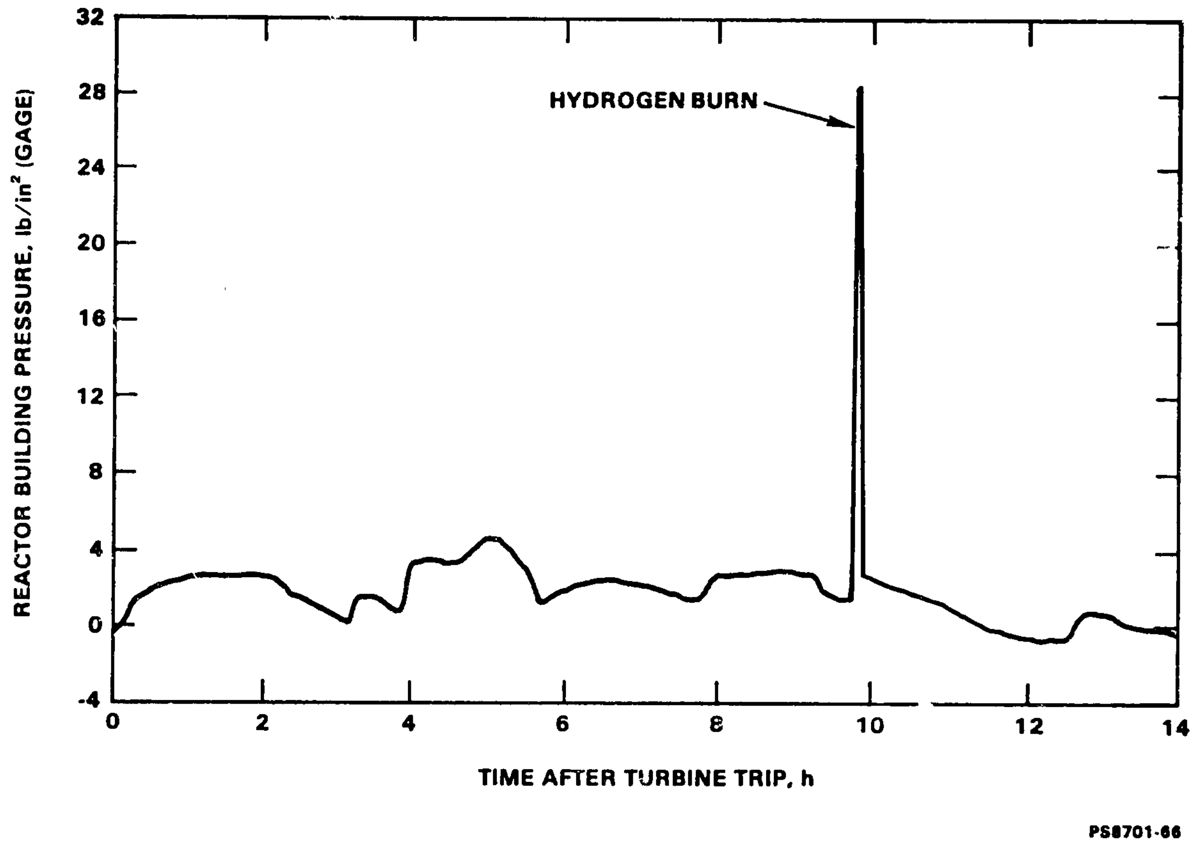

Figure 3-1. Reactor Building Pressure Versus Time (NSAC 1980).

Key references for each of these topics are discussed in the following sections.

3.2.1 Analysis of Hydrogen Generation, Release, and Mixing

This subject has been addressed by Baker (1983), Bloom et al. (1983), Cole (1979), Henrie and Postma (1983a), NSAC (1980), Postma and Hilliard (1985), Rogovin (1980), Thomas (1985), and Zalosh et al. (1985). These studies show that 350 to 500 kg of hydrogen was produced during the first 3 h of the accident, and that most of the hydrogen was released to the containment and was well-mixed during the first 9 h of the accident. This work is further discussed in sections 4.2 and 4.3.

3.2.2 Analysis of the TMI-2 Hydrogen Burn

The first detailed report of the TMI-2 hydrogen burn was reported by NSAC (1980); the TMI-2 burn was more broadly reported by Henrie and Postma (1983a) and by Zalosh et al. (1985). These studies show that the burn probably started in the basement and the flame front progressed rapidly throughout essentially all of the containment. The burn resulted in higher temperatures for longer periods at high elevations and in open regions where the gas-volume-to-heat-sink-area ratio is high. Analyses of the available data and logic relating to the probable burn origin, pathway, and characteristics of the burn are presented in section 4.0.

3.2.3 Analysis of Damage Resulting From the TMI-2 Hydrogen Burn

The evidence of fire damage from the TMI-2 hydrogen burn is unique compared with that in typical fires, since the fire swept through the building so quickly and the heated gases cooled so rapidly that scorching and burning were evident, but none of the many small fires which started were sustained. Therefore, most of the heat damage and burn evidence was preserved. The many instances where flammable materials were not scorched or burned provide additional bases for analyses. Essentially all of the burn damage, both heat and pressure related, is explainable (Alvarez et al. 1982; Alvarez 1984, 1985; Eidam and Horan 1981; Henrie and Postma 1983a; Murphy et al. 1985; Richards and Dandini 1986; Trujillo et al. 1986; Zalosh et al. 1985).

3.2.4 Experimental Studies of Hydrogen Burn Characteristics and Damage

The interest created by the TMI-2 hydrogen burn has resulted in many experimental investigations of hydrogen burn characteristics in both large and small containment vessels and of hydrogen burn damage to wiring and instrumentation (Achenbach et al. 1985; Ashurst and Barr 1982; Benedick et al. 1984; Berlad et al. 1982; Berman and Lee 1984; Berman and Hitchcock 1985; Dandini 1985; Helbert et al. 1984; Hertzberg 1981; Hertzberg and Cashdollar 1983; Kempka et al. 1984; Lee 1981; Ratzel 1985; Ratzel and Shepherd 1985; Sherman 1985; Soberano 1984; Thompson et al. 1987; Torok et al. 1983).

3.2.5 Prevention and Mitigation Studies

As a result of the TMI-2 hydrogen burn, the prevention or mitigation of the damaging effects of hydrogen burn environments have been studied, largely in support of operating licenses for light-water-cooled nuclear power plants in the United States. These studies include the survivability of safety-related components in hydrogen burn environments (Berman 1986; Nelson and Berman 1983, 1984). As a result of many hydrogen control studies, regulatory organizations have established requirements and standards for hydrogen control in water-cooled nuclear power plants (NRC 1985, 1986).

3.3 PREVIOUSLY UNRESOLVED TECHNICAL QUESTIONS

An evaluation of the literature cited in section 3.2 indicated that questions still remained concerning the TMI-2 LOCA which required further investigation and documentation:

1. At what rates and during which time period(s) was the hydrogen generated? (See section 4.3.)

2. Where was the hydrogen stored in the Reactor Cooling System (RCS) until it was released to the containment building? (See section 4.3.)

3. Where in the containment did the hydrogen burn originate and what were the pathways as the flame front moved through the containment? (See section 4.7.2.)

4. Was there any effect of scale evidenced by this large hydrogen burn when compared with burns in smaller enclosures? (See section 4.7.3.)

5. Did a hydrogen detonation occur or was the reaction limited to a deflagration? (See section 4.6.1.)

6. How uniform was the pressure in various parts of the containment during the hydrogen burn and why did the containment pressure as indicated by the B steam generator pressure instrument lag that of the A instrument? (See section 4.7.1 and appendixes A and B.)

7. What was the time-temperature history of the atmosphere in various regions of the containment? (See sections 4.7, 5.1, and appendix C.)

8. What caused the nonuniform lateral scorching of the polar crane pendant cable? (See section 4.7.4.)

9. What was the most likely temperature history of various equipment items exposed to the hydrogen burn and the hot gases left in the wake of the burn? (See sections 4.6.5 and 5.2.)

10. Would a postulated future hydrogen burn in a reactor containment building be worse than the one experienced in the dome of the TMI-2 containment building? (See section 5.2.1.)

11. What design guidelines and steps will ensure that a component will not fail as a result of a TMI-2-type hydrogen burn? (See section 5.2.)

4.0 HYDROGEN GENERATION AND REMOVAL

In this section, the TMI-2 Reactor cooling system and containment building are described and hydrogen generation, storage, release to containment, mixing, burning, controlled recombining, and venting are discussed. The hydrogen burn is characterized and temperatures and pressures are shown as a function of time during the burn and cooldown period.

4.1 REACTOR COOLING SYSTEM AND CONTAINMENT BUILDING FEATURES

The containment building, which was designed to reliably withstand an internal pressure of 65 lb/in² or 450 kPa (gage) with a significant factor of safety, easily contained the 30 lb/in² or 206 kPa (gage) pressure created by the hydrogen burn.

The containment building consists of a large, domed, cylindrical steel shell surrounded by reinforced concrete; the inside diameter and height are approximately 130 ft (40 m) and 190 ft (68 m), respectively. The basement floor is at Elevation 282, the main entry floor at Elevation 305, and the upper floor at Elevation 347 (fig. 4-1). Plan views at each of the three floor levels and from the dome region at Elevation 450 (approximately) are shown in figures 4-2, 4-3, 4-4, and 4-5 (Eidam and Horan 1981). A simplified diagram of the reactor cooling system is shown in figure 4-6 (NSAC 1980).

4.2 DATA SOURCES

Even though no instrumentation had been installed in the TMI-2 containment building to record the characteristics of a hydrogen burn, there were many instruments installed for other purposes that sensed and recorded many of the burn characteristics:

- A stripchart that continuously displayed the containment building pressure (see fig. 3-1)
- A reactimeter that recorded 22 channels of data every 3 s
- An alarm printer that recorded the time when computer-monitored events occurred
- A utility printer that provided special summary, trend, and sequence-of-events reports from the computer when requested by the operator
- A 24-point temperature recorder that printed ambient air temperatures every 6 min at 12 locations in the containment building.

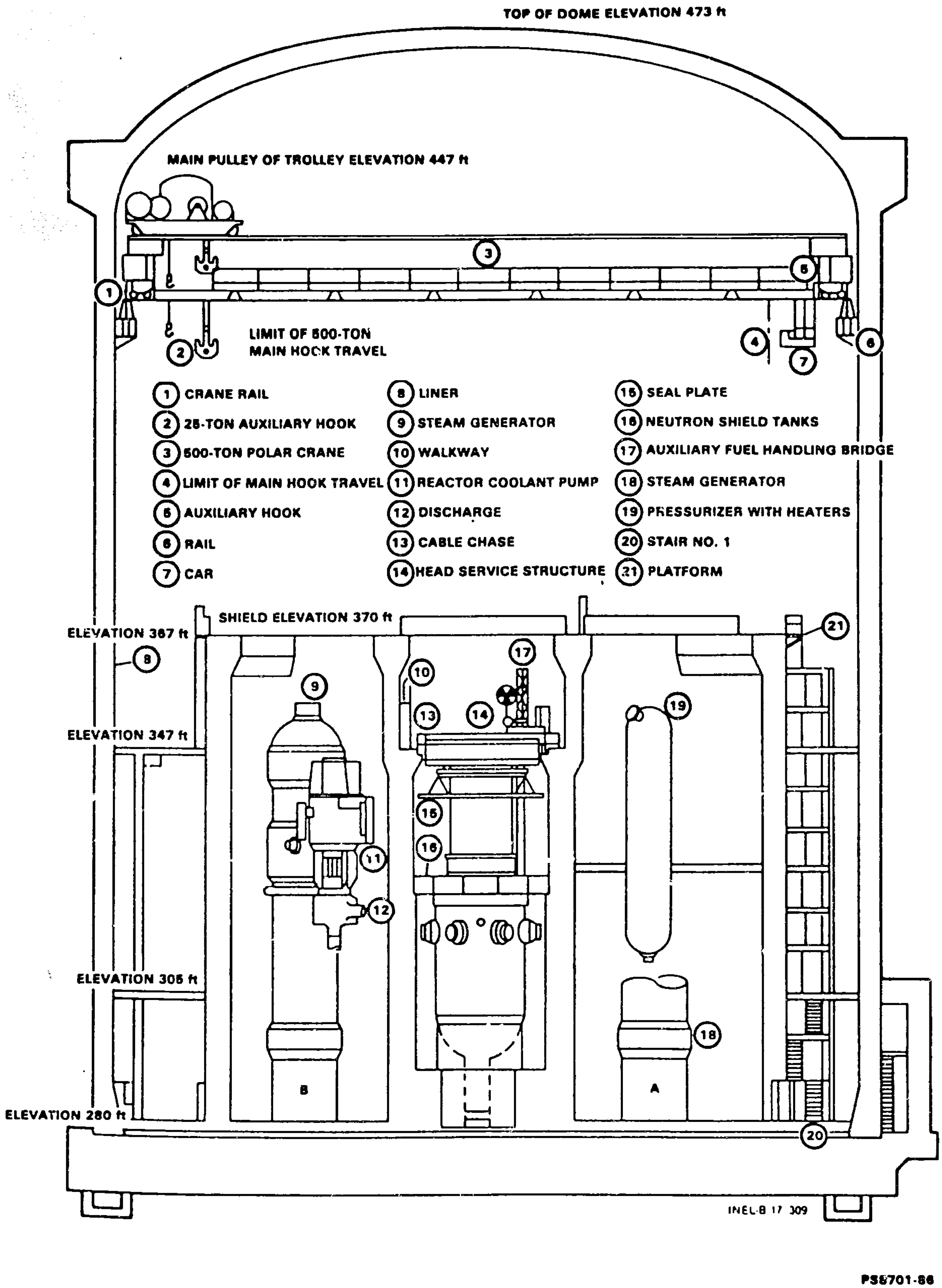

Figure 4-1. Cross Section of the TMI-2 Reactor Containment Building (Looking South).

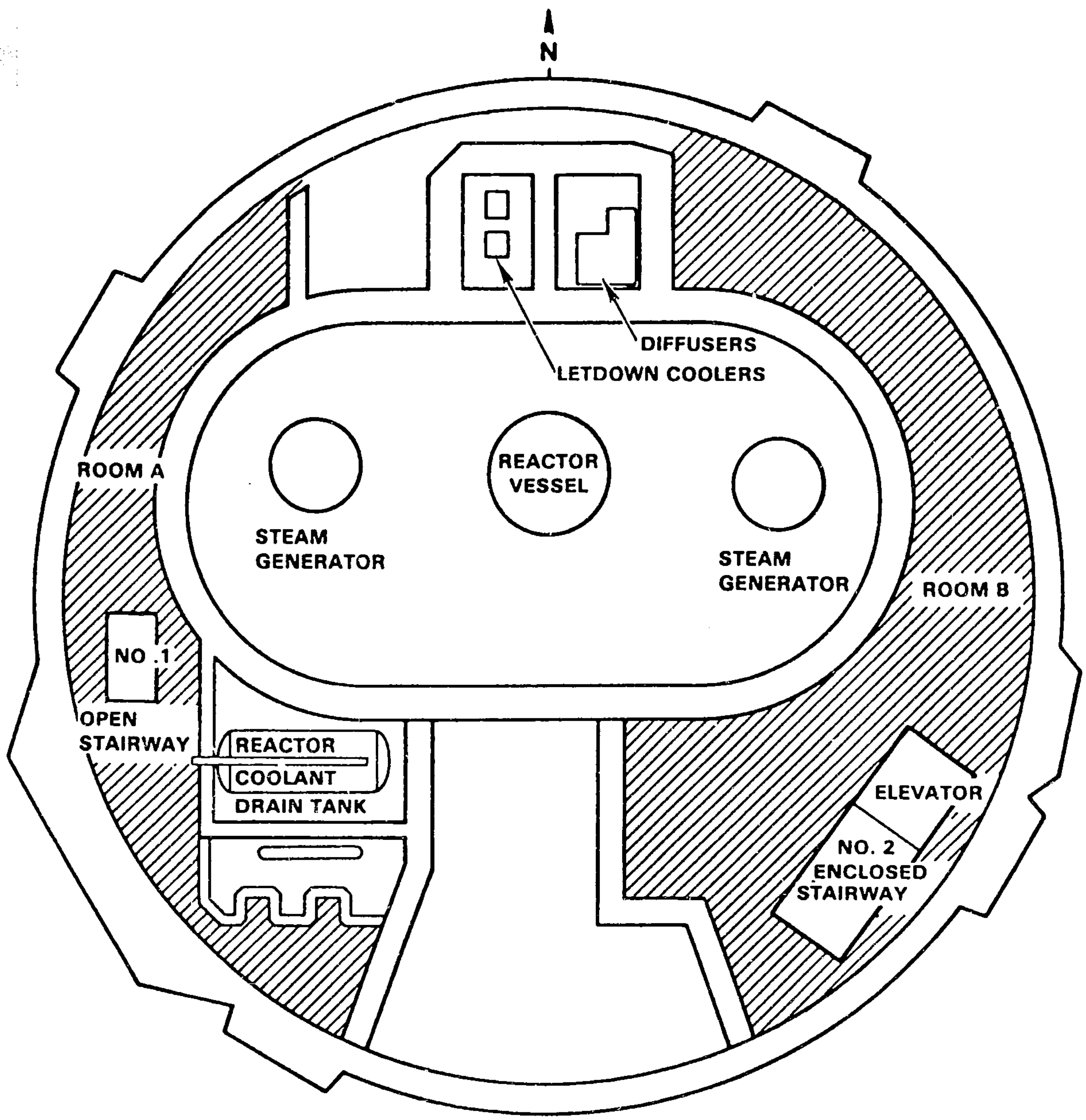

Figure 4-2. Floor Plan View of Elevation 282.

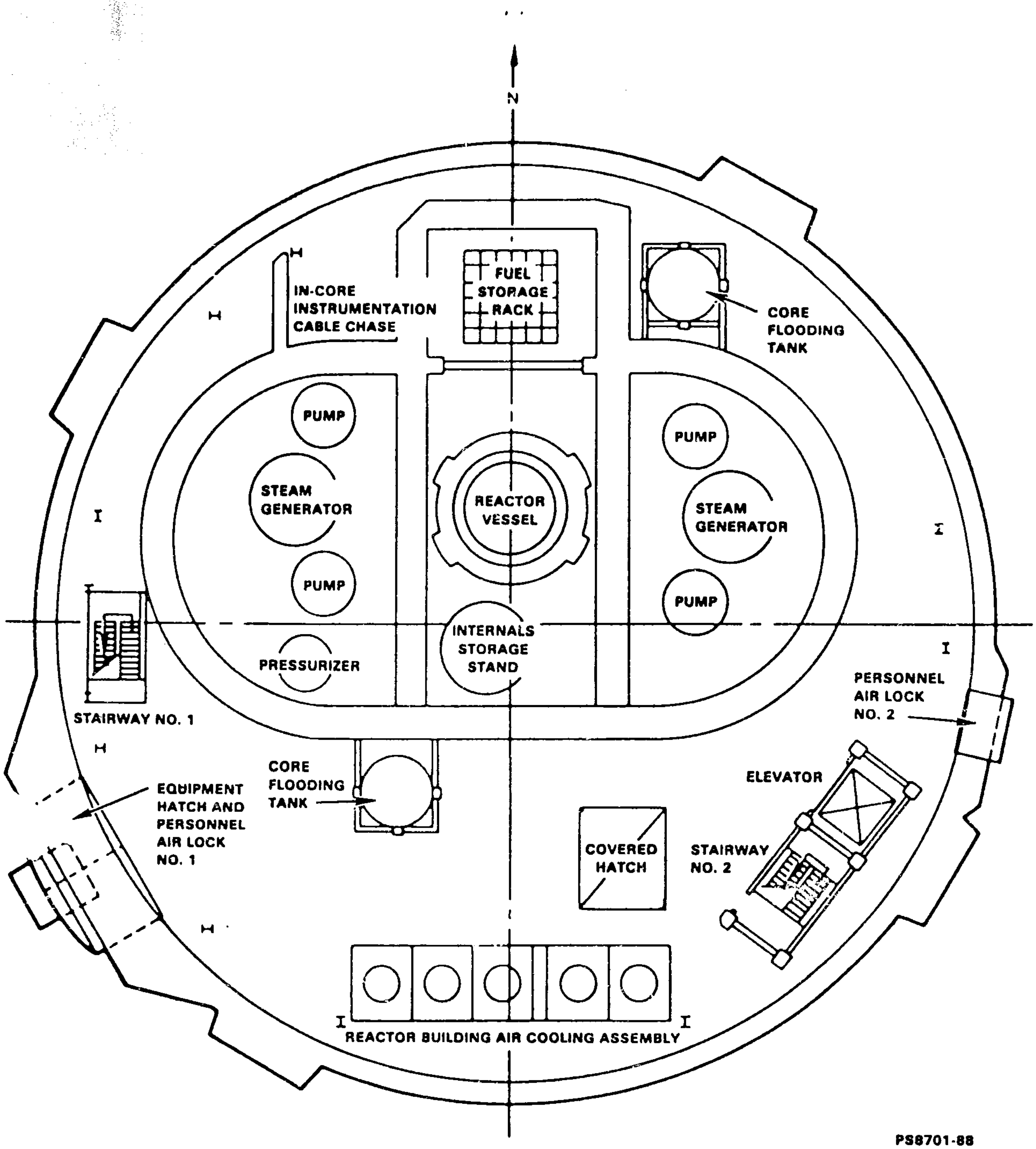

Figure 4-3. Floor Plan of Elevation 305.

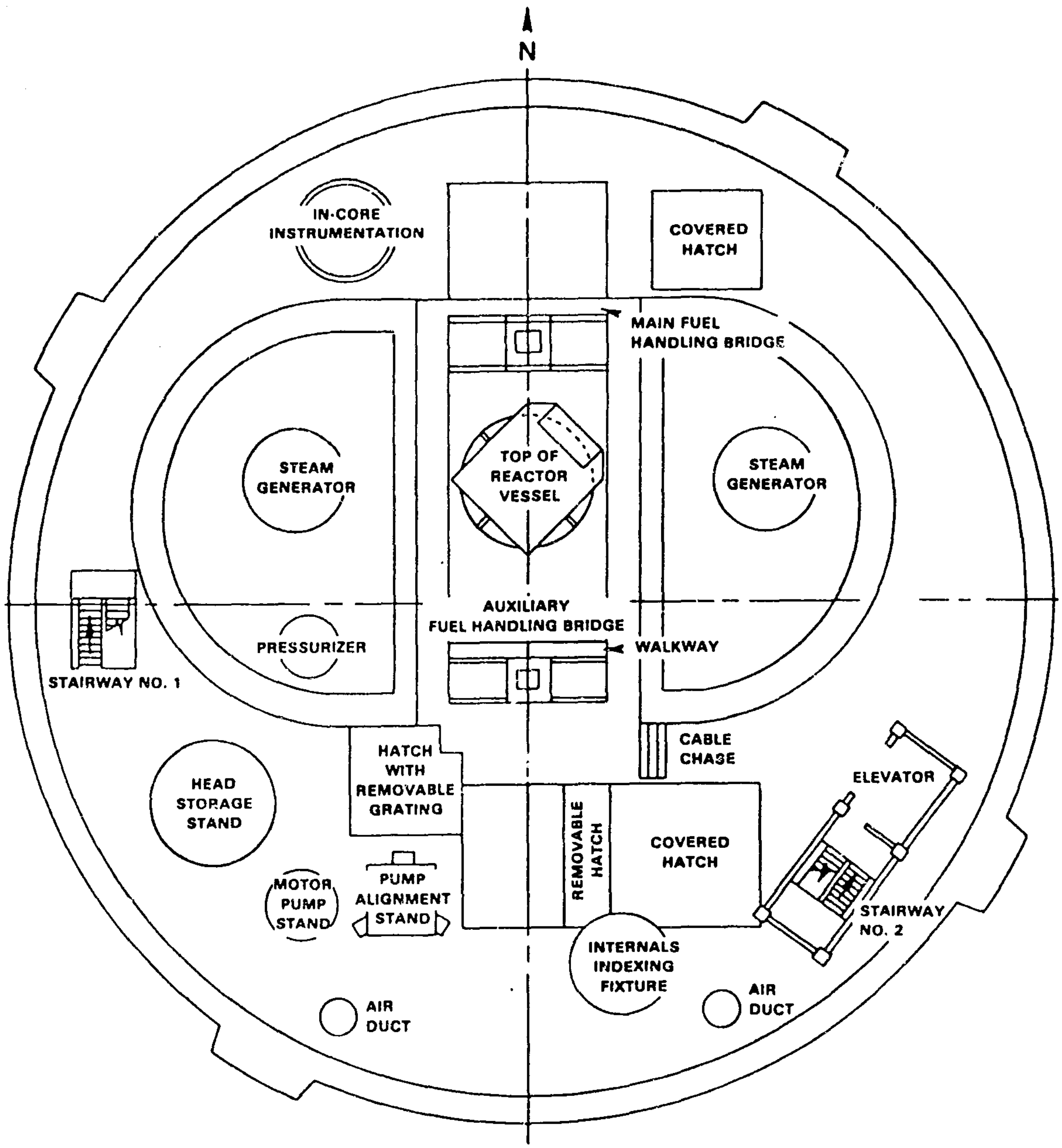

Figure 4-4. Floor Plan of Elevation 347.

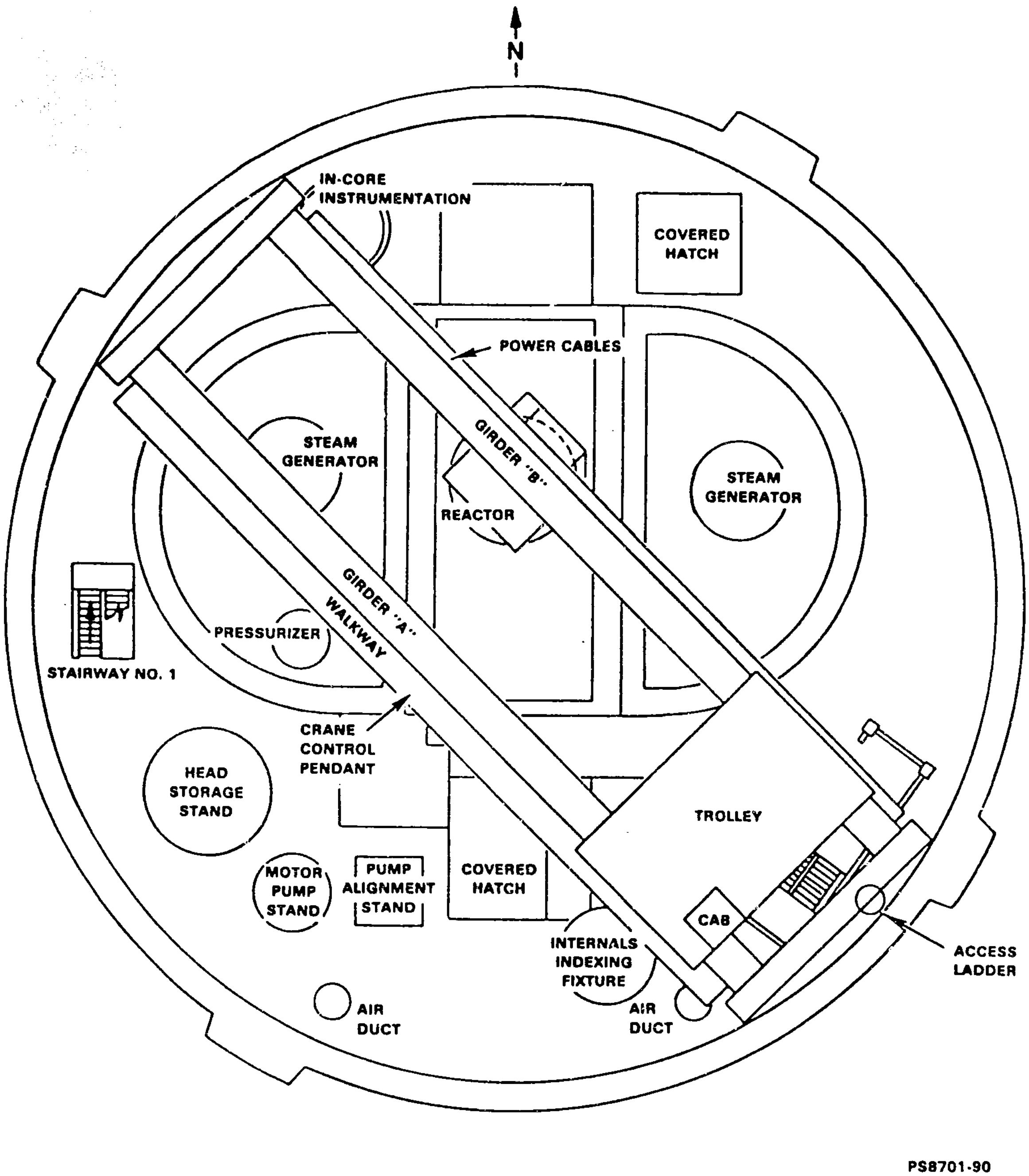

Figure 4-5. Floor Plan at Elevation 450 Showing the Position of the Polar Crane at the Time of the Accident.

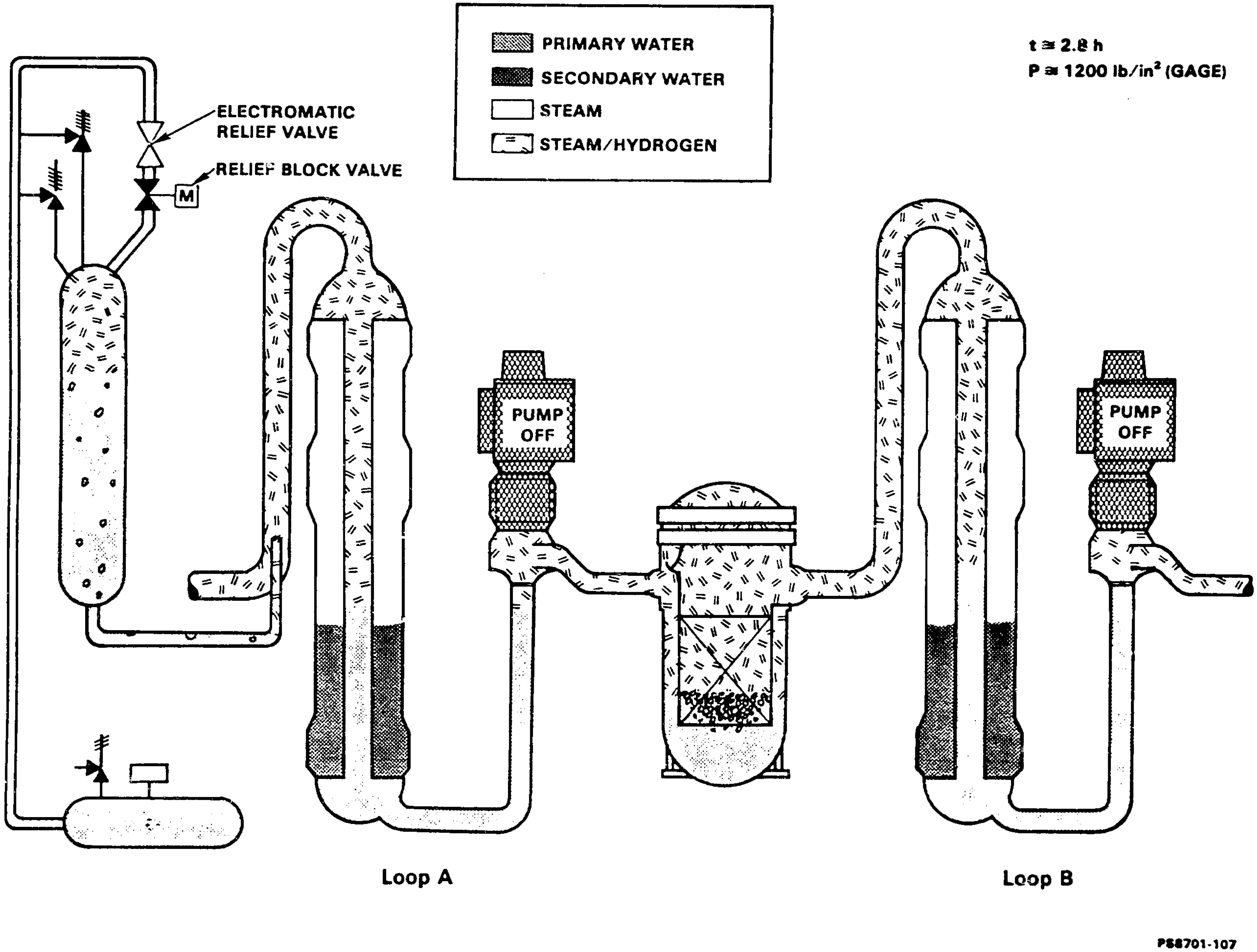

Figure 4-6. Simplified Diagram of the Reactor Cooling System (NSAC 1980).

Because of the infrequency of reports (a 30-s scan period for the computer temperature data and a 6-min period between recorder point printouts) and the relatively large thermal lag built into the rugged temperature sensors, the recorded temperature data have not proven to be as useful as the pressure data in helping to establish the burn characteristics. Conversely, the containment building pressure was continuously recorded on a stripchart and recorded every 3 s by the reactimeter as a change in the reference pressure (containment atmosphere) for the two steam generator pressure monitors. Further, pressure events (pressure switch trips and resets) monitored by the computer were timed to the second on the alarm printer. The sequence-of-events reports recorded on the utility printer indicate the time of each event to the nearest millisecond. The availability of this recorded temperature and pressure data made the TMI-2 hydrogen burn the best-recorded, large-scale (57,600 m^3 or 2,033,000 ft^3), contained, premixed gas burn in history.

4.3 HYDROGEN EVOLUTION AND STORAGE IN THE REACTOR COOLING SYSTEM

Hydrogen is generated in a degrading water-cooled nuclear reactor by radiolysis and metal-water reactions. In the TMI-2 LOCA, hydrogen generated by radiolysis was probably insignificant compared with that generated by the reaction of zirconium with water. Baker (1983) provided data from a number of researches which show that zirconium-water reaction rates are highly temperature dependent. Using these data, figure 4-7 was prepared. Note that the data sources are in reasonably good agreement and that very little hydrogen is generated until zirconium temperatures exceed 1,200 °F (650 °C).

There are many difficulties and uncertainties associated with the calculation of hydrogen generation rates and quantities that occurred during the TMI-2 event. If the calculations rely on the use of empirical metal-water reaction rate versus temperature data, some of the uncertainties include, or are a result of:

- Time the core began to uncover
- Coolant makeup flow rates and boil-down rates
- Changing heat movement means, paths (horizontal and vertical components), and rates with changing water levels, steam generation rates, hydrogen generation rates, and physical changes such as cladding ballooning from overheating and cladding swelling from oxidizing
- Changing surface areas as cracking and flaking of oxide layers expose more unoxidized metal
- Zircaloy melting and relocation to generally colder regions and resulting reduced exposed-surface areas
- Timing and effects of core shifts, core quenching, core collapse, core reheating, etc.

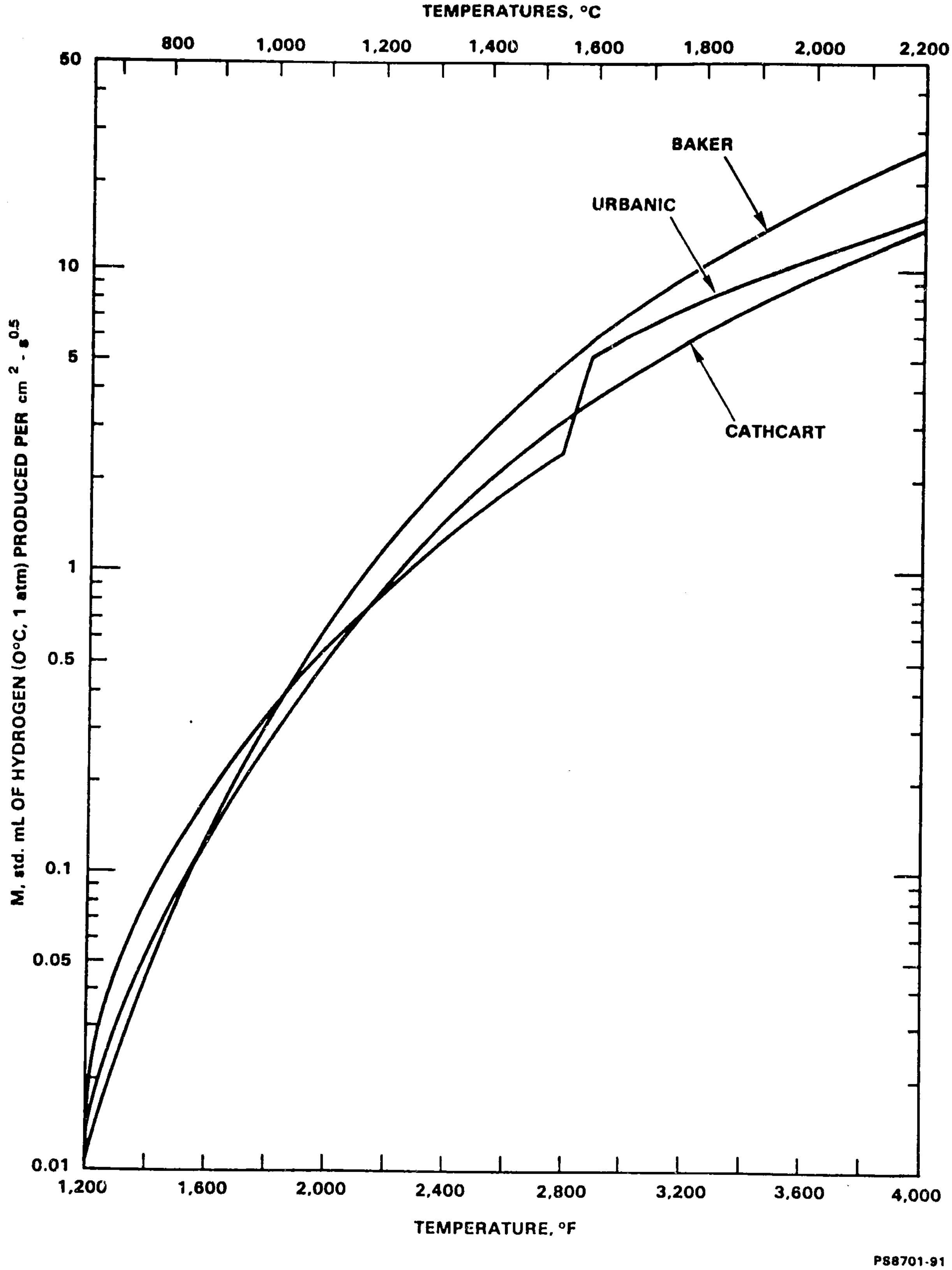

Figure 4-7. Comparison of Zirconium-Water Reaction Correlations.

Another approach to approximating TMI-2 hydrogen generation rates is to evaluate the TMI-2 reactor cooling system thermal-hydraulic data along with available hydrogen accounting information. This approach is presented in section 4.3.1.

4.3.1 Hydrogen Evolution

In the TMI-2 LOCA, steam from the reactor core moved to the pressurizer, out through the pressurizer relief valve to the coolant drain tank, and to the containment building. The water level in the TMI-2 reactor dropped to below the top of the active fuel and the upper region of the core started to overheat as early as 0550; this time is shown as the MAAP best estimate by Kenton et al. (1986). The MAAP best estimate is that by 0610 the water level in the core was below 7 ft (up from the bottom of the 12-ft-high active core section). As the zirconium cladding was uncovered and its temperature approached 1,200 °F (650 °C), hydrogen generation started. Since the zirconium-water reaction is highly exothermic, temperatures rose at increasing rates. By 0612, the amount of hydrogen gas generated was significant enough to block steam flow to the once-through steam generator A (OTSG-A). The secondary side of OTSG-B had boiled dry, and was, therefore, thermally isolated from the primary system. However, the water level in the secondary side of OTSG-A had just been raised to the 50% operating range level (Rogovin 1980). Refluxing was occurring as evidenced by an increased reduction in the primary system pressure. The cold water addition to OTSG-A also reduced steam pressures initially, but the pressure leveled off as temperatures stabilized. Then at 0612, the OTSG-A steam pressure started decreasing again at the same rate it had been decreasing when the secondary side was dry, indicating that it was no longer refluxing. Also, at 0612, the primary system pressure reversed its downward trend and started to increase. One explanation for this behavior would be hydrogen-blocking of OTSG-A and the accumulation of hydrogen and superheated steam in the primary system. Following Kenton et al. (1986), the amount of hydrogen required to effectively block steam flow to OTSG-A would be very small (possibly less than 1 kg), when the secondary water level was near (apparently not more than a few feet higher) that of the primary side. This appears to have been the case, as is shown in section 4.3.2.

After approximately 0610, hydrogen was generated at an increasing rate until approximately 0700 when the core had been quenched and cooled. After the quench, the partially cooled core collapsed and began reheating. Water levels again decreased, as indicated by an analysis of self-powered neutron detector data. However, at 0720:30, a makeup pump (MUP-1C) was started and was left on until the core was completely flooded and the pressurizer was refilled. The cooling effect decreased the system pressure and caused the pressurizer to start to drain and also caused some of the hydrogen and water vapor in the steam generators to flow to the reactor vessel. Reactimeter data show that the only significant steam-generating quench of hot materials caused by operation of the makeup pump started at 0722:30. The system pressure leveled off and flow from the pressurizer stopped for approximately 30 s. Since that transient was so small compared with the one at 0654 or the one to follow at 0745, it is certain that the upper half of the core, in its quenched and collapsed condition, had not overheated to the extent that it produced large quantities of hydrogen for a second time. Water from the makeup pump continued to enter the reactor vessel and at 0728, its level exceeded that of the nozzles; the water then flowed into the hot legs and pressurizer. There is no evidence that the water level in the reactor vessel has ever been below the level of the nozzles since that time. Therefore, the upper half of the core has not been reheated and it can be concluded that essentially all of the damage to the upper half of the core occurred before 0723. An evaluation of the extensive damage to the upper half of the core indicates that approximately 40% (not fully substantiated at this time) of the total zirconium in the core, or approximately 9,400 kg was oxidized in that region. The reaction of that much zirconium with water would produce over 400 kg of hydrogen, or approximately 90% of the total hydrogen accounted for by Henrie and Postma (1983a).

Even after the damaged core had been reflooded and was underwater, coolant flow through the core was blocked by the solid/molten mass of core materials. This mass reheated (from fission product decay heat), remelted, and continued to grow. That condition was terminated by 0748, when approximately 20 tons (Carlson and Cook 1985) of molten core material had flowed laterally and down around the lower core support structure, into the lower head region of the reactor vessel, where it solidified and fragmented. The amount of hydrogen produced during this time period (0723 to 0748) was only a small fraction of that generated earlier. While the molten mass was forming, the area exposed to water was relatively small; when the molten material was quenched, it already contained significant quantities of oxygen. The quantity of hydrogen produced appears to have been approximately 60 kg (460 kg total minus 400 kg produced earlier). There appear to have been no high-temperature core conditions after 0748 that would have resulted in significant hydrogen production from metal-water reactions.

To approximate timing and rates of hydrogen production, an analysis of the RCS pressure history was made, and two bounding sets of assumptions (cases 1 and 2) were established to relate hydrogen produced to system pressure. The results are shown in figure 4-8.

The case 1 analysis is based on the production of 400 kg of hydrogen by 0658, and an arbitrary assumption that the hydrogen generation rate remained constant through the core quench. This analysis indicates that the average hydrogen generation rate (slope) during the last 3 min prior to core flooding was approximately 20 kg/min. To approximate the hydrogen generated during that period, the nominal 20 kg/min generation rate was extended for 3 min to produce approximately 60 kg.

The maximum generation rate during the quench period may have been much higher than 20 kg/min and the total quantity of hydrogen generated may have been much more than 60 kg. The sudden increase in generation rate during the quench might be explained by a geometry change involving

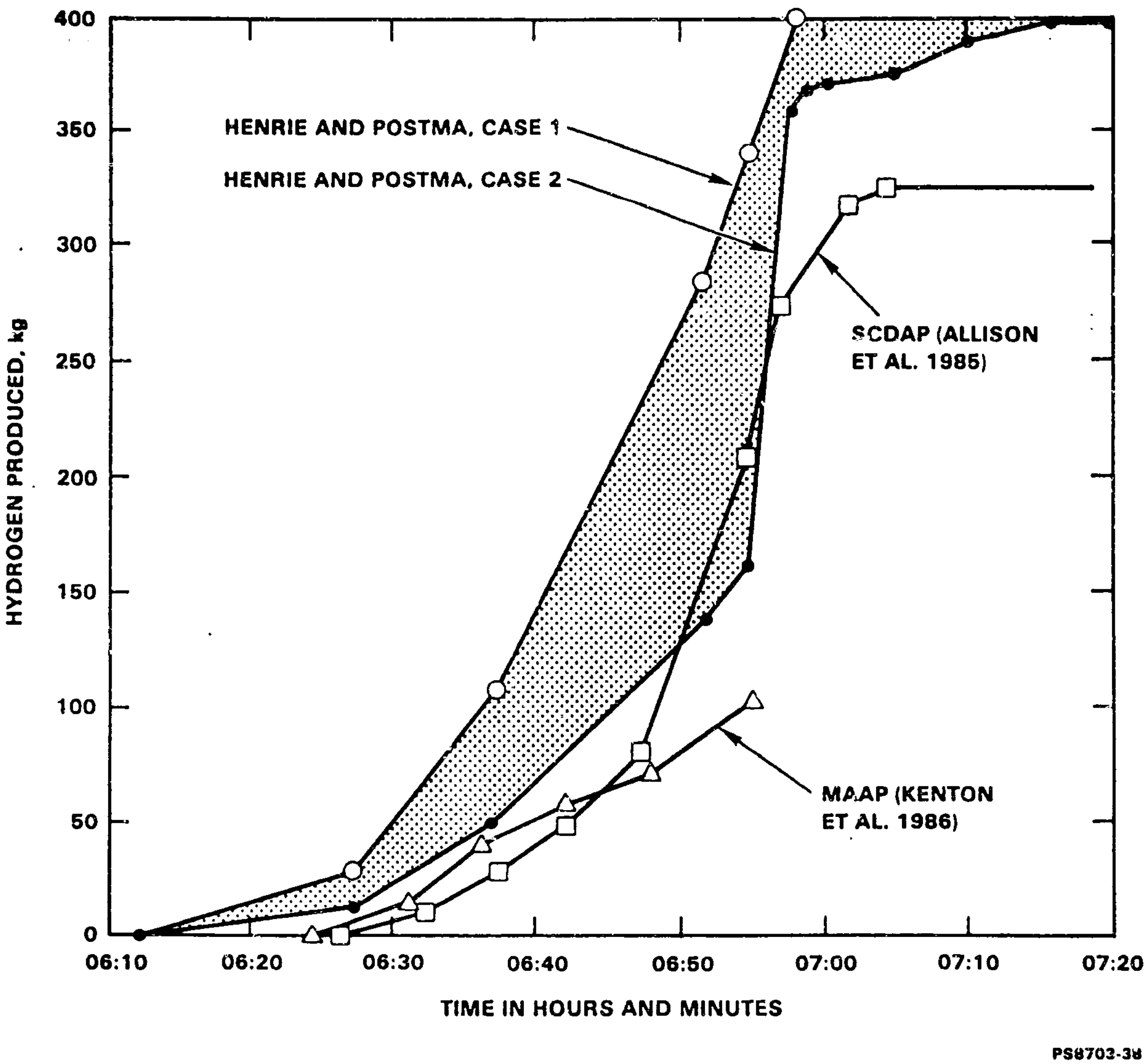

Figure 4-8. Calculated TMI-2 Hydrogen Production from the Zirconium-Water Reaction.

fragmentation of the cladding that greatly increased the area of unoxidized and partially oxidized zirconium exposed to the steam. The resulting increases in reaction rates and temperatures would have been high under those conditions. Case 2 represents these conditions and is based on the assumption that hydrogen generation is proportional to system pressure, even through the quench transient.

An analysis of steam generation rate versus water level in the core was made and compared with the hydrogen generation rates. It appears that for the few minutes preceding the quench, the steam generation rate was low enough to have limited hydrogen production to approximately 20 kg/min, which indicates that for case 1, the reaction may have been steam-limited during that period. The analysis also indicates that the reaction would not have been steam-limited during that period for case 2 conditions; therefore, the increased hydrogen generation rate during the quench would not have been caused simply by the increased availability of water vapor during the quench.

An apparent problem with the case 1 results is that so much energy would have been released from the exothermic metal-water reaction before the quench that it would have caused more damage to the core, core former, and plenum assembly than has been observed. In case 2, more than half of the hydrogen is generated during the core quench. Most of that reaction heat would have been used in the boiling of water, which would minimize metal overheating. Therefore, the case 2 result appears to be more correct than that of case 1. Also, the result of case 2 is much closer than case 1 to that of SCDAP (Allison et al. 1985) and MAAP (Kenton et al. 1986).

From postaccident evaluations of the core debris, core temperatures approached 3,100 K (5,100 °F), the melting point of uranium dioxide (Cook and Carlson 1985). This peak temperature condition probably occurred during the quench period.

4.3.2 Hydrogen Storage in the Reactor Cooling System

The large regions of the RCS that held hydrogen during the accident are the reactor dome, pressurizer, hot legs, and the upper sections of OTSG-A and OTSG-B. The quantity of hydrogen stored in the hot legs and hydrogen-blocked steam generators can be approximated from available system-pressure and steam-pressure data. The steam pressure on the primary side of the near-idle steam generators is essentially identical to that on the secondary side; any difference between the system total pressure and the steam pressure can be attributed to the presence of a noncondensable gas, or hydrogen in this case.

Pressure data from the reactimeter, computer utility printer, and the RC-3A-PT3 stripchart were obtained and correlated. Dynamic conditions and differences in elevation were accounted for in preparing the basis for correcting (calibrating) the stripchart record. A corrected stripchart pressure history for the period 0610 to 0655 was prepared and compared with the composite pressure history prepared by the NSAC (1980). Steam pressures and system pressures above $\sim$1600 lb/in^2 (11,000 kPa) are available from the reactimeter. These data are shown in table 4-1. From those data, the hydrogen concentration at the interface with water in the steam generators can be calculated (total pressure minus steam pressure, divided by total absolute pressure). The hydrogen concentration results are presented in figure 4-9.

Based on the apparently conservatively low assumption that hydrogen concentration decreases linearly from its maximum at the water interface in the steam generators to zero where the hot leg attaches to the reactor vessel, and making appropriate temperature connections, total quantities of hydrogen were calculated. The results are plotted in figure 4-10. Since water in the secondary side of OTSG-B had boiled dry before 0610, hydrogen quantities stored in OTSG-B could not be approximated until after the secondary water level had been raised to the 50% operating range and conditions had stabilized at approximately 0650.

Note from figure 4-9 that hydrogen was apparently accumulating in OTSG-A as early as 0610. Also note from figure 4-10 that at 0712, the calculated total quantity of hydrogen in the two steam generators and hot legs exceeded 300 kg. The void volume in the hot legs and steam generators ($\sim$3,750 ft^3 or 106 m^3) at that time was approximately 63% of the total RCS void volume. (The void volume in the pressurizer was approximately 250 ft^3 or 7 m^3 and the void volume in the reactor vessel was approximately 2,000 ft^3 or 57 m^3.) Since the heat source was in the reactor vessel, the temperature and vapor content there was higher than that in the hot legs and steam generators. Consequently, the amount of hydrogen in the hot legs and steam generators would have been higher than 63% of the total, which indicates good agreement ($>300/>.63 \simeq 400$) with the previously determined total of 400 kg of hydrogen at that time.

4.4 HYDROGEN RELEASE AND MIXING IN CONTAINMENT

Hydrogen and steam were released from the RCS primarily through the pressurizer relief valve (PRV) and piping, to the reactor coolant drain tank (RCDT), then through a failed rupture disk in the discharge duct and on to the containment. The initial hydrogen release occurred between 0612, when hydrogen generation started, and 0619, when the PRV closed. Since hydrogen concentrations and RCS pressures were low at the time, the hydrogen released during that period was probably less than 10 kg. The PRV was opened for a total of 3 1/2 min between 0712 and 0719. From pressure changes, it is estimated that approximately 50 kg of hydrogen was released during that period.

After 0730, water levels were high in the RCS and the hydrogen was trapped (water-blocked) in the reactor dome, steam generators, and hot legs. Approximately 80 kg of this hydrogen escaped between 0830 and 0920 when the PRV was opened, pressures were reduced, and water levels were lowered. The RCS pressure was again increased and the PRV was cycled for an extended period; however, the hydrogen was trapped and little was released.

Table 4-1. Total Pressure in the Reactor Cooling System and Steam Pressure in the Once-Through Steam Generators (OTSG-A and -B), in lb/in^2 (gage), During the Principal Hydrogen Generation Period.

Time	Total pressure		Steam pressure	
	NSAC composite	Current composite	OTSG-A	OTSG-B
0610	610	631	600	a
0612	603	621	591	a
0614.5	615	636	579	a
0627	680	685	518	a
0637	805	831	457	a
0654.5	1200	1244	358	140
0655.5[b]	1674	1674	361	718
0657	1990	1990	354	577
0658	2026	2026	348	545
0700	2043	2043	327	458
0705	2051	2051	281	359
0710	2100	2100	241	363
0712.3[c]	2119	2119	224	370
0715.5[d]	1907	1907	206	375
0718.6[c]	1920	1920	189	377
0719[d]	1887	1887	185	376
0720.5[e]	1883	1883	181	376
0723	1721	1721	163	372
0724	1637	1637	157	370

[a]The secondary side of OTSG-B had boiled dry, therefore, the steam pressure on the primary side is unknown.
[b]After 0655, all data are from the reactimeter.
[c]Pressurizer relief valve opened.
[d]Pressurizer relief valve closed.
[e]Makeup pump (MUP-1C) came on.

PST87-3089-1

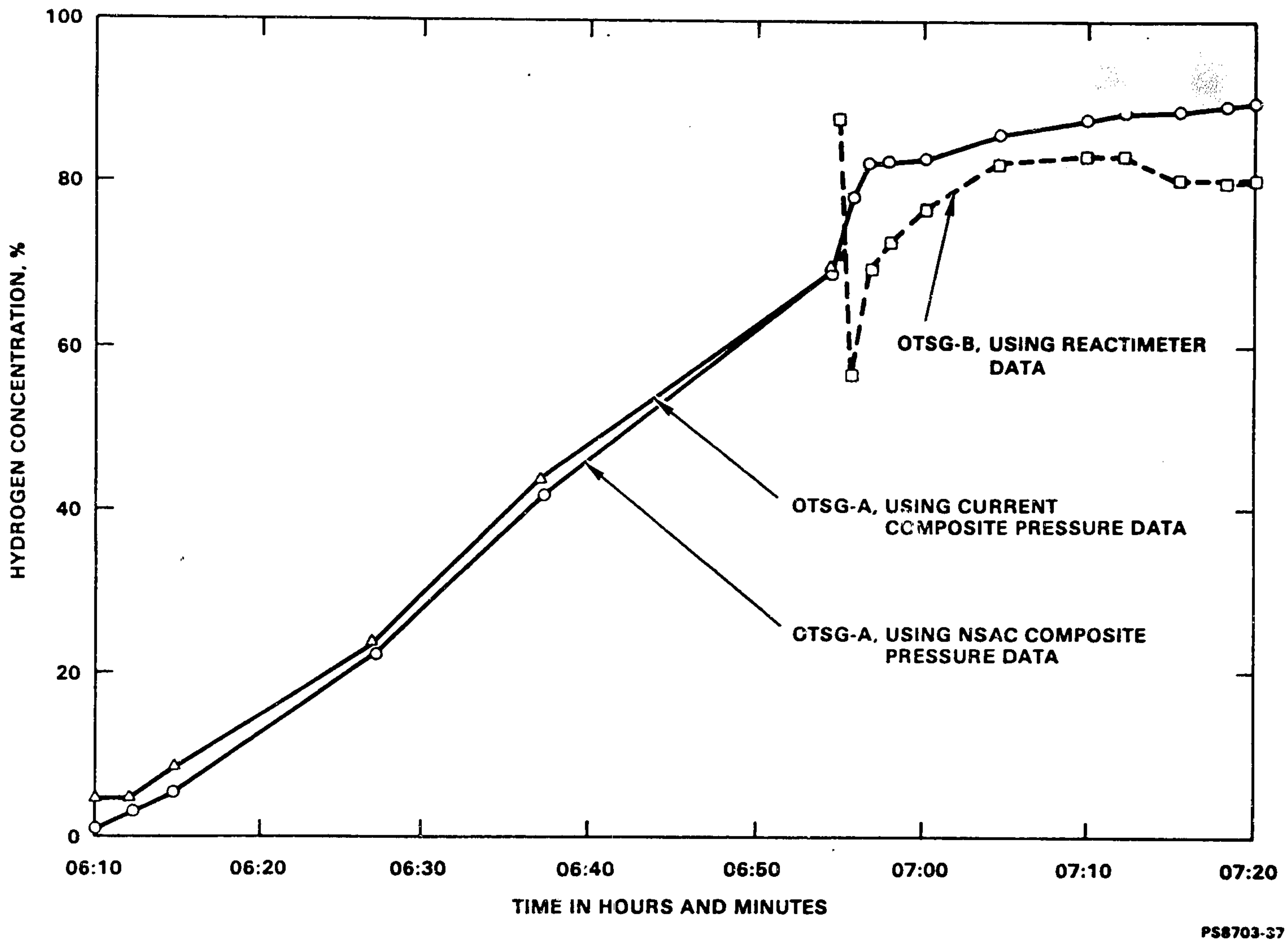

Figure 4-9. Calculated Hydrogen Concentration Versus Time Near the Water Interface in Once-Through Steam Generators -A and -B.

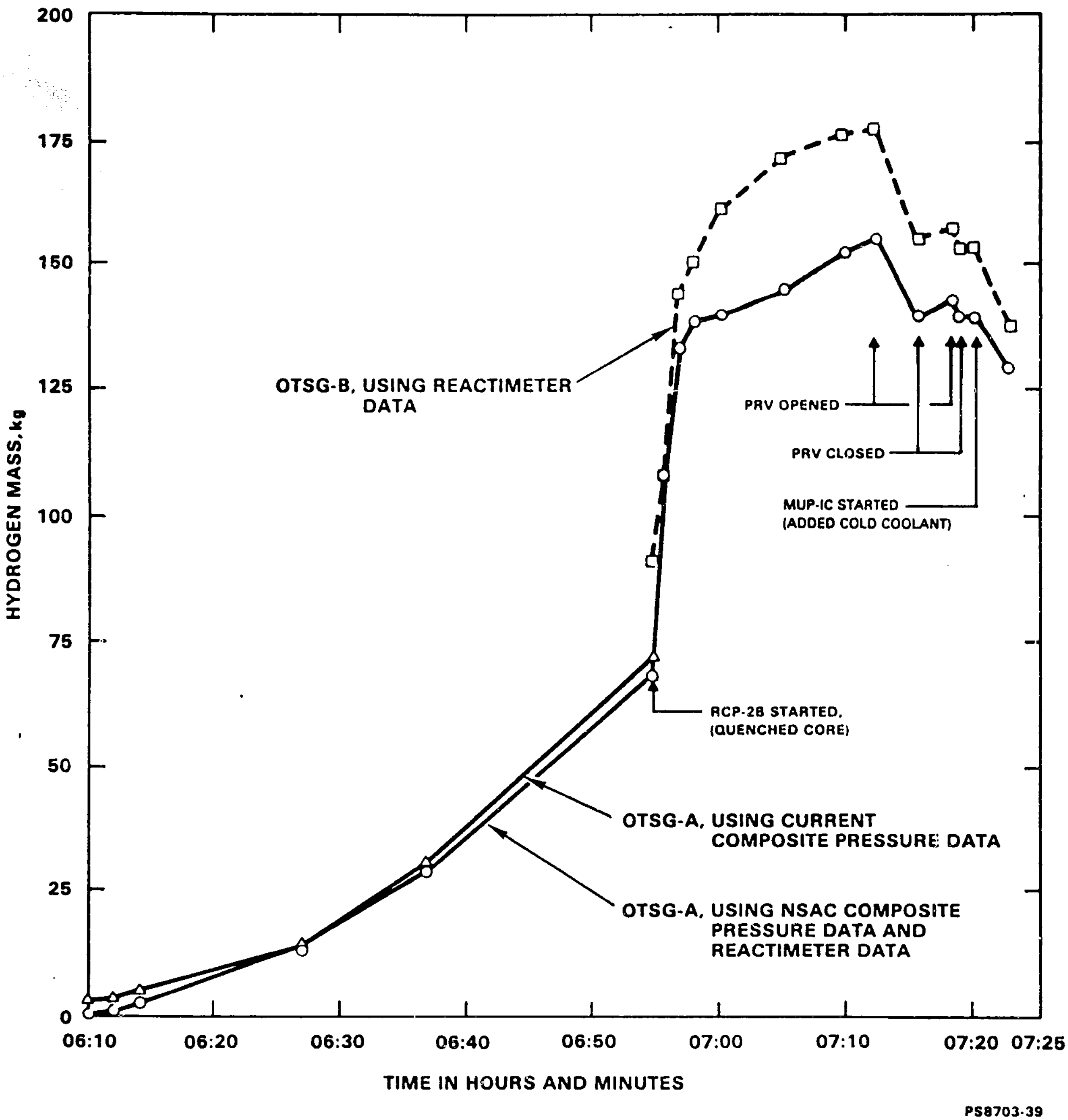

Figure 4-10. Calculated Mass of Hydrogen Versus Time in Hot Legs and Once-Through Steam Generators -A and -B.

At about 1155, the RCS pressure and water level again became low enough to release trapped hydrogen through the open PRV to containment. When the PRV was closed at 1306, approximately 370 kg of hydrogen gas had been released to containment (Henrie and Postman 1983a); therefore, approximately 230 kg of hydrogen was released to the containment building from the RCS between 1155 and 1306.

The RCDT discharge duct terminates below the Elevation 305 floor at a point reasonably close to the west stairway, which is open at each floor. The discharge of steam at this point is confirmed by temperature increases indicated by a sensor (point No. 13 on the multipoint recorder) located at Elevation 326 in the vicinity of the stairway. The sensor reacted quickly to steam discharged from the RCDT exhaust duct, indicating that the steam plume had passed.

The buoyant steam-hydrogen mixture would be expected to spread laterally below the floors at Elevations 305 and 347 and flow upwardly through openings that include many small penetrations, the open stairway, floor gratings, and the 4-in.-wide annular seismic gaps that exist between each floor and the containment shell. Because of its size and proximity, the stairway opening on the west side served as the main pathway for the hydrogen-steam mixture to flow into the room above Elevation 305. Movement was then predominantly upward and to the southeast to the air-cooler inlets. This primary flow path is conclusively shown by a study of the locations of the containment atmosphere temperature sensors and the temperature changes as hot steam-hydrogen mixtures are released from the RCDT.

The hot steam-hydrogen mixture is initially buoyant and tends to stratify in the upper portions of each compartment it enters. The tendency of hydrogen-steam mixtures to stratify is opposed by a number of mixing processes:

- Entrainment by the exiting jet or plume
- Natural convection due to temperature gradients along wall surfaces
- Molecular diffusion
- Momentum of air exiting from air-cooler outlet ducts
- Interroom mixing caused by air flow from the air coolers.

The extent to which these mixing mechanisms would produce a well-mixed atmosphere can be inferred from the results of large-scale containment mixing experiments reported by Bloom et al. (1983). In the cited tests, hydrogen-steam mixtures were released from ducts into an air-filled containment. The diameter of the test vessel was 25 ft; the height was 15 or 50 ft depending on test configuration. While a detailed discussion of mixing test results is beyond the scope of the present study, the following key results are cited as applicable to the TMI-2 incident.

- Turbulent mixing in the jet or plume always caused the hydrogen/steam plume to be greatly diluted by the surrounding atmosphere before the plume reached the top of the test compartment.

- During the hydrogen release period, hydrogen concentrations in the test compartment were much higher than average only in the plume originating from the outlet duct.

- Following the termination of the hydrogen source, significant hydrogen concentration gradients persisted for appreciable times only when active mixing processes were absent and when natural convection was minimal.

- When wall and gas temperatures differed by a few degrees centigrade, natural convection alone was an effective mixing mechanism.

In the TMI-2 containment, all of the mixing mechanisms discussed in this section were operational when hydrogen was being released. Temperature differences of 10 °C to 30 °C typically existed between gas and walls, ensuring the existence of turbulent boundary layers on walls. Also, the coolers recirculated air an average of once every 8 to 9 min. For most of the hydrogen in containment, these mixing processes had more than one hour to operate, making it almost certain that the bulk of the hydrogen would have been well-mixed throughout the containment space.

The relatively small quantity of hydrogen released during the period when the PRV was open immediately before the burn would not have had time to become well-mixed. The gas in this plume would have been enriched in water vapor and hydrogen compared with the remainder of containment. Except for the region of the vent plume and in unvented compartments such as the elevator hoistway and the enclosed stairway, it is unlikely that concentration differences as much as 1% hydrogen could have existed between the upper containment and regions below Elevation 305.

4.5 PREBURN CONDITIONS

Preburn conditions in the containment atmosphere were identified by Henrie and Postma (1983a). The conditions, based on extensive analysis of data, are summarized in table 4-2.

4.6 ENGINEERING ANALYSIS OF KEY BURN PARAMETERS

Several characteristics of hydrogen burns are important in determining damage to the containment building and its contents. These burn characteristics depend on the preburn gas composition and the physical structure of the containment building. In this section, key burn parameters are analyzed to determine the numerical values that apply to the TMI-2 burn and illustrate the degree to which the parameters are expected on the basis of engineering analysis.

Table 4-2. Preburn Conditions.

Parameter	Preburn value
Hydrogen concentration (average)	7.9% (wet basis)
Gas temperature (average)	128 °F (53 °C)
Containment pressure	16.0 lb/in^2 (absolute) (110 kPa)
Water vapor concentration	3.5% (wet basis)
Hydrogen source on	Yes (or just turned off)
Air cooler flow rate	235,000 ft^3/min (absolute) (111 m^3/s)
Atmosphere uniformity	Well-mixed except in source plume
Total gas volume	2,033,000 ft^3 (57,600 m^3)

4.6.1 Deflagration Versus Detonation

Deflagrations are combustions that occur relatively slowly. A flame front propagates from its inception point at speeds well below sonic (based on the speed of sound in the unburned gas) and as a result, the unrestricted sections of a contained atmosphere are compressed at essentially the same rate. Detonations, conversely, involve reactions in wave fronts that propagate through the gas at supersonic speeds (also based again on the sonic velocity in the unburned gas). The shock wave that accompanies the detonation imparts a transient load on structures that is not present in deflagrations. Because containment response to the two reaction types would be considerably different, the TMI-2 hydrogen-oxygen reaction was studied for evidence that would characterize it as a deflagration or a detonation.

4.6.1.1 Preburn Hydrogen Concentration. For mixtures of hydrogen in air with hydrogen concentrations below 14%, detonations are not possible (NSAC 1980). This limit is far above the average hydrogen concentration in the preburn atmosphere at TMI-2 (Henrie and Postma 1983a), and it can be concluded that a detonation was not possible in most, if not all, of the gas volume. Previous studies (Henrie and Postma 1983a) have shown that hydrogen and steam were being vented from the reactor coolant drain tank when the burn occurred. Therefore, the possibility of a detonation in the mixing zone of the release where higher hydrogen concentrations could exist has been considered. The presence of steam in the mixture being released from the drain-tank vent represents a diluting effect that prevents detonable concentrations in the mixing zone. This is illustrated in figure 4-11 where the detonable region is shown on a triangular composition diagram. Compositions in the mixing zone fall on a straight line connecting the source concentration with the mixed or bulk concentration.

The gas exiting from the drain tank would be mostly steam because the water in the drain tank would be close to the boiling point. If the water was 3 °C cooler than the boiling point, the mixture being released would be 91% steam and 9% hydrogen. As indicated by the mixing line on figure 4-11, a detonable concentration is not reached. A hypothetical mixture that would be detonable can be identified by drawing a line from the bulk composition that just intersects the detonable limits. As indicated in figure 4-11, the hypothetical mixture contains approximately 32% hydrogen. This composition corresponds to a mixture saturated with water vapor at a temperature some 10 °C below the boiling point, an unlikely condition at that time.

While the hypothetical mixture of 32% hydrogen represents the leanest source mixture that could produce a detonable concentration in the mixing zone, much higher hydrogen concentrations (lower water concentrations) would be required to produce a large enough gas volume well inside the detonable region to yield a measurable detonation. Therefore, it is concluded that a detonation was impossible in the bulk of the gas, and that the probability of achieving even locally detonable concentrations in the mixing zone was remote.

4.6.1.2 Propagation Velocities. In detonations, the reacting shock wave travels in excess of the speed of sound in the unburned gas. For the TMI-2 preburn gas composition, the sonic velocity is estimated to be 1,230 ft/s (375 m/s); therefore, a sonic wave would travel the maximum dimension of the containment building in less than 0.16 s. However, numerous independent pressure-measuring devices showed that the burn occurred over a time duration longer than 12 s. Based on the measured pressure rise time, which was very long compared with that expected from a detonation, it is concluded that the hydrogen-oxygen reaction proceeded as a deflagration.

4.6.1.3 Mechanical Damage Inside Containment. Mechanical damage resulting from the hydrogen burn is wholly consistent with a deflagration (Eidam and Horan 1981): barrels were partially collapsed and doors opened. If a detonation wave had traveled through the containment, evidence of shattered glass and the translocation of unsecured light-weight structures would be expected. No such evidence exits. It is therefore concluded that the hydrogen-oxygen reaction proceeded as a deflagration rather than a detonation.

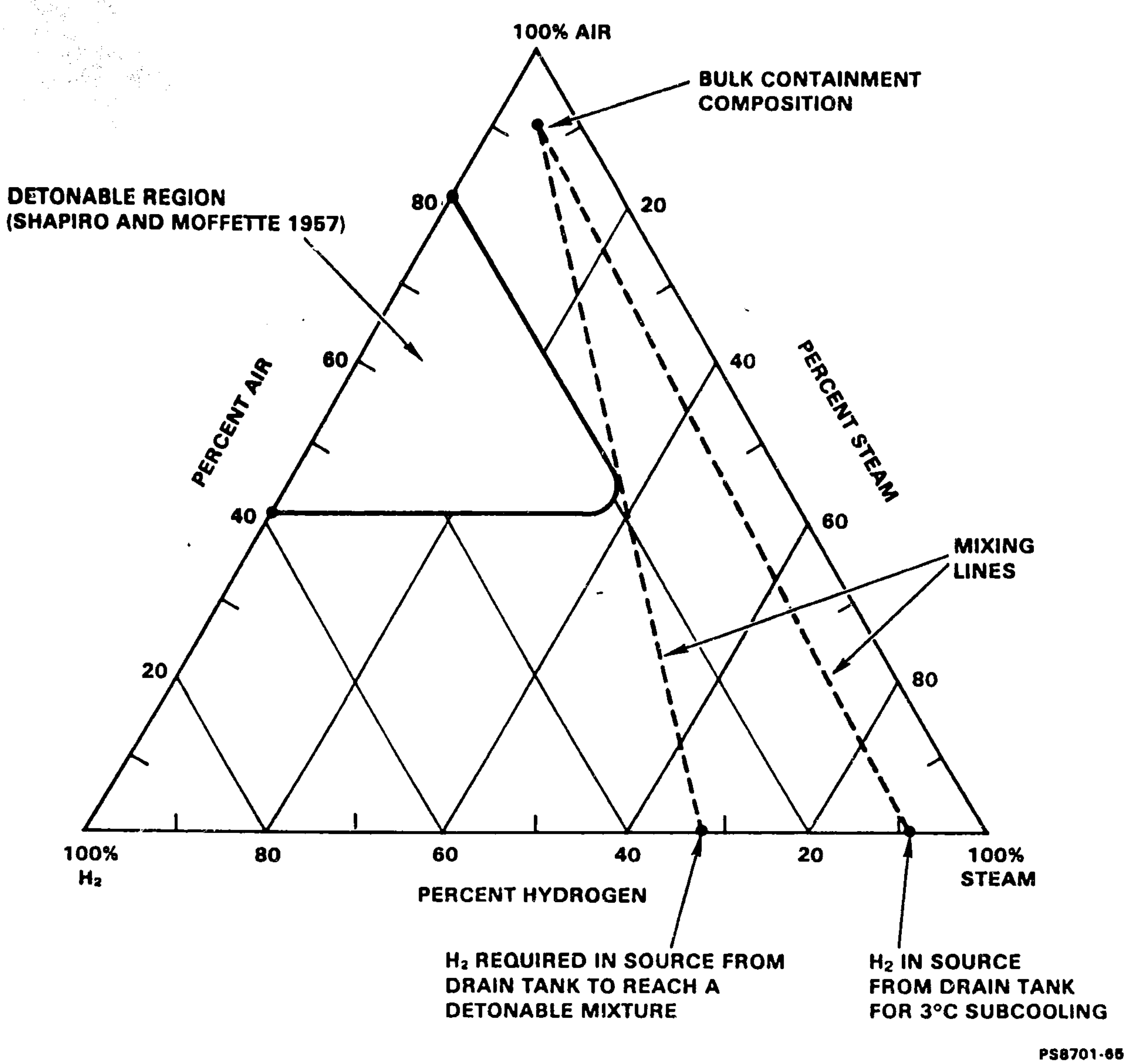

Figure 4-11. Composition Diagram Showing Hydrogen Concentrations in Mixing Zone.

4.6.2 Pressure Rise Rate

During a hydrogen burn in containment, the gas pressure rises as a result of the increase in temperature. The pressure rise rate is, therefore, a reflection of the burning rate and is of interest because it characterizes the burn.

For the TMI-2 burn, pressure rise rates were obtained from pressure data recorded from secondary steam-pressure measuring instrumentation of the OTSG-A and OTSG-B. Pressures obtained from the reactimeter for OTSG-A, starting at the beginning of the burn, are shown plotted in appendix A. Average pressure rise rates are tabulated in appendix B.

4.6.2.1 Pressure Rise Rate and Burning Velocity. The rate at which a flame front propagates through a premixed combustible atmosphere determines the rate at which the chemical reaction occurs on a volumetric basis. The quantity of energy given off per unit volume of gas depends on the initial pressure and volume fraction of the minimum constituent reactant (in this case, hydrogen) in the gas mixture. Increases in both of these factors tend to cause the pressure rise rate to increase until a peak rate is achieved as accelerating and limiting factors develop. These factors include the amount of turbulence present or created by the burn, and the direction of the burn (up, down, or horizontal).

4.6.2.2 Pressure Rise Rate and Ignition Location. Burning velocities are known to be directionally dependent and, therefore, the observed burning rate in the TMI-2 event can be used in determining the origin of the burn initiation. The lower hydrogen concentration limit for upward burning is 4.1%, the limit for horizontal propagation is approximately 6%, and the limit for downward propagation is approximately 9% (Lewis and Von Elbe 1961). Since the premixed hydrogen concentration was lower than the limit for downward propagation, it is concluded that the burn initially propagated upward in order to burn with the high velocity that is consistent with the total burn time. If the burn had started with ignition at a high point in the containment vessel, a much slower and less complete burn would have occurred. From these considerations, it is concluded that the TMI-2 hydrogen burn was initiated with an ignition at a relatively low elevation (below the Elevation 305 floor) in the containment building.

4.6.3 Peak Pressure/Temperature

The peak pressure reached as a result of a hydrogen burn is a reflection of the peak in average gas temperature. Pressure and temperature may be related by means of the ideal gas law and account for the loss of combustible gases and the gain of combustion product gases (Henrie and Postma 1983a). The peak temperature reached depends on the net amount of heat generated by the combustion. The net heat is the difference between the heat of reaction and the heat lost to the surroundings. Since heat lost from the gas during the burn is usually a small fraction of the combustion energy, and which can be accounted for, the peak increase in temperature (and consequently peak pressure) can be related to the percentage of hydrogen burned.

The final gas temperature produced by an adiabatic isochoric hydrogen burn is shown in figure 4-12 as a function of hydrogen percentage burned (Henrie and Postma 1983a). In principle, the peak pressure reached can be used to estimate the percentage of hydrogen burned. The accuracy of the estimate depends in part on how well heat losses during the burn can be accounted for, as well as after-burns. For the TMI-2 burn, Henrie and Postma (1983a) estimated that the peak pressure reached was consistent with a burn of 6.8% hydrogen. It was further estimated that 1.1% hydrogen remained in the containment after the burn; therefore, the preburn hydrogen concentration was estimated to be 7.9%.

4.6.4 Postburn Cooldown Rate

The rate at which the containment atmosphere cools after a hydrogen burn is important because the temperature-time history determines the heat pressure that causes materials and equipment in containment to be heated. The degree of heatup in turn challenges the integrity of a receptor so damage analyses can be done only after the time-temperature history of the ambient atmosphere is defined.

A simplified heat transfer analysis of the atmospheric cooldown rate was performed with two key objectives in mind: (1) allow receptor heatup analyses to be performed and (2) illustrate the degree to which the actual cooldown rate agreed with predictions based on a simple heat transfer model.

The work reported here is based largely on the earlier work of Henrie and Postma (1983a). The hand calculational model described by Henrie and Postma (1983a) was improved (by allowing for intercompartmental flows and by explicitly accounting for heat transfer to sprays) and reduced to a BASIC code that was run on a personal computer. The basis for these calculations and the results are presented in appendix C. (Note from figure C-3 how closely the average temperature points based on the OTSG-A and OTSG-B measured pressure points compare with the predicted average curve.) Since the same calculational techniques were used to predict time-temperature profiles in the upper containment (above Elevation 347) and lower containment (D-rings and below Elevation 347), those profiles are quite accurate and should be useful in evaluating burn evidence or projecting burn potentials in those regions.

4.6.5 Burn Damage Characteristics

A hydrogen burn within the containment building would produce burn damage with characteristics that reflect the pulse-type heating and the properties and locations of specific receptors. In this section, burn damage characteristics are summarized to illustrate the degree to which they are expected on the basis of a premixed hydrogen combustion event.

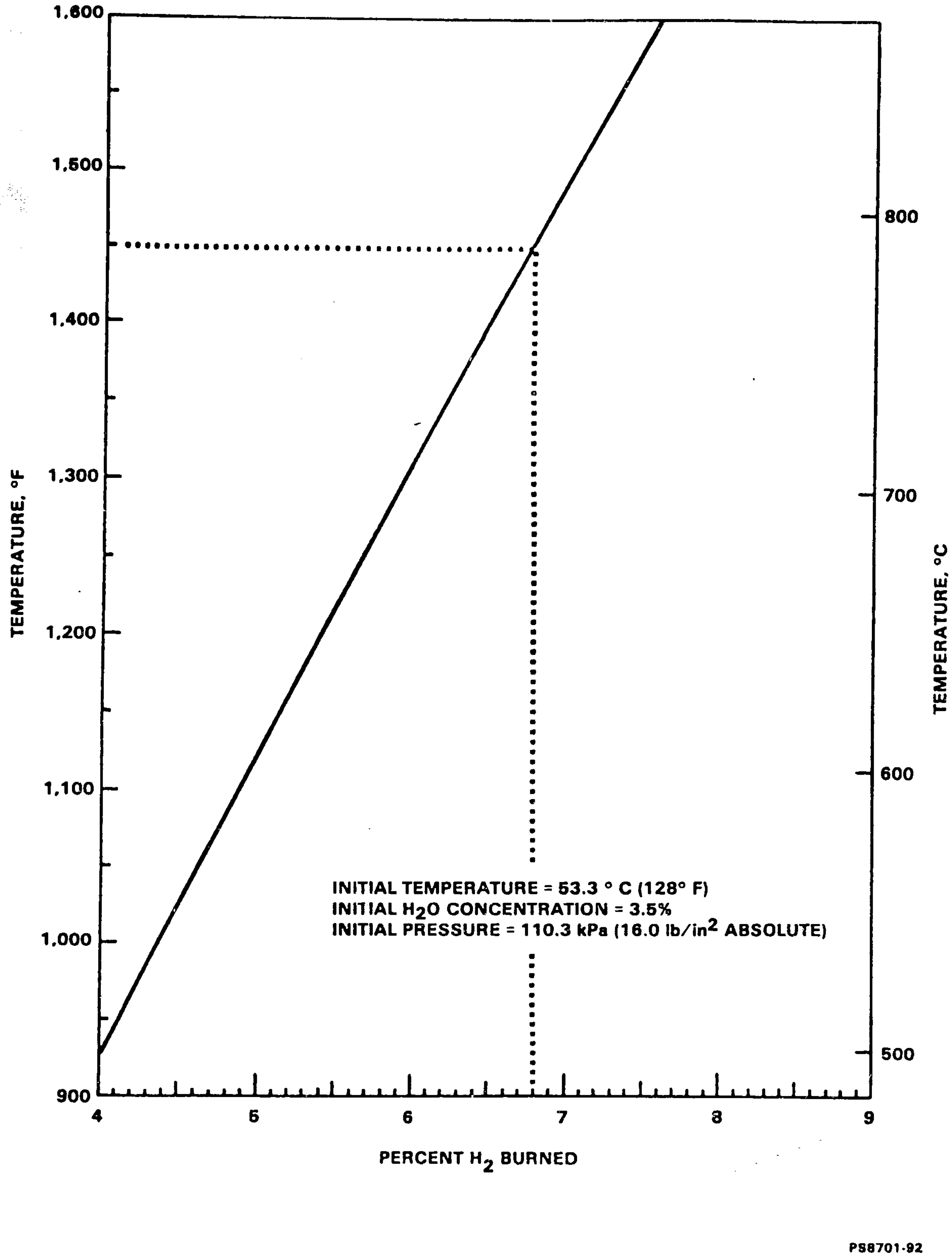

Figure 4-12. Predicted Containment Temperature for an Adiabatic Isochoric Hydrogen Burn (Henrie and Postma 1983a).

4.6.5.1 Effect of Receptor Materials Properties. Studies of burn damage (Alvarez et al. 1982; Henrie and Postma 1983a; Schutz and Nagata 1982) and reviews of in-containment photographs (Eidam and Horan 1981) indicate that noticeable damage was sustained only by thin materials (paper manuals, plastic sheeting, and items made from thin plastics e.g., telephones and buttons on instruments) and material with a low-thermal diffusivity (wooden planks, plastic rope, and the polar crane pendant cable). The susceptibility of these materials to burn damage is as expected on the basis of heat transfer analyses that predict the heatup of surfaces exposed to a hot gas (Alvarez et al. 1982; Henrie and Postma 1983a). Temperatures of these susceptible materials can become high enough to cause melting, pyrolysis, or burning. Materials of appreciable thickness and high-thermal diffusivity (metals) can not be heated to temperatures hot enough to undergo burn damage. Thus, as expected, most containment surfaces (painted steel or concrete) did not suffer apparent burn damage. Therefore, it is concluded that the materials which were observably damaged were those expected to be most susceptible to being heated to damage-threshold temperatures by the hydrogen burn.

4.6.5.2 Effect of Receptor Location. The location of a receptor can be important if the temperature-time history of the ambient gas is affected by its location inside the containment. As discussed in section 4.6.4, the heat pressure in lower containment volumes is less intense than in upper containment because lower containment compartments have higher surface-to-volume ratios. Studies of TMI-2 photographs led Henrie and Postma (1983a) to conclude that observed burn damage was less severe in lower compartments as a result of lower heat pressure in those rooms. Differences in damage to telephones located at different elevations are cited as illustrative of this expected effect.

For locations within a large volume, stratification is expected to cause gas temperature to increase with height. Thus, damage to susceptible materials would be expected to increase with height in upper containment. Studies of burn damage to the polar crane pendant cable (Trujillo et al. 1986) do indeed show observable damage to the outer sheath to increase with height. As an added note, it is postulated that the effect of height on damage would have been even more noticeable if containment sprays had not activated. Spray operation mixes the containment atmosphere as well as causes a faster cooldown.

Susceptors located next to massive heat sinks may be protected from overheating. First, heat transfer from the susceptor to the sink can limit susceptor temperature. Second, the gas in the boundary layer adjacent to the sink can be much cooler than bulk gas and small susceptors may be exposed only to the cooler gas of the boundary layer. Henrie and Postma (1983a) cite as an example a telephone cable lying on a steel table is apparently undamaged; an adjacent section of cable, suspended in midair, shows significant damage.

4.6.5.3 Effect of Surface Moisture. As noted by Henrie and Postma (1983a), the presence of water on susceptors can greatly limit heatup of the susceptor. It was estimated that the latent heat of vaporization of a water film approximately 0.5-mm (0.02-in.) thick was equal to the total amount of heat transferred to a surface by the burn. Therefore, wet objects would be affected much less by a burn than dry ones.

Preburn events at TMI-2 included numerous openings of the primary system relief valve. While much of the steam released to containment was no doubt removed by containment coolers, there was ample opportunity for condensate to wet materials located near the steam vent or in drip locations. As noted earlier (Henrie and Postma 1983a; Alvarez 1984) the presence of sorbed moisture can explain the apparent lack of damage to receptors located in wet regions; similar receptors located away from those wet areas were damaged.

4.6.5.4 Overpressure Damage. While the containment building itself was not damaged by the pressure spike caused by the hydrogen burn, 50-gal drums were partially collapsed and doors on the enclosed stairwell and elevator were sprung (Eidam and Horan 1981). Consistent with pressure differential calculations, unsealed containers (typified by electrical boxes and LOCA ducts) were apparently undamaged by the pressure spike.

All of the observed responses to the pressure spike are as expected for a hydrogen deflagration and it is concluded that further analyses of mechanical damage is unnecessary.

4.7 CHARACTERISTICS OF THE HYDROGEN BURN

In a contained burning event, the pressure rise results from the change in gas temperature and the depletion and addition of gas molecules resulting from the burn. Therefore, the average containment gas temperature and pressure data are interrelated and complementary (see section 4.6.3).

A composite of the available data showing the average containment gas temperature and pressure over the entire burn and cooldown period are shown in figure 4-13. Also shown is the theoretical projection of the burn temperature if it had occurred instantly. The difference indicates that cooling during the burn caused a reduction in the peak pressure and temperature of 5 lb/in^2 (35 kPa) and 110 °C, respectively. Three anomalies are shown by figure 4-13:

- The apparent drift of the OTSG-A pressure data starting at about 1351:30
- The abrupt downward spike indicated at 1352:05, when the OTSG-A and OTSG-B data went off-scale low
- The apparent 3-s lag in the OTSG-B pressure data during the hydrogen burn.

The first anomaly is attributed to a slow rise (2 lb/in^2 or 14 kPa in 45 s) in steam pressure in OTSG-A and is inconsequential. The second anomaly has been thoroughly studied (Henrie and Postma 1983b) and was

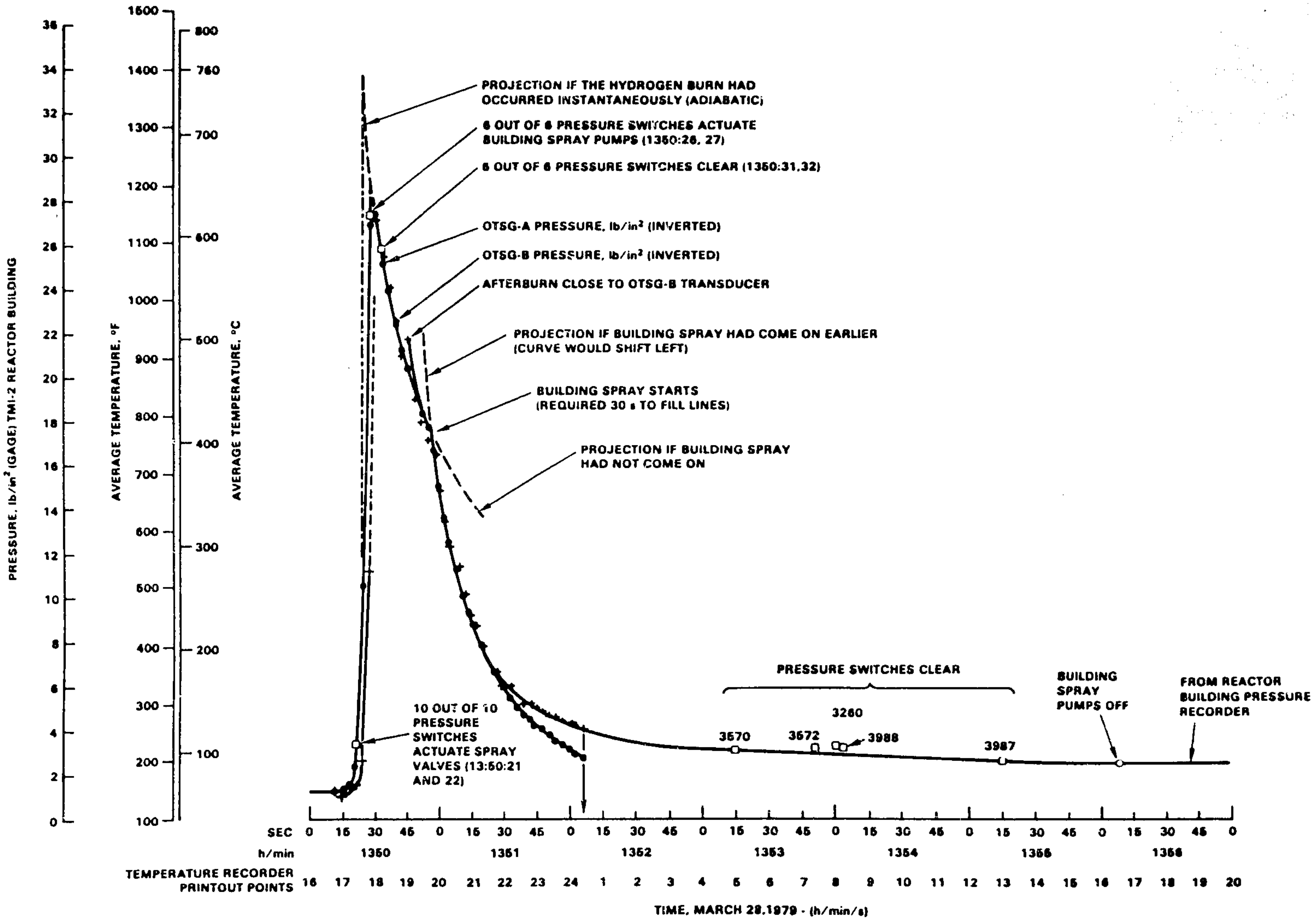

Figure 4-13. Composite TMI-2 Containment Average Temperature and Pressure Versus Time.

determined to an electrical malfunction, probably a ground fault, which affected all of the reactimeter signals. The third anomaly had not been satisfactorily resolved prior to this report.

4.7.1 Pressure Differences During the Burn

An evaluation of available, accurately timed pressure data and an analytical study of expected pressure differences in partially sealed compartments during the hydrogen burn indicate the following (see appendixes A and B).

- During the burn when the containment pressure was at 3.6 lb/in^2 (gage) (25 kPa), the pressure in room B (see fig. 4-2) (below Elevation 305 on the east side) was lagging behind that of most of the rest of the containment by approximately 0.425 s. The pressure rise rate during that period was approximately 1.3 lb/in^2-s (9 kPa/s); therefore, the pressure in room B was approximately 0.5 lb/in^2 (3.4 kPa) lower than that in most of the rest of the containment.

- The OTSG-A pressure transducer was providing accurately timed pressure data for most of the containment regions. The OTSG-B pressure transducer was providing pressure data that was approximately 3 s behind what was actually occurring in room B.

- The most plausible explanation for the delay in the OTSG-B pressure measurements is that the transmitter was underwater, and that its pressure reference point (located on the bottom of the transducer and covered by a small, fine-mesh screen) was more than 95% plugged in the upward or in-flow direction by debris that had been floating on the water as it rose to the transducer level.

Two other significant enclosed regions that could have had pressures that differed from most of the containment volume are the elevator hoistway and the adjacent enclosed stairwell. It is likely that pressure differences versus time for these enclosures were similar to those described for room B. No pressure transmitters or switches were monitoring pressures within these enclosures; however, observations of structural damage provide some insight concerning pressure differentials that existed. The large elevator doors at Elevations 305 and 347 were bowed outward from the elevation hoistway (Eidam and Horan 1981). Also, the hinged door at Elevation 326 that swings outward into the containment from the elevator hoistway had a damaged latch and was bowed outward above and below its latch. In an earlier picture (Eidam and Horan 1981, Figure 15), the section of this door below its latch appeared to bow inward, which is misleading. It appears that this elevator door may not have been forced open. The closure arm is undamaged, but is disconnected. The hinged door at Elevation 305, which swings outward into the containment from the enclosed stairwell, was forced open. It was then badly bent as it was thrust against a pipe support structure (Eidam and Horan 1981). Since no other enclosed stairway doors were damaged, it appears that the latch on the Elevation 305 door may not have been well-secured. Tests reported by Zalosh et al. (1985) indicate that the latch on a similar door failed at a pressure difference of 0.6 to 0.7 lb/in² (5 kPa).

The damage and lack of damage indicate that the pressure in the elevator hoistway may have been slightly more than 0.5 lb/in² (4 kPa) higher than that in the surrounding containment. The positive pressure differential in the enclosed stairway was probably less than 0.5 lb/in² (3 kPa) because of venting through the doorway at Elevation 305. It is not known whether the gas in the two enclosures burned at the same time or whether a significant pressure difference existed between the two enclosures at some time. There are no doorways between the two enclosures and no structural damage has been observed in the wall that separates the enclosures.

Pressure differentials varied between the containment atmosphere and smaller enclosures such as sealed 55-gal drums, ventilation ducting, and light bulbs. The pressure differential across sealed 55-gal drums was so great (∽2 atm), compared with the drum's ability to resist external pressures (∽1 atm), that the drums collapsed (Eidam and Horan 1981). Similarly, some of the large-diameter ventilation ducting would not be capable of withstanding high external pressures. However, the ducts are open at both ends, and flow calculations show that when exposed to the known containment pressure rise rates, the pressure differential across the duct wall would be much less than that which would cause the ducts to collapse. The smaller, well-sealed enclosures such as light bulbs, which did not collapse, were able to withstand the 2-atm pressure pulse.

4.7.2 Burn Origin and Pathways

Though the exact origin of the hydrogen burn is unknown, the following evaluation of available data and known hydrogen-burn characteristics identifies the region where the burn was probably initiated.

The hydrogen concentration in the mixed containment gas was less than 9%, which is the lower limit for downward burning. Therefore, if the ignition source had been high in the containment, burning would have been very slow and only as a result of turbulence and downdrafts. However, the burning of approximately 57,600 m^3 (2,033,000 ft^3) of gas apparently occurred in the relatively short time of 12 s. This means that the burning was predominately upward and lateral and must have been initiated somewhere in the lowest containment level (below the floor at Elevation 305).

As discussed in section 4.7.1, data from the accurately timed 3.58 lb/in² or 25 kPa (gage) pressure switches show that the pressure in room B (below Elevation 305 on the east side) was lagging that in the west side and above Elevation 305. Therefore, the burn must have been initiated on the west side. This reasoning indicates that the hydrogen burn originated in room A (below Elevation 305 on the west side).

This conclusion is further supported by the fact that the reactor coolant drain tank vents to room A; therefore, hydrogen concentrations would be highest and more easily ignitable in that region. Typical spark ignition sources equivalent to an automobile spark plug are relatively weak and will not reliably ignite hydrogen-air mixtures below 9% hydrogen (Carlson et al. 1973). Also, it is known from the actuation of a computer-monitored temperature switch, that the pressurized relief valve (RC-V2) was opened sometime between 1349 and 1349:30. It was closed again, probably within a few seconds to a minute, and may have been open when the hydrogen burn was initiated at approximately 1350:15.

Therefore, it is likely that there would have been a hydrogen-rich region in room A and up from the open stairwell and other openings in the Elevation 305 floor at the time the burn was initiated. This hydrogen-rich region may have acted as a rapidly burning torch predominately up to the air coolers at Elevation 330 (where it would have been rapidly cooled as shown in table C-3, and probably quenched), and also up the open stairwell through the floor at Elevation 347. This probably initiated containment atmosphere burning at all three levels within the first 6 s of the burn. Considering the pressure history and heat lost during the burn, less than 5% of the burning took place in the first 6 s, less than 40% in the next 3 s, and more than half of the burning occurred in the last 3 s. The rapid burning during the last 3 s resulted from the large, highly turbulent flame front that had developed and also because the remaining gas had been compressed to almost half of its original volume.

The predominant burn pathway would have been up the west side in the region of the open stairwell, across to the east beneath the upper dome and the Elevation 305 and 347 floor levels, then down the east side in a rolling motion at each of the two upper levels.

It is likely that the atmosphere in the D-rings ignited through openings below Elevation 305, then burned vertically upward. There are a number of temperature switches in the D-rings, which actuated during the hydrogen burn, showing that the atmosphere in the D-rings burned. However, these switches are scanned and reported only once each 30 s and therefore do not add significantly to the determination of the burn path.

Because of the location (low and east) and partial isolation of room B, it is presumed that the room B atmosphere was near the last to burn. Prior to its burning, gas from the regions above and adjacent would have been flowing into room B (see appendixes A and B). With a pressure differential of 0.5 lb/in^2 (3.4 kPa), peak velocities through the many openings probably exceeded 75 m/s (250 ft/s). When burning in room B finally occurred, its pressure would have increased to above that of the rest of the containment, and the gas flow would have reversed to the outward direction. The large steel cover plates over openings in the Elevation 305 floor would have raised at the time of the pressure pulse, thereby increasing the venting area. This was the probable cause of misalignment of the cover plates reported by Eidam and Horan (1981).

The other significant volumes of partially isolated gas that were likely near the last to burn were in the elevator hoistway and the adjacent enclosed stairwell. Since these volumes are not directly connected to the containment ventilation system, hydrogen concentrations were probably lower there than in any other significant containment region. Diffusion before the hydrogen burn may have increased hydrogen concentrations to above the lower flammability limit (Zalosh et al. 1985). Containment gas flow into these enclosures caused by the rise in containment pressure during the hydrogen burn would have further increased the hydrogen concentrations. Burning occurred in both of these shafts, as evidenced by the door damage described in section 4.7.1, probably from the bottom up and probably near the end of the containment hydrogen burn.

4.7.3 Effect of Geometry and Large Scale

Even though laminar burning velocities in lean hydrogen-air mixtures are relatively slow and stable, the buoyant and pressure-driven movement of a flame front can cause a transition to turbulent burning. In large, unrestricted, vertically upward burning environments, resistance to gas flow is very low and buoyant effects of the hot gases in and behind the flame front result in high-vertical velocities. In closed systems (or partially closed systems where burning starts at a closed end), the expansion caused by the heating of the gases in the flame front accelerates the flame front. In systems where the unburned gases are made turbulent by fans, water sprays, or by the forced movement past fixed obstacles, turbulent burning occurs and the velocity of the flame front can be accelerated by an order of magnitude (Hertzberg 1981). All of these conditions existed in the TMI-2 containment at the time of the hydrogen burn except the water sprays, which came on approximately 30 s after the flame front had passed through the containment.

From the pressure rise data, it is evident that over 90% of the 57,600 m^3 (2,033,000 ft^3) of gas burned in the last 6 s. A similar fraction of the burning of much smaller containers of similar gas mixtures ($\sim$8% hydrogen in air) have been observed to burn in approximately the same time period (Hertzberg 1981; Thompson et al. 1987). Therefore, it is evident that geometry and scale have a significant effect on burning rates. The TMI-2 hydrogen burn may be the first large-scale environment to clearly demonstrate the significant effects of scale.

In the large-scale tests conducted at the U.S. Department of Energy's Nevada Test Site (NTS) (Thompson et al. 1987), flame-front movement was monitored. In test P-13 (7.8% hydrogen), the flame front accelerated from an initial vertical velocity of 3.7 ft/s (1.1 m/s) to 18 ft/s (5.5 m/s) during the 4- to 5-s period. The flame front could not be accurately measured after that time.

Many small-scale tests are equipped with fans to premix the gases and to determine the effect of fan-induced turbulence. The fans may circulate the gases 100 to 1,000 times per hour and always cause turbulent burning that results in high-burn velocities. However, in large containment buildings, the effect of fans (5 to 10 air changes per hour) in the air coolers have a much smaller effect on inducing turbulent burning, except in the regions of the fan inlets, air outlets, and ducts. The containment sprays in the large-scale NTS tests induced much more turbulent burning than the fans. Therefore, even though all five blowers in the TMI-2 air coolers were operating at the time of the hydrogen burn and were recirculating the containment air on an average of once every 8.6 min, the containment sprays were off; a comparison with tests without fans or sprays operating is made in figure 4-14. In the smallest vessel, the ignition was in a central position, 6 ft (2 m) above the bottom. In the NTS vessel, the igniters were near the bottom. In the TMI-2 containment, the ignition location could have been as high as 20 ft above the basement floor and still be below the floor at Elevation 305 (see section 4.7.2). Note that the burning times and pressurization rates (slopes) shown in figure 4-14 are similar.

An analysis by Hertzberg (1981) has concluded that burning in the 12-ft-dia. vessel was laminar throughout the entire burn period. If the vessel had been much larger, turbulent burning would have occurred. The depressurization or cooling rate in the small vessel is shown to be greater than for the larger vessels. This difference results from the higher surface-to-volume ratio (more cooling area per fuel element). The surface-to-volume ratios of the TMI-2 containment and the much smaller NTS test vessel are similar because there are more compartments and equipment in the TMI-2 containment.

There are minor differences in peak pressures reached in the examples shown in figure 4-14. The peak pressure from the 8.5% hydrogen in air mixture in the smaller vessel was depressed approximately 4 lb/in^2 (27 kPa) as a result of the more rapid cooling that occurred during the burn. The 7.8% hydrogen in air mixture in NTS-P13 was depressed as a result of incomplete burning prior to the time of the peak pressure. (Note that an afterburn occurred several seconds later.) It appears that more than 96% of the hydrogen burned in each case, except for TMI-2. Henrie and Postma (1983a) estimated that an average of 1.1% hydrogen remained in the TMI-2 containment after the hydrogen burn, which would indicate an 85% burn efficiency and a 3 to 5 lb/in^2 (20 to 35 kPa) reduction in peak pressure. Taking these differences into consideration, the test results shown in figure 4-14 are in remarkably good agreement.

The similar pressure rise rates imply that similar fractions of the total volumes were burning on a similar time basis. Since volume is a cube function of a characteristic length, the average burning velocity would be somewhat proportional to the cube root of the volume. On this basis, the average burn velocity in the 12-ft sphere would be expected to be 23% of that in the NTS sphere, and the average burn velocity in the TMI-2 containment would be 302% of that in the NTS sphere. Since a flame-front velocity measured during the rapidly burning period of the NTS P-13 test was 18 ft/s (5.5 m/s), comparable peak velocities in the 12-ft sphere and the TMI-2 containment would be projected to be 4.1 ft/s (1.3 m/s) and 54 ft/s (16.5 m/s), respectively. It is evident from other tests that this particular effect of scale (peak velocity proportional to diameter) would

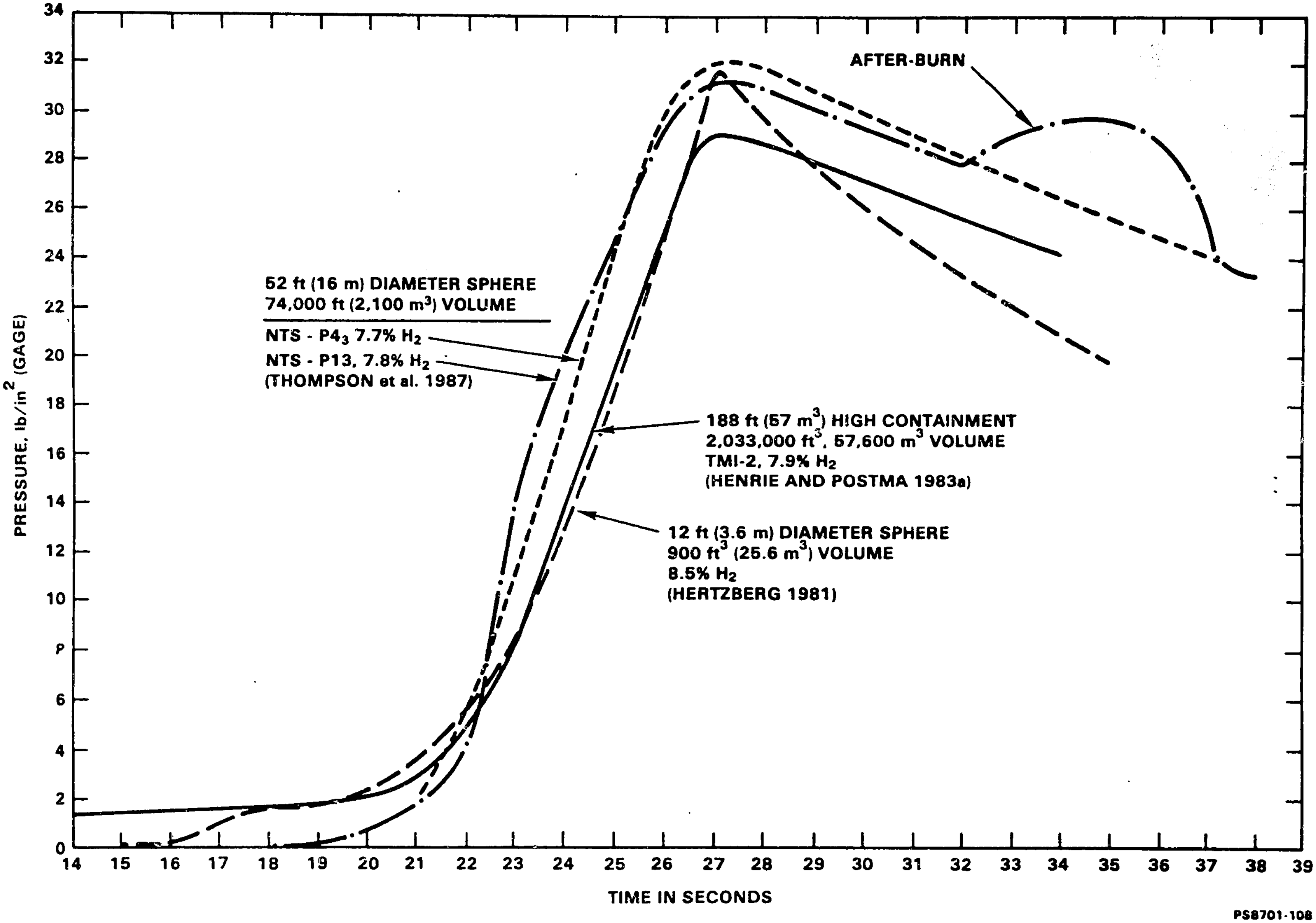

Figure 4-14. Comparison of Pressure Histories During the Burning of Hydrogen in Three Vessels Having Greatly Different Sizes.

not be maintained when hydrogen concentrations greatly exceed 8% or when high initial turbulence exists. Under those conditions high-velocity turbulent burning would occur throughout the burn, regardless of vessel size.

4.7.4 Compression and Radiant Heating

In containment, a burn is considered by definition to occur on a constant volume basis. However, if the burn occurs over a relatively long time (many seconds), the burning of any single unit volume (i.e., 1 L or 1 ft^3) occurs very rapidly and burns more on a constant-pressure basis. Constant-pressure burning is cooler than constant-volume burning because of the expansion cooling that occurs during the constant-pressure burn. In a closed system, the energy difference between constant-volume and constant-pressure burning of a small volume of the gas goes into a slight compression heating of the remaining (burned and unburned) volume. Henrie and Postma (1983a) calculated gas temperatures of the initial unit volume, the middle unit volume (burn starting at 2 atm absolute), and the last unit volume of TMI-2 containment gas to burn, assuming no heat loss during the burn. Using the same calculational techniques, but also accounting for heat loss during the burn, the temperatures of unit volumes of gas assumed to burn at 0, 3, 6, 9, and 12 1/2 s into the burn were approximated. The results are shown in figure 4-15. Note that the first unit volume to burn cools significantly during the first 6 s and remains cooler than the gas, which burns later. The gas that burns at 6 s is so affected by subsequent compression heating that it becomes approximately 55 °C hotter than the gas, which burned last.

This condition would be partially offset by the preheating of the unburned gases by radiation from the burned gases. Even though emissivity and absorptivity coefficients are low for hydrogen, oxygen, and nitrogen gases, these coefficients are significant for water vapor. The average water vapor fraction in the containment gas just prior to the hydrogen burn was calculated to be 3.5% (Henrie and Postma 1983a). The water vapor fraction in the burned gas would be approximately 7% higher than in the unburned gas since the hydrogen gas would have been converted to water vapor. Emissivity correlations by Smith and Shen (1980) indicate that the emissivities (or absorptivities) for 20 m (65 ft) of these burned and unburned gases at 2 atm absolute would be approximately 0.6 and 0.5, respectively. Therefore, the ability for radiant heat transfer from the hot burned gas to the relatively cool unburned gas is good. The extent of the radiant heating of the unburned gas was not further quantified.

The water vapor fraction on the west side near the open stairwell would have been considerably higher than 7% due to its proximity to the reactor coolant drain tank vent. Hydrogen and steam were either venting or had just been venting from the reactor cooling system through the drain tank (see sections 4.4 and 4.7.2). Therefore, emissivities for the wet burned gas in that region would have been relatively high. Also, if the hydrogen concentration in the region of the open stairwell was high at the time it burned, the resulting gas temperature would have been higher than average and the

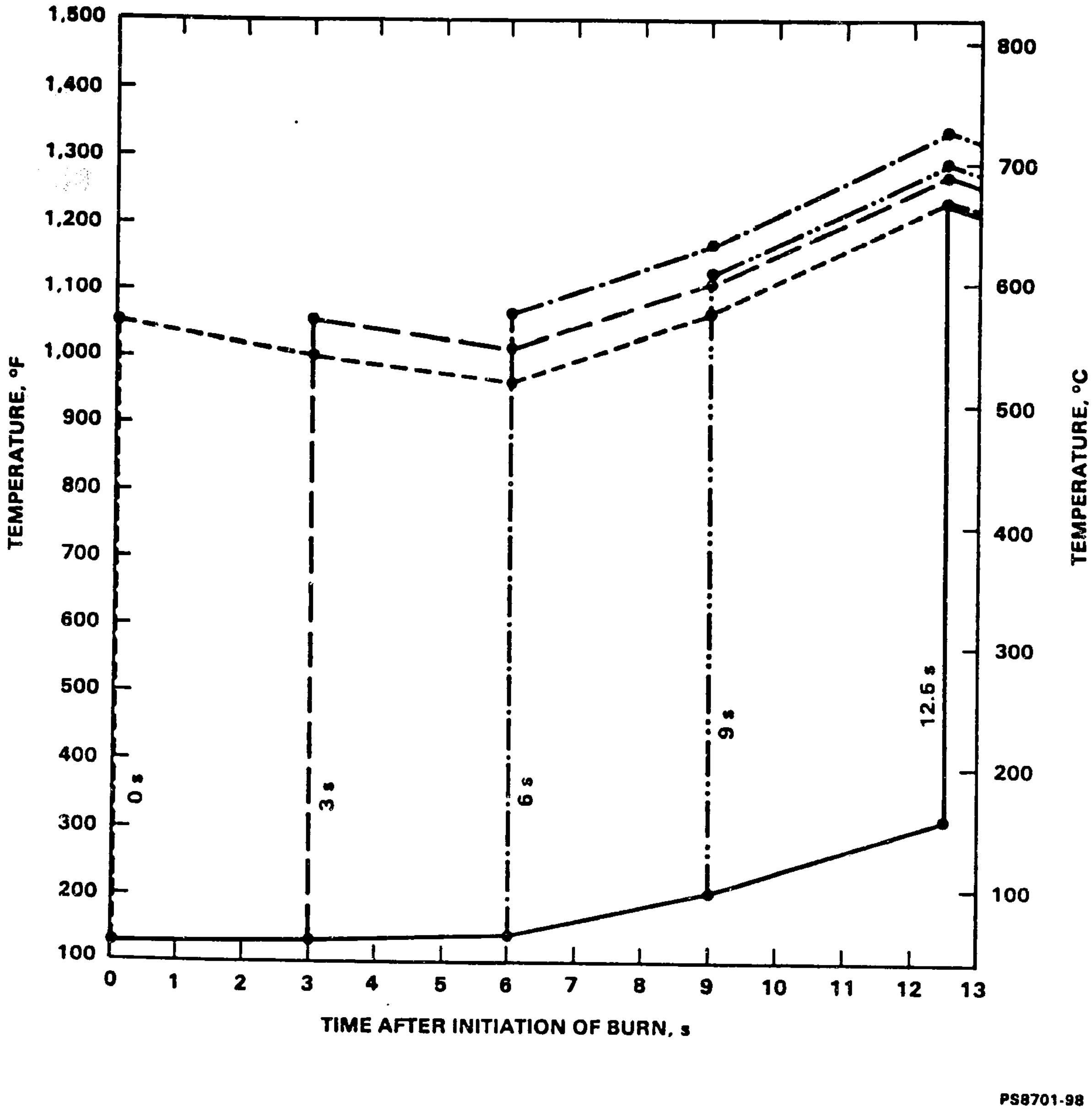

Figure 4-15. Thermal Effects of Burning, Compression Heating, and Cooling on Unit Volumes of TMI-2 Containment Gas, Which Burned at the Times Shown.

radiant heating effect would have been much higher, since it is a function of the fourth power of the absolute temperature. Further, since the gas in the region of the open stairwell was ignited early in the burn (during the first few seconds), the time for heat transfer to surrounding objects before the containment sprays started would have been relatively long. Some or all of these conditions were apparently in effect, since it has been determined (Trujillo et al. 1986) that the side of the polar crane pendant cable, which was the most severely discolored/scorched/burned, was facing directly toward the open stairwell (west) and to the region just south of that which is toward the path these gases would have taken to the inlet of the containment air coolers.

4.8 POSTBURN HYDROGEN

Previous evaluations (Henrie and Postma 1983a) indicate that 1.1% hydrogen remained in containment after the hydrogen burn. Most of this was probably in compartments below the Elevation 305 floor, but would have dispersed rapidly.

The pressurizer relief valve was again opened (shortly after 1400) for a little more than 1 hour. This increased the hydrogen concentration in containment by an estimated 0.6%. Between March 31 and April 2, 1979, enough hydrogen was released to containment from the reactor coolant system to increase the hydrogen concentration by approximately 0.5%, which brought the total to approximately 2.2%. The hydrogen recombiner developed by Rockwell International started removing hydrogen from containment on April 2, 1979, at 1530. Recombiner operation was terminated on May 1, 1979, after it had removed 112 kg of hydrogen gas (and 56 kg of oxygen gas) from containment, and the hydrogen concentration was down to 0.7%. Some of the residual 28 kg of hydrogen leaked or diffused from the containment during the following year and the remainder was vented to the atmosphere in June 1980.

The quantities of hydrogen added to and removed from containment are summarized in table 4-3. Approximately 460 kg (230 kg-mol) of hydrogen gas entered and was removed from containment. Essentially all of this hydrogen was probably produced by the zirconium-water reaction. Since 1 mol of zirconium reacting with 2 mol of water liberates 2 mol of hydrogen, 230 kg-mol of hydrogen represents the oxidation of 115 kg-mol, or 10,500 kg (23,000 lb), of zirconium. The TMI-2 reactor core contains a calculated 23,600 kg (52,000 lb) of zirconium. Therefore, the zirconium oxidized by the metal-water reaction is equal to approximately 45% of the total zirconium in the reactor core. It should be noted that hot zirconium cladding can mix with adjacent uranium dioxide fuel. This process would, of course, not produce hydrogen. Therefore, more zirconium cladding may have been destroyed than would be indicated by the amount of hydrogen that was accounted for.

Table 4-3. Containment Hydrogen Balance.

Time	Hydrogen added		Hydrogen removed		Hydrogen inventory	
	dry (%)	kg	dry (%)	kg	dry (%)	kg
March 28, 1979						
1350	8.2	370			8.2	370
1352			7.1	319[b]	1.1	51
1500	0.6	24[a]			1.7	75
April 1, 1979	0.5	21[a]			2.2	96
May 1, 1979	1.1	44[a,c]	2.6	112[d]	0.7	28
June 1980			0.7	28[e]		0
Total		459		459		

[a]From reactor cooling system.
[b]Hydrogen burn.
[c]From waste gas decay tanks.
[d]Rockwell International hydrogen recombiner.
[e]Vented to atmosphere (some may have diffused/leaked earlier).

5.0 PREDICTED HEATUP OF EQUIPMENT EXPOSED TO A HYDROGEN BURN IN A CONTAINMENT BUILDING

In this section, results of heat transfer calculations are presented that illustrate the degree to which objects in a containment building would be heated by a hydrogen burn. These results include the temperature transient that would be expected for certain types of equipment exposed to a hydrogen burn transient, how various physical parameters affect the peak temperatures reached as a result of a hydrogen burn, and how equipment could be designed so that the temperature transient it endures would be limited to values below its design limit.

5.1 BASIS FOR PREDICTED TEMPERATURE TRANSIENTS

The time-temperature history of the containment atmosphere was predicted on the basis of a single premixed hydrogen-air mixture burn that mirrored the one that occurred at TMI-2. Postburn temperatures and pressures were chosen for an adiabatic-isochoric hydrogen burn. The cooldown rate was then predicted by means of a two-compartment heat transfer model that accounted for:

- Heat transfer to walls by convection and radiation
- Heat transfer to containment coolers
- Heat transfer to water sprays
- Intercompartment flows (work and mixing).

The containment gas temperatures predicted by this model are shown in figure 4-5 and are discussed in section 4.6.4 and appendix C. As expected, the temperature in the upper, main room of the containment building cooled more slowly than in the smaller subcompartments (with their higher surface-to-volume ratios). To ensure the use of an adequately conservative temperature profile, the one predicted for the large room above Elevation 347 was used in these analyses. Since the temperatures are higher for a longer time in a large room than they would be in smaller, more congested compartments, the predicted peak temperatures of equipment would be higher and, therefore, more conservative.

The containment gas temperatures predicted by the model are shown in figure 5-1. The information is the same as that shown in the upper curve of figure 4-5, but it is extended for a longer time period and includes a projection for no-spray operation. As indicated by the curves of figure 5-1, the initiation of sprays at 32 s causes a rapid drop in temperature as compared to the no-spray case.

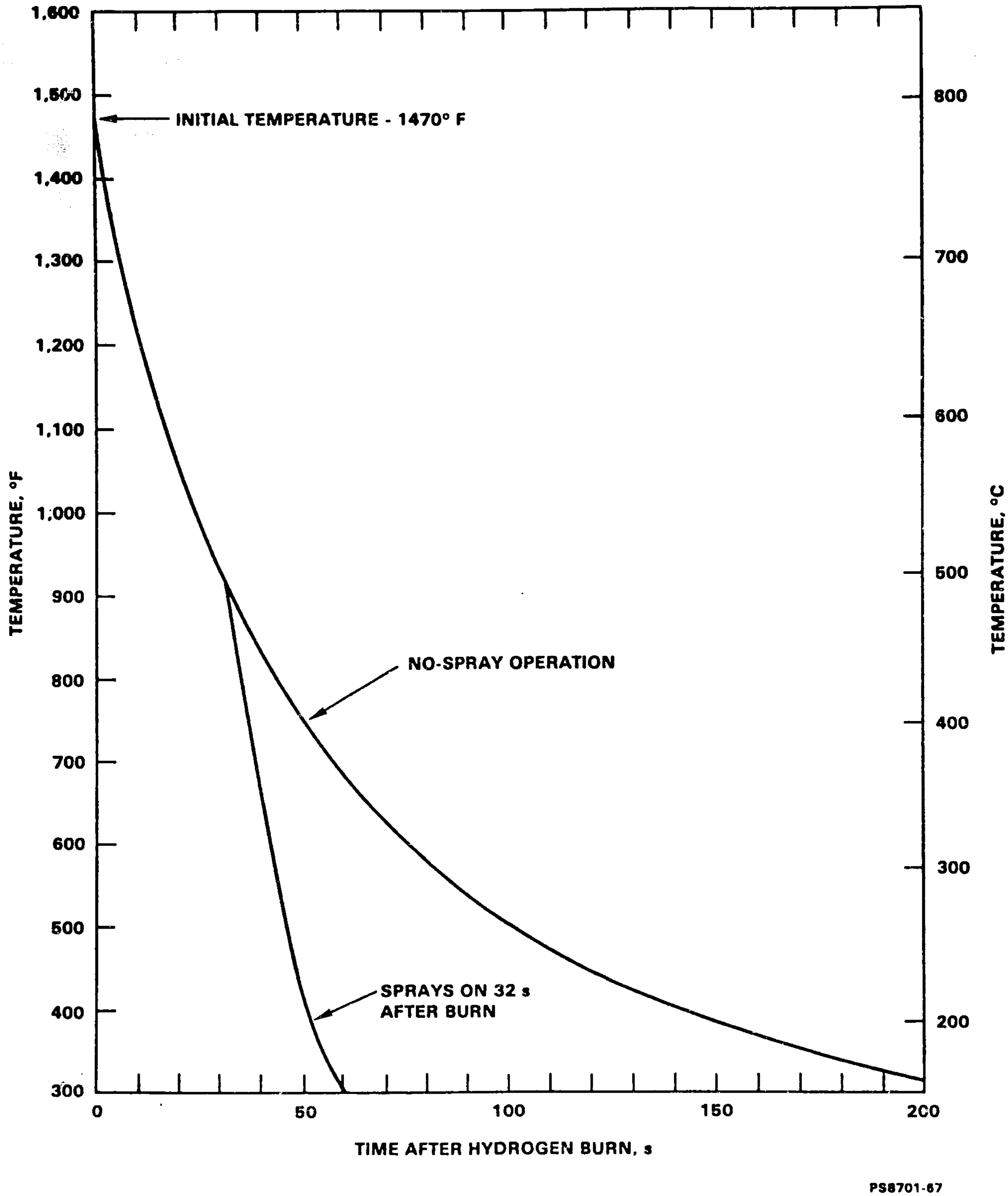

Figure 5-1. Predicted Average Gas Temperature in Upper Containment (Above Elevation 347) Versus Time Following a Postulated Instantaneous Hydrogen Burn.

Perhaps the most important aspect of the cooldown curves shown in figure 5-1 is the limited duration of high temperatures. This limited time at temperature, in turn, limits the degree to which equipment can be heated by the assumed hydrogen burn.

A parametric heating analysis of components exposed to the hot gas transient shown in figure 5-1 is presented in appendix D.

5.2 DESIGN GUIDELINES FOR PROTECTING EQUIPMENT

In this section, some of the most important considerations (see appendix D) that affect the design of equipment for survivability are summarized. Implicit in the following discussions is the assumption that equipment would be designed on the basis of heat transfer analysis. In instances where performance adequacy is marginal, operability would be ensured by redesign or verified by testing.

5.2.1 Definition of Time-Temperature History For Ambient Atmosphere

A first step in a heatup analysis is the determination of the temperature-time history of the containment atmosphere. The heat pressure of the ambient atmosphere determines the driving force that causes the heatup of the receptor being analyzed. The temperature-time history is calculable from a specification of burn parameters. Burn parameters include preburn hydrogen concentration, initial temperatures, containment geometry, and the operability of containment heat-removal devices (coolers and sprays). While the time-temperature history would, in theory, be different for each set of burn parameters, the TMI-2 burn in the containment dome (see fig. 5-1) is viewed as a baseline or standard burn that can be used (at least as a point of departure) for analyzing equipment heatup. The possible use of the TMI-2 temperature-time history as a base case is supported by the following factors:

- The preburn hydrogen concentration, ~8%, is higher than would be expected in containments with deliberate ignition systems, and probably close to an upper limit determined by adventitious ignition sources. (If multiple sequential hydrogen burns are postulated without adequate cooling between burns, further analysis would be necessary.)

- The assumption of an adiabatic, isochoric hydrogen burn does not allow for cooling that would occur during the burn, and therefore, a higher-than-actual initial peak temperature results.

- The surface-to-volume ratio for upper containment in TMI-2 is typical for the large dry containments, and less than those for smaller containments or other smaller compartments in containments. Thus, the cooldown rate of the hot gases following the hydrogen burn in the TMI-2 upper containment was at or near a minimum value, and the heat pressure was at or near a maximum.

- The assumed location of equipment in the upper containment, where convective and radiative heat transfer can occur at all exposed surfaces, is an extreme case. In most instances, equipment is mounted near floors at lower elevations. The proximity of equipment to surfaces (mounting platforms, floors, and walls) and at lower elevations in subcompartments will lower the heatup by limiting radiation view factors and establishing boundary layers that minimize circulation of the gases.

5.2.2 Specification of Maximum Temperature Allowable for Receptor

As a second step in designing for hydrogen burn protection, it is suggested that a peak-allowable temperature be specified for the receptor. This specification, based on the temperature capability of the receptor, allows the design of an enclosure that will prevent the receptor from exceeding the specification.

5.2.3 Determination of Thermal Properties and Geometrical Configuration of Receptor and Protective Enclosure

The thermal properties of the receptor that need to be known for a heatup analysis include density, heat capacity, and thermal conductivity. Geometrical configurations of receptor and enclosure (if any) need to be defined well enough to permit volumes, areas, and thicknesses in the direction of heat movement to be specified.

5.2.4 Base Case Heatup Analysis

After the heat pressure of the ambient atmosphere is specified and the geometry and thermal properties of the receptor and enclosure are known, a first- or base-case analysis can be made using nominal properties for enclosure walls. A comparison of peak receptor temperature with the design maximum will indicate whether an enclosure is needed, an increase in enclosure wall thickness is needed, or whether surface insulation should be added.

5.2.5 Iterative Analyses For Enclosure Design

If the base-case heatup analysis shows the receptor to be underprotected (or overprotected), the nominal design parameters can be changed accordingly and the heatup analysis repeated. This procedure can be repeated until a sufficiently economic and protective enclosure design is developed.

5.2.6 Receptors With Natural Protective Enclosures

Many types of electrical equipment have metal cases or housings that serve as enclosures and which may make the use of additional protective enclosures unnecessary. Examples include solenoid valves, limit switches, and enclosed electric motors (see section 6.0). Examples of equipment that survived numerous hydrogen burn transients without separate protective enclosures are described in Achenbach et al. (1985).

5.2.7 Design Example

In order to illustrate the design approach described in this section, it is postulated, and demonstrated more completely in appendix D, that a single teflon-covered wire can be protected from a premixed hydrogen combustion event. It is assumed that the wire covering is teflon, the outside diameter is 0.16 in., and that the copper core is 0.064 in. (#14).

Step 1. The heat pressure for this case is assumed to be that experienced in the upper containment volume during the TMI-2 hydrogen burn event, with the water spray on at 32 s, as shown in figure 5-1.*

Step 2. The maximum recommended service temperature for this material, as specified by Materials Selector (1971), is 550 °F (280 °C). Therefore, the design task is to prevent the temperature of the wire covering from exceeding 550 °F (280 °C).

Step 3. From Materials Selector (1971), the thermal properties of teflon are: conductivity = 0.14 Btu/h-°F/ft, density = 137 lb/ft^3, and heat capacity = 0.25 Btu/lb-°F.

Step 4. As a base case it was assumed that the wire was exposed directly to the containment atmosphere. The predicted wire-surface temperature for this case is shown in figure 5-2, where a peak of 580 °F (304 °C) is seen to occur at 35 s after the burn. Since the predicted peak temperature exceeds the design limit, some degree of protection is required.

Step 5. As a first design step, a steel tube with a wall thickness of 0.10 in. was provided as a conduit to protect the wire. The temperature history for both the wire surface and the conduit are illustrated in figure D-9 in appendix D. It is assumed that the hydrogen in the conduit burns. The wire surface temperature is seen to peak at 204 °F (96 °C) and the conduit temperature peaks at 259 °F (126 °C). Since a sector of the

*While spray operation is a realistic assumption for most hydrogen-burn accident scenarios, it is recognized that it would be more conservative to assume no-spray operation. The temperature history for the no-spray case is also shown in figure 5-1; figures D-7 and D-12 in appendix D show the increased thermal effects under the conditions of no-water spray.

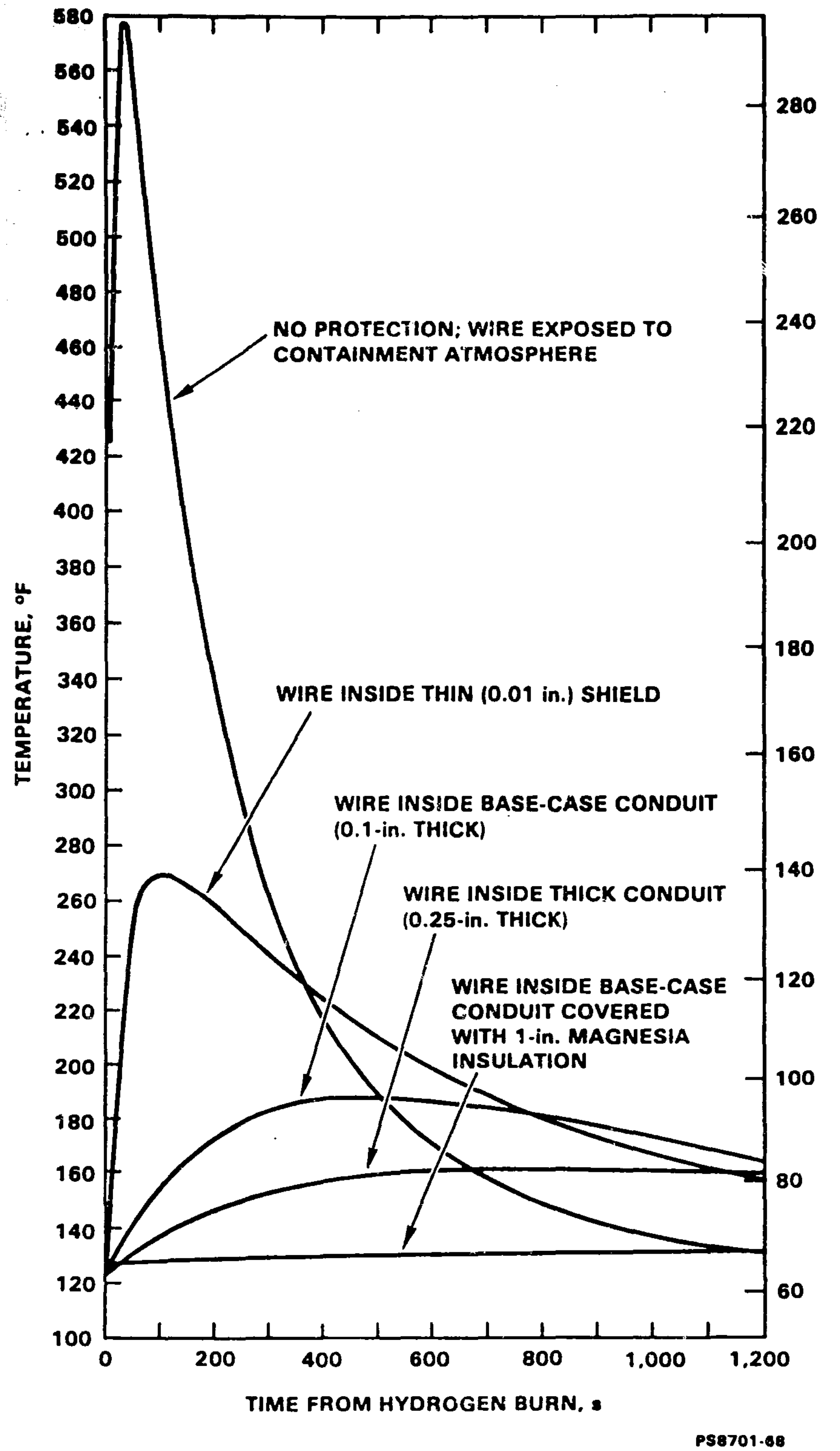

Figure 5-2. Comparison of Wire-Surface Temperatures for Different Protective Conduits.

wire would contact the conduit, the predicted peak conduit temperature (259 °F or 126 °C) should be compared with the maximum design temperature (550 °F or 288 °C). Since the predicted temperature is far below the design limit, it is concluded that for a teflon-insulated wire, a typical conduit provides adequate protection from the hydrogen burn. Note the wire covering would have been acceptable even if the maximum design temperature had been as low as 259 °F (126 °C), which is the conduit temperature.

6.0 EQUIPMENT THAT SURVIVED THE TMI-2 HYDROGEN BURN

As described earlier in this report, the only items that showed thermal damage as a result of the hydrogen burn were those which were thin, had low thermal-diffusivity characteristics, and had the ability to discolor, char, or burn. Therefore, cloth, plastic, paper, and wood products typically showed burn damage (Eidam and Horan 1981; Alvarez 1984). Electrical wiring, instruments, and other equipment contained in conduit, cabinets, or similar enclosures typically did not receive thermal damage. However, the long-term effects of moisture caused considerable degradation of electrical cables, connectors, and equipment (Helbert et al. 1984; Meininger et al. 1985).

Examples of large electromechanical equipment that survived the TMI-2 LOCA and hydrogen burn were the five axial-flow fans that are part of the containment air-handling system. The fans were manufactured by the Joy Industrial Equipment Company (Model No. 48-26-1170/870, Part No. 500722-66). The electric motors for the fans were 150/75 hp, 1,200/900 rpm, totally enclosed air-over (TEAO) types, which were provided by the Reliance Electric Company.

Each of the five fans was operating at approximately 22.2 m^3/s (47,000 actual ft^3/min) before, during, and long after the hydrogen burn. The fans and motors were not only directly exposed to the containment atmosphere, but were forcing this atmosphere past them at high velocities (250 ft/s or 75 m/s at fan blade tips and 90 ft/s or 27 m/s past motor fins). Therefore, the rate of convective heat transfer to the fan blades and motor fans during and after the hydrogen burn would have been very high. However, the fan blades are made of cast stainless steel and, therefore, have good strength at high temperature, and the motor casing is so massive that the temperature rise from the burn transient would not have been high.

The TEAO feature of the motor prevents direct contact of the motor windings with the atmosphere surrounding the motor. Therefore, the windings would remain relatively cool. The motor insulation is type H-RN, which is high-temperature and radiation resistant. The insulation is also protected by the motor housing. Each electrical conductor (motor power leads) leading from the junction box on the blower housing to the motor housing is in an individual conduit, physically spaced from other conduits. The individual conduits are collectively surrounded by a single waterproof conduit. This provides excellent thermal isolation of the electrical insulation from the containment atmosphere. These special design features were intended to meet the Institute of Electrical and Electronic Engineers standards that were in effect at the time the equipment was sold to ensure that the equipment would operate through a LOCA. Successful qualification testing was performed. The end result is the blowers not only survived the LOCA, but a severe hydrogen burn environment as well.

7.0 REFERENCES

Achenbach, J. A., R. B. Miller, and V. Srinivas, 1985, Large-Scale Hydrogen Burn Equipment Experiments, EPRI NP-4354, Electric Power Research Institute, Palo Alto, California.

Allison, C. M., S. T. Polkinghorne, and M. S. Sohal, 1985, SCDAP/MOD1 Analysis of the Progression of Core Damage During the TMI-2 Accident, EGG-SAR-7104, EG&G Idaho, Inc., Idaho Falls, Idaho.

Alvarez, N. J., 1984, Assessment of Extent and Degree of Thermal Damage to Polymeric Materials in the Three Mile Island Unit 2 Reactor Building, GEND-IWF-023, Vol. VI, Lawrence Livermore National Laboratory, Livermore, California.

Alvarez, N. J., 1985, Assessment of Thermal Damage to Polymeric Materials by Hydrogen Deflagration in the Three Mile Island Unit 2 Reactor Building, American Chemical Society Symposium Series 293, 189th American Chemical Society Meeting, Miami Beach, Florida.

Alvarez, N. J., D. G. Beason, and G. R. Eidam, 1982, Investigation of Burn Damage in the Three Mile Island Unit 2 Reactor Building, GEND-INF-023, Volume 1, Lawrence Livermore National Laboratory, Livermore, California.

Ashurst, W. T. and P. K. Barr, 1982, "Discrete Vortex Simulation of Flame Acceleration Due to Obstacle-Generated Flow," in Proceedings of the Second International Workshop on the Impact of Hydrogen on Water Reactor Safety, Albuquerque, New Mexico.

Baker, L., Jr., 1983, An Assessment of Existing Data on Zirconium Oxidation Under Hypothetical Accident Conditions in Light-Water Reactors, ANL/LWR/SAF 83-3, Argonne National Laboratory, Argonne, Illinois.

Benedick, W. B., J. C. Cummings, and P. G. Prassinos, 1984, Combustion of Hydrogen: Air Mixtures in the VGES Cylindrical Tank, NUREG/CR-3273, SAND 83-1022, Sandia National Laboratories, Albuquerque, New Mexico.

Berlad, A. L., R. Jaung, and W. T. Pratt, 1982, "Electric Cable Insulation Pyrolysis and Ignition Resulting from Potential Hydrogen Burn Scenarios for Nuclear Containment Buildings," in Proceedings of the Second International Workshop on the Impact of Hydrogen on Water Reactor Safety, Albuquerque, New Mexico.

Berman, M. and J. T. Hitchcock, 1985, "Hydrogen Deflagrations and Diffusion Flames," in Proceedings of the Twelfth Water Reactor Safety Research Information Meeting, NUREG/CP-0058, Vol. 3, Gaithersburg, Maryland.

Berman, M., 1986, "Recent Developments in Hydrogen Technology," Hydrogen Behavior and Nuclear Reactor Safety, Vol. II, Chapter 2, CRC Press, Inc.

Berman, M. and J. H. S. Lee, 1984, "Containment Loads Due to Hydrogen Combustion," in Proceedings of International Conference on Containment Design, Canadian Nuclear Society, Toronto, Ontario, Canada.

Bloom, G. R., L. D. Muhlestein, A. K. Postma, and S. W. Claybrook, 1983, Hydrogen Mixing and Distribution in Containment Atmospheres, EPRI NP-2669, Electric Power Research Institute, Palo Alto, California.

Carlson, L. W., R. M. Knight, and J. O. Henrie, 1973, Flame and Detonation Initiation and Propagation in Various Hydrogen-Air Mixtures with and Without Water Spray, AI-73-29, Rockwell International, Canoga Park, California.

Carlson, E. R. and B. A. Cook, 1985, "Chemical Interaction Between Core and Structural Materials," in Proceedings of the First International Information Meeting on the TMI-2 Accident, CONF-8510166, EG&G Idaho, Inc., Idaho Falls, Idaho.

Cole, R. K., 1979, Generation of Hydrogen During the First Three Hours of the Three Mile Island Accident, NUREG/CR-0913, Sandia National Laboratories, Albuquerque, New Mexico.

Cook, B. A. and E. R. Carlson, 1985, "TMI-2 Core Debris Analysis," in Proceedings of the First International Information Meeting on the TMI-2 Accident, CONF-8510166, EG&G Idaho, Inc., Idaho Falls, Idaho.

Dandini, V. J., 1985, Testing of Nuclear Qualified Cables and Pressure Transmitters in Simulated Hydrogen Deflagrations to Determine Survival Margins and Sensitivities, NUREG/CR-4324, Sand 85-1491, Sandia National Laboratories, Albuquerque, New Mexico.

Eidam, G. R. and J. T. Horan, 1981, Color Photographs of the Three Mile Island Unit 2 Reactor Containment Building: Volume I - Entries 1, 2, 4, 5, 6, GEND-006, EG&G Idaho, Inc., Idaho Falls, Idaho.

Helbert, H. J., N. S. Cannon, D. R. Chick, and M. R. Donaldson, 1984, TMI-2 Cable/Connections Program, FY-84 Status Report, GEND-INF-056, EG&G Idaho, Inc., Idaho Falls, Idaho.

Henrie, J. O. and A. K. Postma, 1983a, Analysis of the Three Mile Island Unit 2 Hydrogen Burn, RHO-RE-SA-8 Rev 2 (also GEND-INF-023, Vol. IV), Rockwell Hanford Operations, Richland, Washington.

Henrie, J. O. and A. K. Postma, 1983b, Analysis of Three Mile Island Unit 2 Reactor Cooling System Transients, GEND-INF-023, Vol. V, EG&G Idaho, Inc., Idaho Falls, Idaho.

Hertzberg, M., 1981, "Flammability Limits and Pressure Developments in H_2-Air Mixtures," in Proceedings of the Workshop on the Impact of Hydrogen On Water Reactor Safety, Vol. III, NUREG/CR-2017.

Hertzberg, M. and K. L. Cashdollar, 1983, "Flammability Behavior and Pressure Development of Hydrogen Mixtures in Containment Volumes," Thermal-Hydraulics of Nuclear Reactors, Vol. 1, American Nuclear Society, La Grange Park, Illinois.

Kempka, S. N., A. C. Ratzel, A. W. Reed, and J. E. Shepherd, 1984, "Post-Combustion Convection in an Intermediate-Scale Vessel," in Designing For Hydrogen in Nuclear Power Plants, presented at the Joint ASME/ANS Nuclear Engineering Conference, Portland, Oregon.

Kenton, M. A., R. E. Henry, A. Sharon, M. Epstein, G. R. Thomas, L. J. Rudy, M. Meerbaum, and J. Azzarello, 1986, Simulation of the TMI-2 Accident Using the MAAP Modular Accident Analysis Program, Version 2.0, EPRI-NP-4292, Electric Power Research Institute, Palo Alto, California.

Lee, J. L., 1981, A Study of Damageability of Electrical Cables in Simulated Fire Environments, Final Report EPRI NP-1767, Research Project 1167-1-1, Electric Power Research Institute, Palo Alto, California.

Lewis, B. and G. Von Elbe, 1961, Combustion, Flames, and Explosions of Gases, Academic Press, Inc., New York, New York.

Materials Selector, 1971, Materials Engineering, 74 (4), p. 358.

Meininger, R. D., D. R. Chick, C. P. Cannon, M. E. Yancey, M. R. Dinsel, and F. T. Soberano, 1985, TMI-2 Cable Connections Program Status Report, GEND-INF-068, EG&G Idaho, Inc., Idaho Falls, Idaho.

Murphy, M. B., G. M. Mueller, and W. C. Jennigan, 1985, Analysis of the TMI-2 Dome Radiation Monitor, GEND-INF-063, Sandia National Laboratories, Albuquerque, New Mexico.

Nelson, L. S. and M. Berman, 1983, Mitigation of Damaging Effects of Hydrogen Combustion in Nuclear Power Plants, SAND 83-1862C, Sandia National Laboratories, Albuquerque, New Mexico.

Nelson, L. S. and M. Berman, 1984, "Reduction of the Damaging Effects of Hydrogen Combustion in Nuclear Power Plants," in Designing for Hydrogen in Nuclear Power Plants, presented at the Joint ASME/ANS Nuclear Engineering Conference, Portland, Oregon.

NRC, 1985, Hydrogen Control Requirements, 10 CFR Part 50.44, U.S. Nuclear Regulatory Commission, Washington, D.C.

NRC, 1986, Standards for Combustible Gas Control Systems in Light-Water-Cooled Power Reactors, Title 10, Code of Federal Regulations, Part 50.44, U.S. Nuclear Regulatory Commission, Washington, D.C.

NSAC, 1980, Analysis of Three Mile Island - Unit 2 Accident, Appendix HYD, NSAC 80-1, NSAC-1, Nuclear Safety Analysis Center, Electric Power Research Institute, Palo Alto, California.

Postma, A. K. and R. K. Hilliard, 1983, Hydrogen Generation, Distribution and Combustion Under Severe LWR Accident Conditions--A State of Technology Report, HEDL-TME 82-7, Westinghouse Hanford Company, Richland, Washington.

Ratzel, A. C., 1985, Data Analyses for Nevada Test Site (NTS) Premixed Combustion Tests, SAND 85-0135, Sandia National Laboratories, Albuquerque, New Mexico.

Ratzel, A. C. and J. E. Shepherd, 1985, Heat Transfer Resulting From Premixed Combustion, Publication HTD-45, American Society of Mechanical Engineers, New York, New York.

Richards, E. H. and V. J. Dandini, 1986, Analysis and Testing of the HP-R-214 Dome Monitor Cable from Three Mile Island Unit 2, GEND-INF-072, Sandia National Laboratories, Albuquerque, New Mexico.

Rogovin, M., ed., 1980, Three Mile Island - A Report to the Commissioners and the Public, Volume I and Volume II, U.S. Nuclear Regulatory Commission, Washington, D.C.

Schutz, H. W. and P. K. Nagata, 1982, Estimated Temperatures of Organic Materials in the TMI-2 Reactor Building During Hydrogen Burn, GEND-INF-023, Vol. II, EG&G Idaho, Inc., Idaho Falls, Idaho.

Sherman, M. P., 1985, "Hydrogen Flame Acceleration and Detonation," in Proceedings of the Twelfth Water Reactor Safety Research Information Meeting, NUREG/CP-0058, Vol. 3, Gaithersburg, Maryland.

Shapiro, Z. M. and T. R. Moffette, 1957, Hydrogen Flammability Data and Application to PWR Loss-of-Coolant Accident, WAPD-SC-545, Bettis Plant, Pittsburgh, Pennsylvania.

Smith, T. F. and Z. F. Shen, 1980, Evaluation of Coefficients For the Weighted Sum of Gray Gases Model, E-TFS-80-007, University of Iowa, Iowa City, Iowa.

Soberano, K. T., 1984 Final Report on the In Situ Testing of Electrical Components and Devices at TMI-2, GEND-040, EG&G Inc., Idaho Falls, Idaho.

Thomas, G. R., 1985, The TMI Accident: Fission Product Release and Cleanup, Electric Power Research Institute, Palo Alto, California.

Thompson, R. T., R. C. Torok, D. S. Randall, J. S. Sullivan, L. B. Thompson, and J. J. Haugh, 1987, Large-Scale Hydrogen Combustion Experiments, EPRI Report NP-3878, Electric Power Research Institute, Palo Alto, California.

Torok, R., K. Siefert, W. Wachtler, R. R. Gay, P. M. Gloski, and J. W. Wanless, 1983, Hydrogen Combustion and Control Studies in Intermediate Scale, EPRI Report NP-2953, Electric Power Research Institute, Palo Alto, California.

Trujillo, R. E., E. H. Richards, and C. P. Cannon, 1986, Analysis of the Polar Crane Pendant Cable from Three Mile Island - Unit 2, GEND-INF-069, Sandia National Laboratories, Albuquerque, New Mexico, and Westinghouse Hanford Co., Richland, Washington.

Zalosh, R. G., R. A. Beier, R. K. Dean, M. W. Earley, and E. A. Veal, 1985, Analysis of the Hydrogen Burn in the TMI-2 Containment, EPRI NP-3975, Factory Mutual Research Corporation, Norwood, Massachusetts.

APPENDIX A

MEASURED TIME/PRESSURE LAG IN ONCE-THROUGH STEAM GENERATOR-B

The most accurate containment pressure data available are provided from 16 computer-monitored pressure switches. The alarm printer indicates the second these pressure switches actuate (trip or reset). When the operator requests a sequence of events involving these switches, the actuation times to the millisecond are recorded on the utility printer. These pressure switch data have been correlated with the once-through steam generator (OTSG) pressure data and plotted as shown on figure A-1. The 28 lb/in² (190 kPa) pressure switch data points were plotted as horizontal lines covering the time (second) of the reported actuations. The reactimeter data for OTSG-A were adjusted to match the accurate pressure switch data points by inverting and adding a 65.3-s time correction, a 3.3 lb/in² (23 kPa) zero correction, and a 7.7% span correction. The OTSG-A data were similarly adjusted, except the zero correction was 266.9 lb/in² (1,830 kPa). (Note that the OTSG-B data could have been made to fit the accurate pressure switch data. However, the fit would have been less certain since the OTSG-B data have only one point near the peak and the OTSG-A data would then have been 3-s early, which is an impossible situation.)

The alarm printer indicates that nine out of the ten 3.58 lb/in² (25 kPa) pressure switches were actuated during the second prior to 1350:21; the tenth switch actuated during the second prior to 1350:22. Additional information from a sequence-of-events report on the utility printer shows that four of these switches tripped between 1350:21:000 and 1350:21:440. The switch that the alarm printer recorded tripping during the 1-s period prior to 1350:22 actually tripped at 1350:21:440. The data show that the 1-s period reported on the alarm printer ends 0.29 to 0.44 s after the reported time.

All 16 of the pressure switches are located in the auxiliary building and sense the pressure on the B (east) side of the containment building through 28 to 65 ft-long tubes. All of the pressure sensing points are located at Elevations 319 or 324 except for one at Elevation 293, which is the 3.58 lb/in² (25 kPa) (gage) switch and was the last to trip. The sensing point of this single switch is, therefore, separated from that of the other switches by the floor at Elevation 305. Further, the sensing point at Elevation 293 is located close to and in direct communication with the OTSG-B pressure transducer. Therefore, the accurately timed pressure data can be used to determine the pressure-time delay across the Elevation 305 floor and the OTSG-B pressure response delay at the pressure range near 3.6 lb/in² (25 kPa) (gage).

The accurately timed pressure switch data from the auxiliary printer were compensated for the time delay caused by the various sensing tube lengths. The compensated average trip time for the three switches sensing the pressure above Elevation 305, based on 30-ft-long sensing tubes, was 1350:21:015. This is 0.425 s before the same pressure was reached below

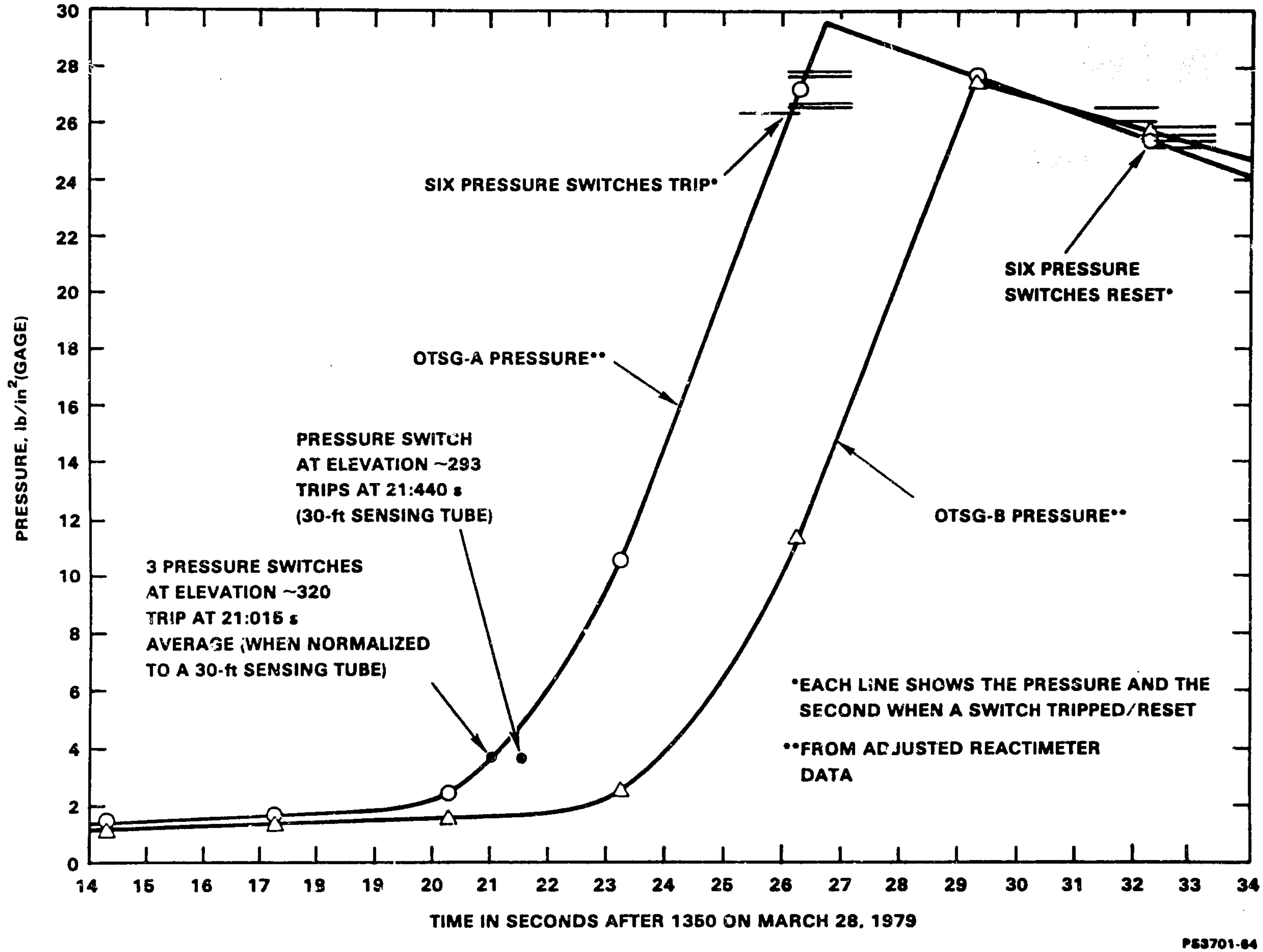

Figure A-1. Containment Pressures During the Hydrogen Burn.

Elevation 305 on the B (east) side. The pressure rise rate at that time was approximately 1.3 $lb/in^2/s$ (8 kPa/s) as determined by the slope of the pressure curve (fig. A-1) at 3.6 lb/in^2 (25 kPa) (gage). Therefore, at that time the pressure drop across the Elevation 305 floor on the B side appears to have been approximately 0.5 lb/in^2 (3.4 kPa).

The timing delay in the pressure data provided by the OTSG-B pressure transducer is approximately 3 s (see fig. A-1). There are two OTSG-B pressure transducers mounted on open racks at different elevations and it is not known which transducer was reporting to the reactimeter. The higher transducer, SP-6B-PT2, is located on rack 428 at Elevation 288. The lower transducer, SP-6B-PT1, is located on rack R-13 at Elevation 284 and would have been under water at that time. Because of the signal delay experienced by the OTSG-B pressure transducer, it is believed that the lower, submerged transmitter was involved. Calculations (Henrie and Postma 1983) backed by water-flow measurements through the screen at the bottom of the pressure transducer show that the delay would have been less than 0.2 s, with a pressure lag of less than 0.5 lb/in^2 (3.4 kPa) as a result of having its reference opening under water. Therefore, simply submerging the instrument in water would not have caused the measured 3-s delay. Since the instrument continued to function normally at the end of the burn, it is highly improbable that its sensitive mechanism compartment could have been filled with water and somehow caused the delay. Even more improbable would be an electronic timing error associated with the transducer or that its reactimeter channel would correct itself after indicating four consecutive 3-s delays. Therefore, the most likely explanation for the delay is a highly restrictive (more than 95%) inflow blockage at the screen (approximately 3/8 in. in dia.) at the bottom of the transducer, which would delay its response to the changing reference pressure. This could have been caused by floating debris coming in contact with the bottom of the transducer as the water level in the basement area rose up to the level of the transducer. Note that this blockage would not affect outflow from the transducer reference port, and therefore, the transducer would function normally after the maximum pressure had been reached. Note also that the approximately 3-s time delay could remain relatively constant even though the pressure rise rate was increasing, since the inflow through the reference port would increase with the increasing pressure difference across the port.

REFERENCE

Henrie, J. O. and A. K. Postma, 1983, Analysis of the Three Mile Island Unit Hydrogen Burn, RHO-RE-SA-8, REV 2 (also GEND-INF-023, Vol. IV), Rockwell Hanford Operations, Richland, Washington.

APPENDIX B

CALCULATED PRESSURE DIFFERENCES
BETWEEN COMPARTMENTS

The pressure transient caused by a hydrogen burn would be expected to create pressure differences between compartments in which the burn is proceeding at different times and rates. The closed stairwell and elevator shaft are examples of relatively isolated regions where burning could be expected to be initiated at different times than the bulk of the containment. Physical evidence, i.e., the doors of the elevator shaft and stairwell, shows that a significant pressure difference existed between these regions. Another region of interest is the compartment that houses the reference leg of the pressure transmitter for the B steam generator. As noted in appendix A, the pressure response of the once-through steam generator (OTSG)-B instrument lagged that of the OTSG-A instrument and the numerous pressure switches. One possible explanation for the indicated time lag is the postulated lack of a burn in the B cubicle. This explanation is possible only if flow communication is so restricted that a relatively high pressure drop could exist. The following paragraphs present an engineering analysis which suggests that the maximum predicted pressure drop is far below the value indicated by the instruments.

The difference in compartment pressures indicated by the A and B steam generator pressure instruments is listed in table B-1. An examination of the data of table B-1 shows that significant pressure differences for the two instruments were recorded for three times, 9, 12, and 15 s. For longer times, the two instruments track together quite well. Of particular interest is the peak pressure difference of 15.9 lb/in^2 (109 kPa) indicated at 15 s. Pressure differences this high, if authentic, would generate gas flows with near-sonic speeds through the many openings which exist, and would tend to quickly equalize pressures.

Table B-1. Pressure Differences Indicated by Instruments on OTSG-A and OTSG-B.

	Pressure (lb/in^2 gage)		
Time (s*)	OTSG-A	OTSG-B	ΔP
0	1.4	1.4	0
3	1.4	1.2	0.2
6	1.6	1.4	0.2
9	2.4	1.6	0.8
12	10.4	2.6	7.8
15	27.2	11.3	15.9
18	27.6	27.3	0.3
21	25.2	25.6	-0.4

*Time after 1350:12 on March 28, 1979.

The room where the B pressure transmitter reference leg is located lies between floors at Elevations 282 and 305 and in the eastern semicircle outside the D-ring walls. The southeastern end of the room is a concrete wall that blocks gas flow. Gas passages exist at the northern part of the room. Openings for gas flow also exist from above the Elevation 305 floor through uncovered parts of the seismic gap and through pipeways and other openings in the Elevation 305 floor.

A study of drawings of the containment structure led to the conclusion that the gas flow path could be represented as a combination of series and parallel openings as illustrated in figure B-1. The horizontal path between rooms A and B contain three restrictions shown as orifices 1, 2, and 3 in figure B-1. Orifice 4 represents the combined openings through the floor at Elevation 305.

A precise determination of the flow areas for the four pinch points identified in figure B-1 proved to be difficult to define. The three series of doorway-type openings are partially blocked with structures (pipe, supports, and mesh-type doors). Also, water on the floor reduced the vertical height that was open to flow. The openings from above Elevation 305 were many, and were partially blocked by steel cover plates. While up-to-date information on the openings was obtained from drawings and descriptions of the openings and the ducts and cover plates partially blocking them, the estimated area totals were rounded off and are subject to considerable uncertainty. Estimates of these areas, identified in figure B-1, are listed in table B-2.

Table B-2. Estimated Flow Areas for Openings into Room B.

	Flow area (ft^2)	
Restriction[a]	Best estimate	Minimum
1	30	15
2	30	25
3	30	25
4	50	33

[a]See figure B-1.

A transient flow model was developed to predict the pressure differences that could occur under burn conditions which would cause the pressure differences to be a maximum. Key assumptions of the flow model include the following:

- Pressure-time history for the regions outside room B was indicated by the OTSG-A instrument and the many pressure switches (see fig. A-1)

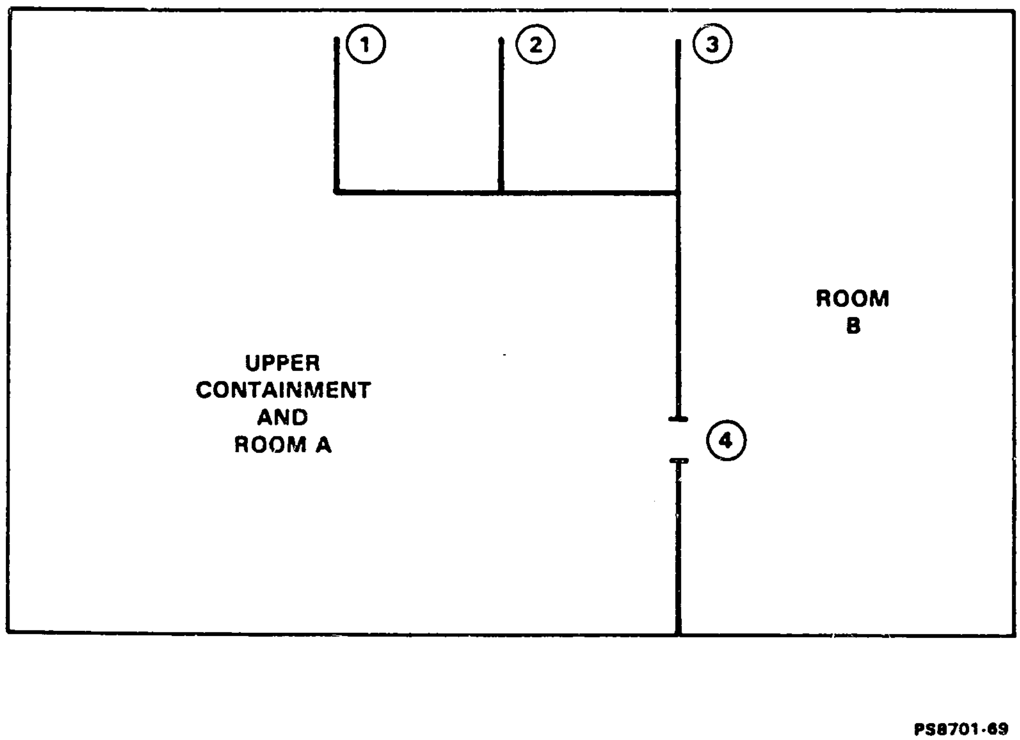

Figure B-1. Schematic of Flow Paths from Upper Containment and Room A Into Room B.

- No hydrogen burning occurred within room B until at or near the end of the burn above Elevation 305

- Flow areas were assigned the minimum value (see table B-2)

- Flow resistance was computed using the orifice equation with a coefficient of 0.6.

The pressure-time history (for volumes outside room B) used in the calculations was formulated on the basis of an initial pressure of 1.3 lb/in^2 or 9 kPa (gage) and the pressure rise rates listed in table B-3. Gas volumes between flow restrictions 1 and 2 and between flow restriction 2 and 3 were neglected in the flow model. Room B was assigned a volume of 50,000 ft^3 (1,416 m^3) on the basis of its dimensions.

Table B-3. Pressure Rise Rates in Upper Containment Resulting From Hydrogen Burn.

Time period (s)	Pressure rise rate	
	(lb/in^2-s)	(kPa/s)
0 - 3	0.07	0.48
3 - 4	0.10	0.69
4 - 5	0.17	1.2
5 - 6	0.48	3.3
6 - 7	1.0	6.9
7 - 8	2.6	18
8 - 9	4.0	27
9 - 12.5	5.6	38
12.3 - 15	-0.8	-5.5

The predicted pressure difference between Room B and the main containment space is shown as a function of time in figure B-2. As indicated by the curve of figure B-2, the pressure difference was computed to be negligible for the first 5 s. A peak pressure difference of 0.68 lb/in^2 (4.7 kPa) was computed at 9.4 s. This predicted peak pressure difference is a factor of 23 less than the maximum pressure difference (15.9 lb/in^2 or 109 kPa difference; see table B-1) indicated by the two transmitters. Because this predicted pressure difference is an upper limit type of number, and because the value indicated by the instrument is 23 times this value, the conclusion is that the indicated value is wrong. Such a high-pressure difference across the relatively large openings in room B could not have been produced by the hydrogen burn that occurred. As noted in appendix A of this report, the most plausible explanation for this anomaly appears to be blockage at the sensor inlet by floating debris.

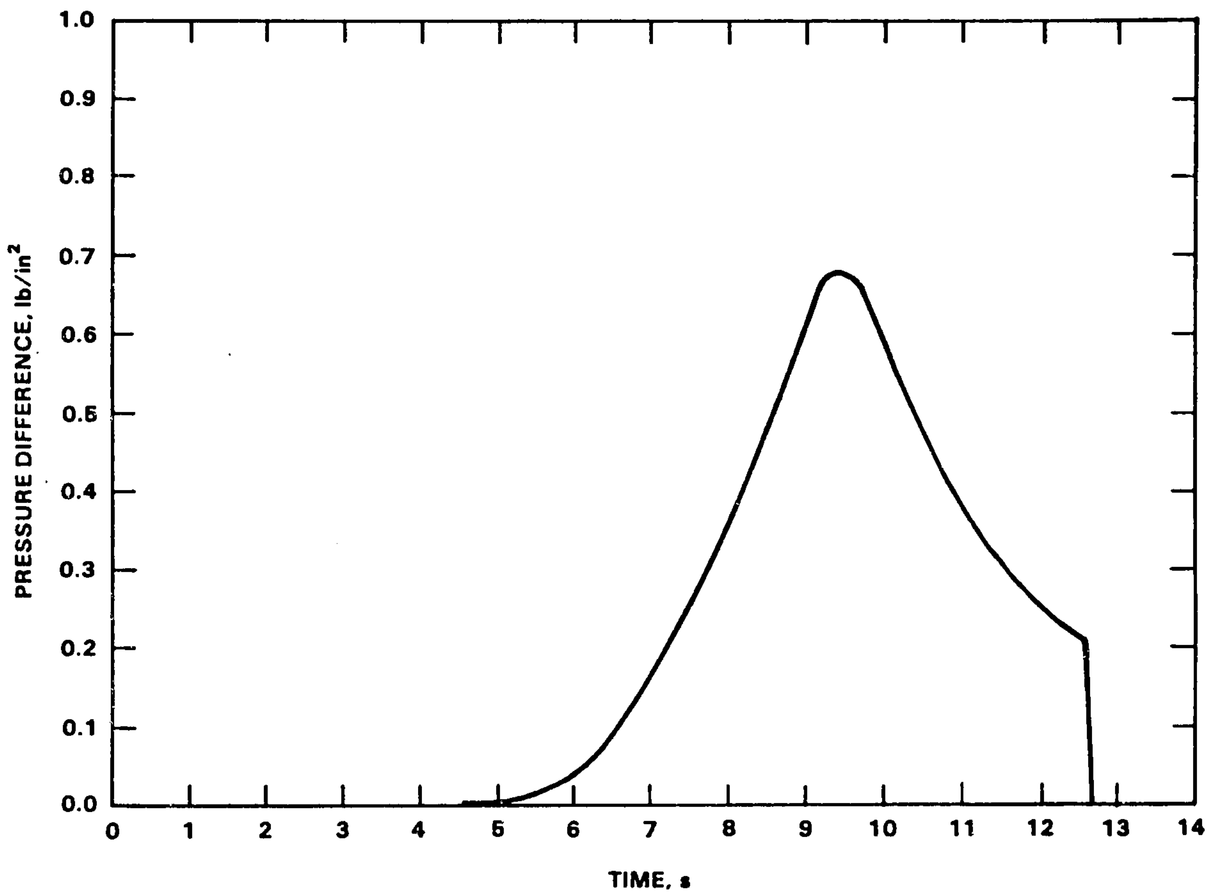

PS8701-97

Figure B-2. Predicted Pressure Difference Between Upper Containment and Room B.

APPENDIX C

DESCRIPTION OF CONTAINMENT GAS HEAT-TRANSFER PROCESSES AND PARAMETERS

The two-compartment cooldown model used herein is shown schematically in figure C-1. The upper containment region, volume 1, consists of the space above the D-rings and above the operating floor at Elevation 347. Volume 2 consists of the remainder of containment. Heat-transfer surface areas and gas volumes for three containment regions, as estimated by Henrie and Postma (1983), are listed in table C-1. Surface areas and volumes applicable to volume 2 of the cooldown model can be obtained by adding the values for the first two regions listed in table C-1 (i.e., the region inside D-rings and the region below Elevation 347).

Table C-1. Heat Transfer Surface Areas and Gas Volume (Henrie and Postma 1983).

Area or volume	Inside D-rings	Below Elevation 347	Above Elevation 347	Total containment
Uninsulated equipment[a]	17	39	34	90
Painted steel liner[a]	3	55	77	135
Concrete[a]	35	84	26	145
Total uninsulated area[a]	55	178	137	370
Gas volume[b]	211	428	1,394	2,033

[a]Thousands of square feet.
[b]Thousands of cubic feet.

Gas flows are induced by the air coolers and by differential cooling rates between different regions. Numerical values for gas flow rates passing through the air coolers and distribution ducts were based on results of analyses presented by Henrie and Postma (1983). Duct flow areas and design flow rates are reproduced in table C-2. For loss-of-coolant accident (LOCA) conditions, it was established that the flow rate per fan was 47,000 actual ft^3/min (22.2 m^3/s). Since five fans operated, the total flow rate exiting from the cooler is calculated to be 235,000 actual ft^3/min (111 m^3/s). The calculated flow rate into volume 1 is 54,000 actual ft^3/min (25.5 m^3/s), which is the total multiplied by the fraction specified in table C-2. The remaining cooler flow, 181,000 actual ft^3/min (85.5 m^3/s), is assumed to discharge into volume 2.

Intercompartmental flow rates were computed from the difference in cooldown rates in the two compartments, under the constraint that atmospheric pressure in the two rooms was equal. Sensible heat carried by the intercompartmental gas flows was accounted for; work done by the flowing gas was also accounted for. Prior to the operation of containment sprays, the faster cooldown in the lower compartment caused gas to flow from compartment 1 to compartment 2. The rapid cooling of compartment 1 by sprays caused a reversal of the flow direction from compartment 2 to compartment 1.

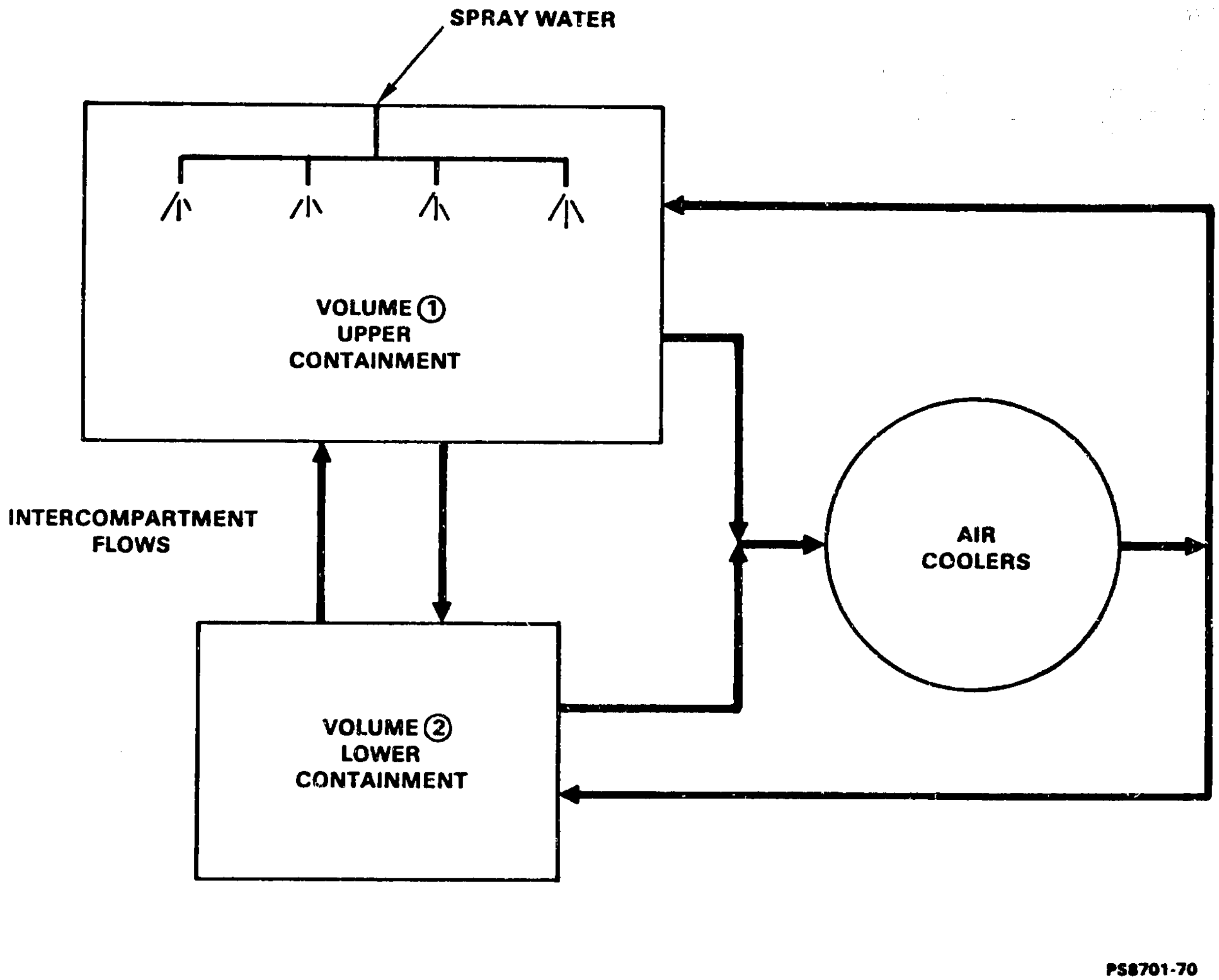

Figure C-1. Compartmentalization and Material Flows for Cooldown Model.

Table C-2. Flow Areas of Ducts Leaving Air Cooler (Henrie and Postma 1983).

Duct description	Duct diameter (in.)	Flow area (ft^2)	Fraction of total flow area	Design flow rate (actual ft^3/min)	Fraction of total flow
D-ring					
East	72	28.3	0.70	79,210	0.66
West	84	38.5		65,810	
Elevation 282					
East	40	8.7	0.1	23,840	0.11
West	8	0.4		1,140	
LOCA Duct					
East	42	9.6	0.20	25,000	0.23
West	42	9.6		25,000	

Heat transfer to surfaces in containment was dominant at early times (following the hydrogen burn) as compared to heat extracted by the coolers and work and sensible heat involved in the intercompartmental flows. Following Henrie and Postma (1983), empirical data were used to define heat transfer coefficients to surfaces. The empirical data were extracted from earlier studies of hydrogen burns by Carlson et al. (1973) and implicitly accounted for convection, radiation, and condensation. Overall heat transfer coefficients from two sets of data are reproduced in figure C-2. Data applicable to the TMI-2 hydrogen burn were obtained by interpolation between the two curves of figure C-2. The interpolation was based on specific volume of the contained gas; for the TMI-2 burn, the specific volume was intermediate between the values shown in figure C-2. These data appear to be in good agreement with Ratzel and Shepherd (1985).

Heat removal by the air coolers was predicted on the basis of flow and design parameters. Steady state outlet gas temperatures computed by Henrie and Postma (1983) are reproduced in table C-3.

The inlet gas temperature to the coolers was obtained as a weighted average of the temperatures in the two compartments. The weighting factor used was the mass flow rate from each compartment.

Heat transfer from the containment atmosphere to containment sprays is rapid compared to heat removal by containment coolers and to heat transfer to solid surfaces in containment. Analyses of spray heat transfer showed that a highly accurate model, applicable to all containment conditions, was too complex to be within the scope of the present study. The analyses which were completed showed that most spray drops would completely evaporate when atmosphere temperatures were higher than approximately 400 °F (204 °C).

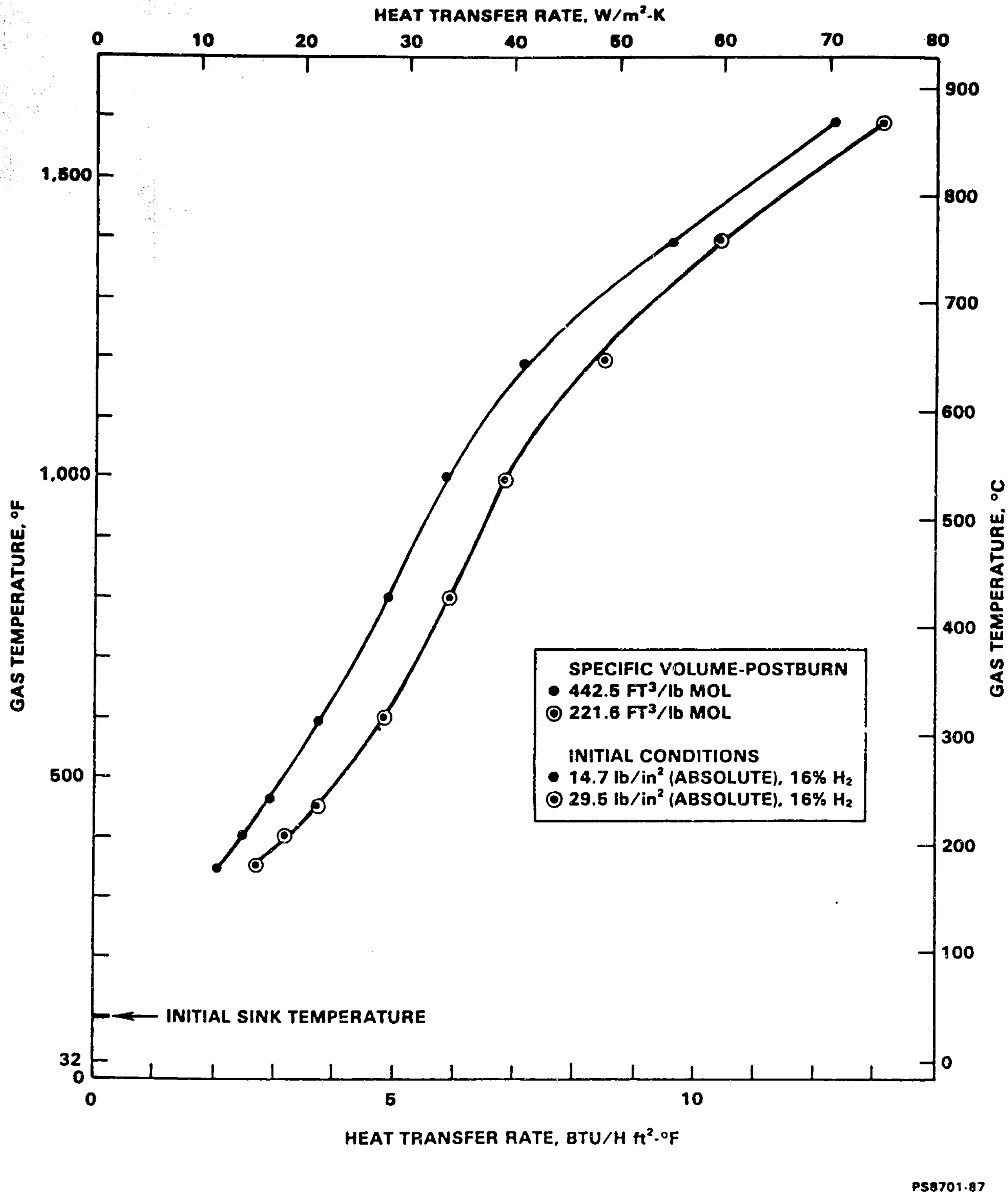

Figure C-2. Overall Heat Transfer Rate Versus Gas Temperature for Different Gas Mixtures.

Only very large drops or liquid sprayed against a surface would not be evaporated by the containment atmosphere. Therefore, a simplified model of spray cooling was based on total evaporation of 80% of sprayed liquid. An estimated 20% of spray was assumed to remain as liquid. Heat removal caused by sprays was computed by accounting for heatup of liquid, evaporation of liquid, heatup of vapor, and work done by the vapor against the containment atmosphere.

Table C-3. Predicted Outlet Temperature of Air Coolers, Steady State (Henrie and Postma 1983).

Gas inlet temperature		Gas outlet temperature	
°C	°F	°C	°F
704	1300	188	370
649	1200	173	344
593	1100	159	318
538	1000	144	292
427	800	116	240
316	600	88	190
204	400	59	138

The predicted cooldown transient is depicted graphically in figure C-3; the three solid curves represent containment atmosphere temperatures as predicted by the heat transfer model. The upper curve applies to upper containment gas, the lower curve to gas in the lower region of the containment, and the middle curve represents the containment average. The average temperature is one that yields the same containment pressure as the two-volume model. The cooldown calculations were begun at the time of a theoretical instantaneous burn. For the hypothetical burn, initial gas temperatures can be computed for an adiabatic burn, and as noted by Henrie and Postma (1983), the beginning values selected here allow for a lower burn efficiency (residual hydrogen 2.1%) in the lower compartment as compared to the upper compartment (residual hydrogen 0.7%).

As expected, the lower compartment cools more rapidly than the upper compartment, which is caused by the higher surface-to-volume ratio of the lower volume and the higher gas flow to and from the coolers as compared to the upper volume. The spray cooling effect is quite important in the upper volume but has a barely discernible effect on the gas in the lower room. This small but observable change in cooldown rate of the lower volume at the time of spray initiation is attributed to expansion work. It should be noted that these predictions do not apply for temperatures lower than approximately 400 °F (205 °C) because the assumption of spray evaporation and the implicit treatment of steam condensation used in this model would not apply for lower temperatures.

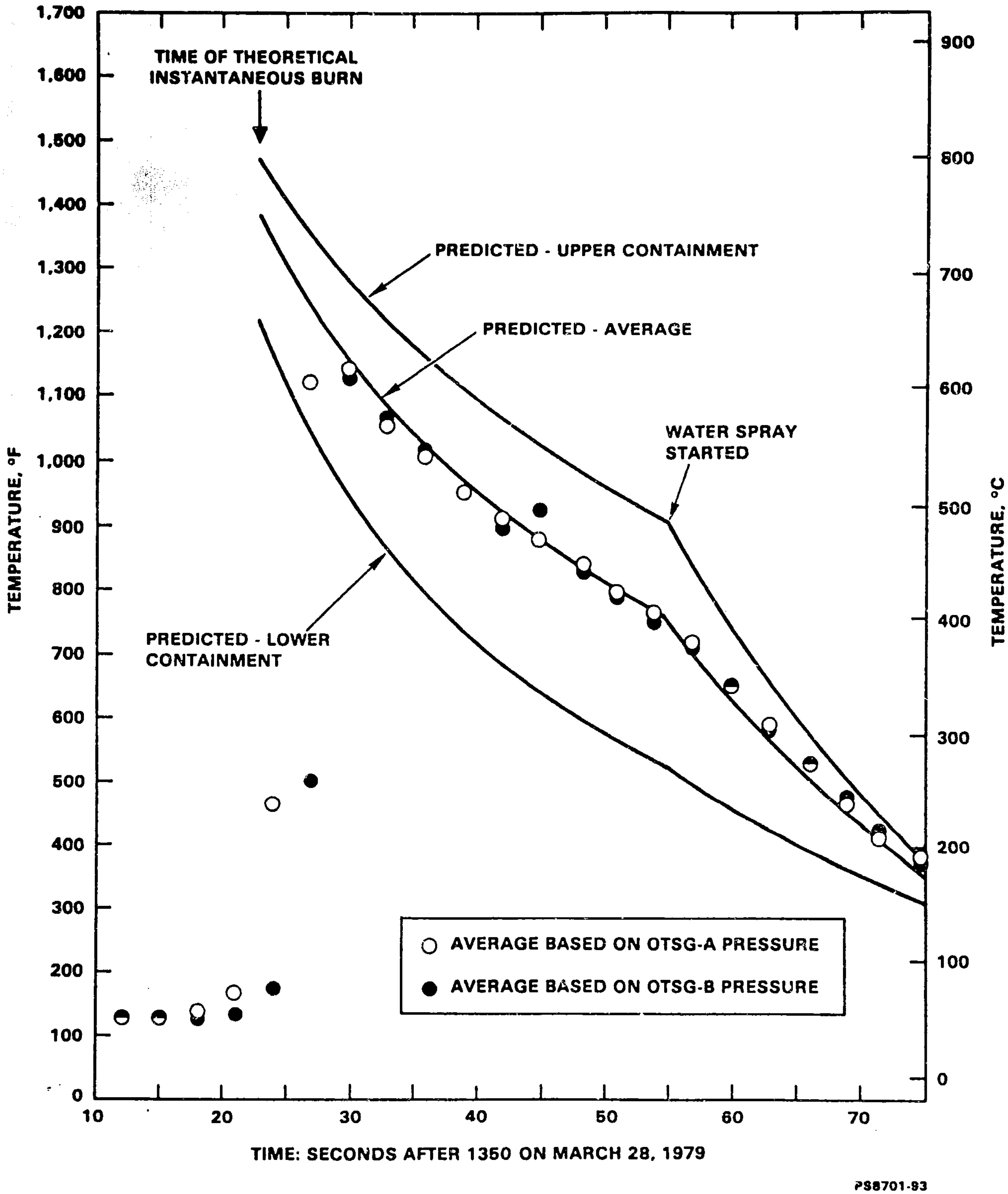

Figure C-3. Predicted and Observed Containment Gas Cooldown.

Also shown in figure C-3 are temperature data points that were computed from pressures obtained from measuring devices associated with the once-through steam generator. The temperatures were computed from the pressures using the ideal gas law and material balances that accounted both for the disappearance of gas moles and, as a result of the burn, the increase in gas moles resulting from spray evaporation.

The following statements summarize the results of comparing the cooldown model with data from TMI-2.

- The average temperatures predicted by the model agree very well with average temperatures inferred from TMI-2 pressure measurements. From this agreement, it is concluded that the model realistically accounts for heat transfer from the containment atmosphere. Because the model was based on ordinary engineering correlations, it is concluded that the observed cooldown rate was as expected.

- Gas temperatures in the upper containment volume are typically 250 °F to 400 °F (120 °C to 205 °C) hotter than in lower regions. Therefore, the challenge to equipment located high in containment would be significantly greater than equipment located in the compartments of the lower containment.

- Water sprays have a dominant effect on gas cooldown rates and spray cooling needs to be factored into analyses of equipment survivability related to hydrogen burns.

REFERENCES

Carlson, L. W., R. M. Knight, and J. O. Henrie, 1973, Flame and Detonation Initiation and Propagation in Various Hydrogen-Air Mixtures With and Without Water Spray, AI-73-29, Rockwell International, Canoga Park, California.

Henrie, J. O. and A. K. Postma, 1983, Analysis of the Three Mile Island Unit 2 Hydrogen Burn, RHO-RE-SA-8, REV 2 (also GEND-INF-023, Vol. IV), Rockwell Hanford Operations, Richland, Washington.

Ratzel, A. C. and J. E. Shepherd, 1985, Heat Transfer Resulting from Premixed Combustion, Publication HTD-45, American Society of Mechanical Engineers, New York, New York.

APPENDIX D

PARAMETRIC ANALYSIS OF COMPONENT HEATING FOLLOWING A POSTULATED HYDROGEN BURN

D.1 INTRODUCTION

The heatup of material (the receptor) located in the containment atmosphere was predicted from a heat transfer model that is depicted in figure D-1. As is evident from the figure, the emphasis is on the heatup of electrical wires located inside a protective enclosure. This system would be typified by electrical wires inside panel boxes and conduits. Important features of the heatup model include the following.

- Steel enclosure: The steel enclosure provides heat transfer isolation with respect to the containment building atmosphere. An opening in the enclosure allows inflow and outflow to maintain gas pressure equilibrium inside and outside. However, the enclosure is assumed to suppress flow-through convection of the outside atmosphere. A specified area of the wall is assumed to be mounted against a massive structure, and therefore, not heated by the containment atmosphere.

- Wire receptor: An internal electrical wire, of cylindrical geometry, is assumed to be suspended in the atmosphere inside the enclosure. The wire is assumed to be comprised of an outer elastomeric sheath covering a copper conductor.

The exposed part of the steel enclosure is heated externally by convection and radiation from the containment atmosphere. All walls exchange heat with internal gas by convection and radiation. Heat exchange by radiation between the enclosure and the wire surface is also accounted for.

The internal wire is heated by convection and radiation. The elastomeric portion of the wire is divided into nodes to permit the temperature distribution through the wire to be calculated. Internal gas is heated initially by compression or by an internal hydrogen burn. Heating by inflowing gas (due to more rapid cooling inside) is accounted for as is work done by inflowing and outflowing gas.

Two versions of the heatup model were developed. One uses a cylindrical conduit as the steel enclosure and the other uses a rectangular box geometry for the enclosure.

Input parameters for the heatup model are listed in table D-1.

D.2 PARAMETRIC ANALYSIS FOR WIRE-IN-CONDUIT GEOMETRY

A parametric analysis was carried out to illustrate how the various parameters affect the temperature-time history of the wire receptor. Cases were selected by changing individual parameters from those that applied to a base case.

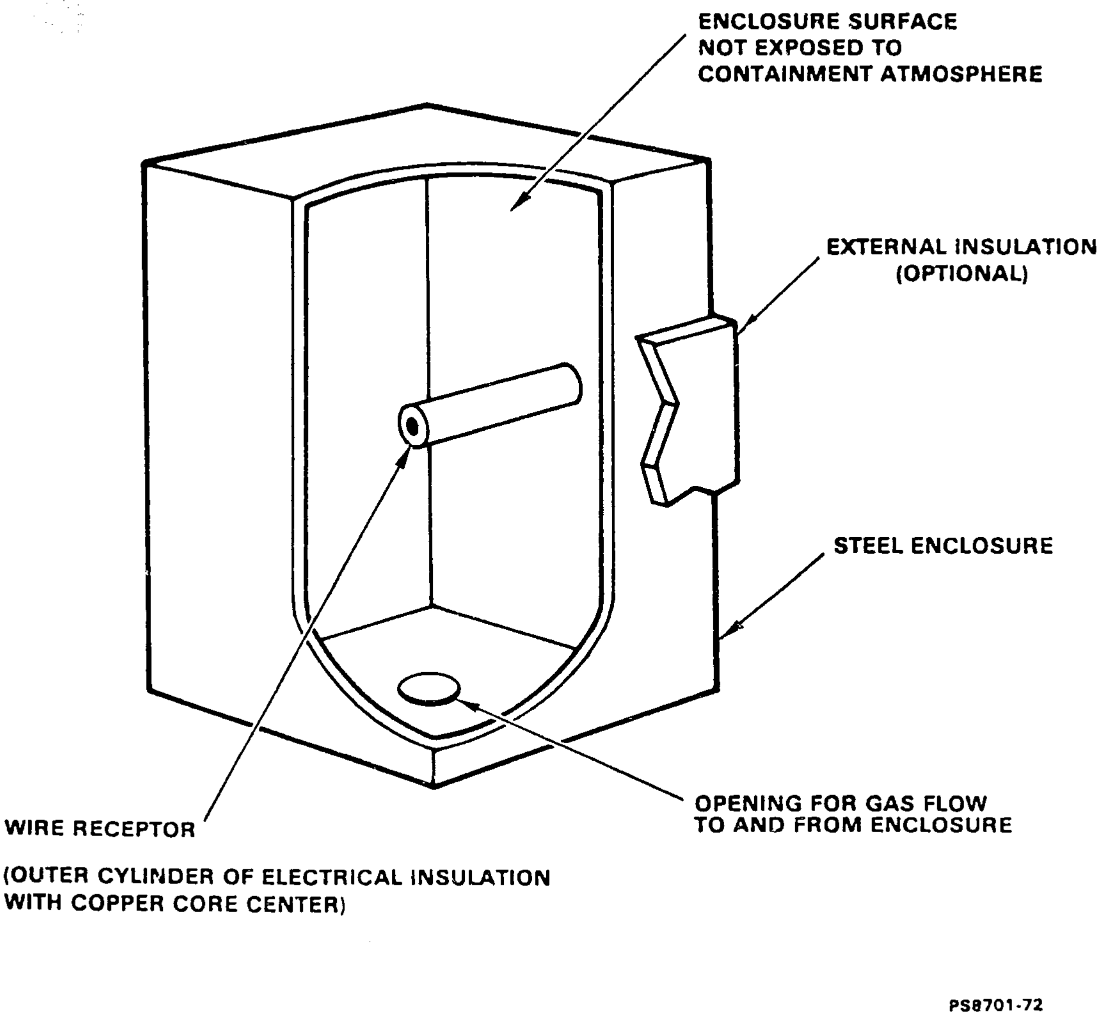

Figure D-1. Schematic View of Equipment Heatup Model.

Table D-1. Input Parameters For Heatup Model.

Parameter	Comments
Internal burn	If no burn, compression heating only
External insulation	Parameter is thickness/conductivity ratio
Thickness of steel	Assumed to be uniform
Enclosure surface area	Total for enclosure
Surface fraction exposed	Fraction of enclosure exposed to containment
Internal volume	Internal volume of enclosure
Outside diameter	Outer diameter of wire receptor
Copper diameter	Diameter of copper core of wire
Length	Length of wire inside enclosure
Conductivity	Thermal conductivity of wire insulation
Density	Density of wire insulation
Number of nodes	Conduction nodes in wire insulation
Time of sprays	Time for start of containment sprays

D.2.1 Base Case Parameters

The base case was characterized by a bare-steel conduit, 2-in. outer diameter and 0.1-in. thick, containing 20 wires, and in which an internal hydrogen burn occurred simultaneously with the burn in containment. Containment sprays were assumed to start at 32 s after the burn, but it was assumed that spray drops did not directly contact the conduit. Input parameters, as described in table D-1, were given the values listed in table D-2.

Representative results of the base-case calculation are presented in figure D-2 where temperatures of containment gas, the steel conduit, and the surface of the wire are shown as a function of time. The steel conduit reaches a peak temperature of 255 °F (124 °C) at 60 s; the surface of the wire reaches its maximum of 190 °F (88 °C) at some 500 s. The temperatures are much lower than the gas temperature, illustrating the protection provided by a simple conduit.

D.2.2 Effect of Internal Hydrogen Burn

While the base case assumed a hydrogen burn inside the conduit, it is conceivable that flame would not propagate into the conduit, and that the initial gas temperature would be determined by compression heating of the preburn containment atmosphere. Results for the no-internal-burn case are

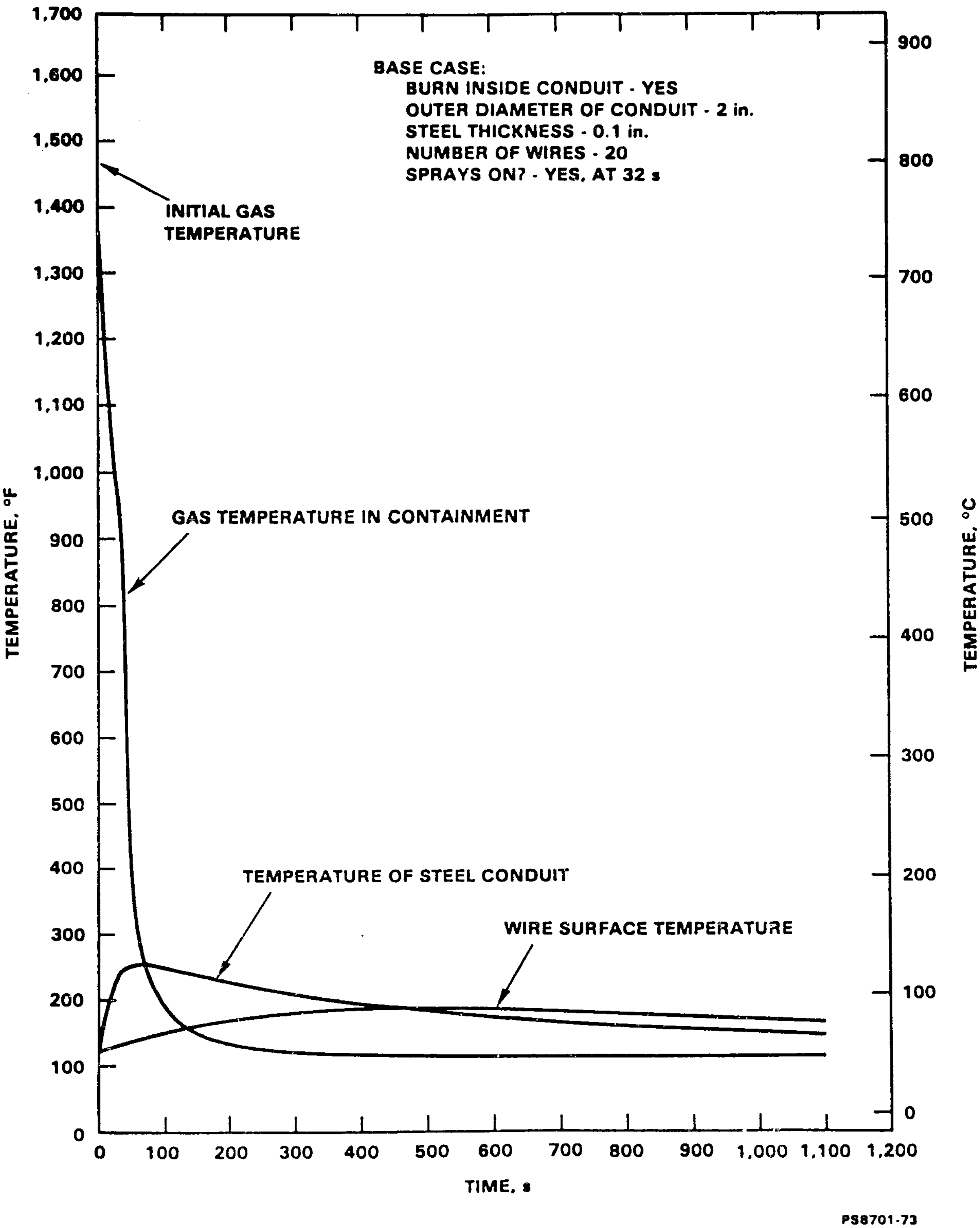

Figure D-2. Heatup of Wire in Conduit for a Hydrogen Burn.

Table D-2. Base Case Parameters.

Parameter	Value
Internal burn	Yes
External insulation	0 s °F ft^2/Btu
Steel thickness	0.1 in.
Surface area	0.5236 ft^2
Fraction exposed	1
Internal volume	0.0218 ft^3
Outside diameter of wire	0.16 in.
Diameter of copper core	0.064 in.
Length of wire	20 ft
Thermal conductivity	0.14 Btu/h/°F-ft
Heat capacity	0.25 Btu/lb
Density of elastomer	137 lb/ft^3
Number of nodes	3
Time of spray start	32 s

shown in figure D-3. It is evident from the curves of figure D-3 that the internal burn, or lack of it, has little influence on the time-temperature history for either the wire surface or the steel conduit. Peak temperatures are predicted to be only about 2 °C lower when no burn occurs as compared to the internal burn case.

The minor effect of the internal hydrogen burn is as expected when the very low mass of gas inside the conduit is accounted for, as compared to the wires and the steel conduit. The quantity of energy released by the internal gas as it cools from 1470 °F (800 °C) to the solid material temperatures is quite small compared to the thermal energy required to heat the solid materials to their peak temperatures.

D.2.3 Effect of Conduit Wall Thickness

One way to limit the temperature rise of a conduit is to make the conduit thicker. A test was made using a conduit wall thickness of 0.25 in.; the results presented in figure D-4 show that the peak conduit temperature is reduced from 254 °F to 184 °F (123 °C to 84 °C) when conduit thickness is increased to 0.25 in. from 0.1 in. Likewise, the peak wire surface temperature is reduced to 161 °F from 186 °F (72 °C from 86 °C) when the conduit thickness is increased by this amount. These results illustrate the general principle that massive bodies of highly conducting materials experience a much smaller temperature rise than lightweight bodies when both are exposed to a short-term burn transient typified by a premixed hydrogen/air combustion.

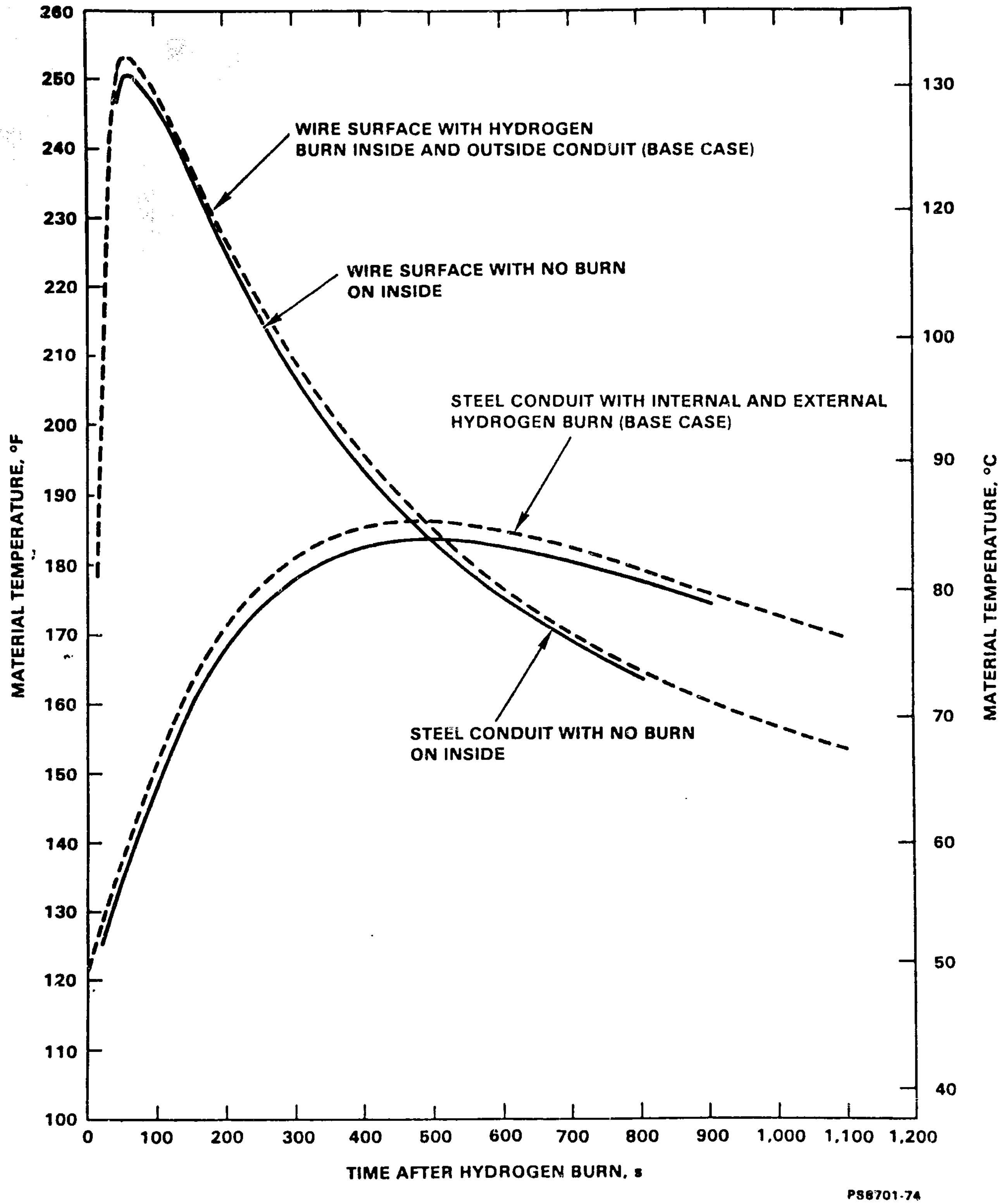

Figure D-3. Effect of Internal Hydrogen Burn on Heatup of Conduit and Internal Wires.

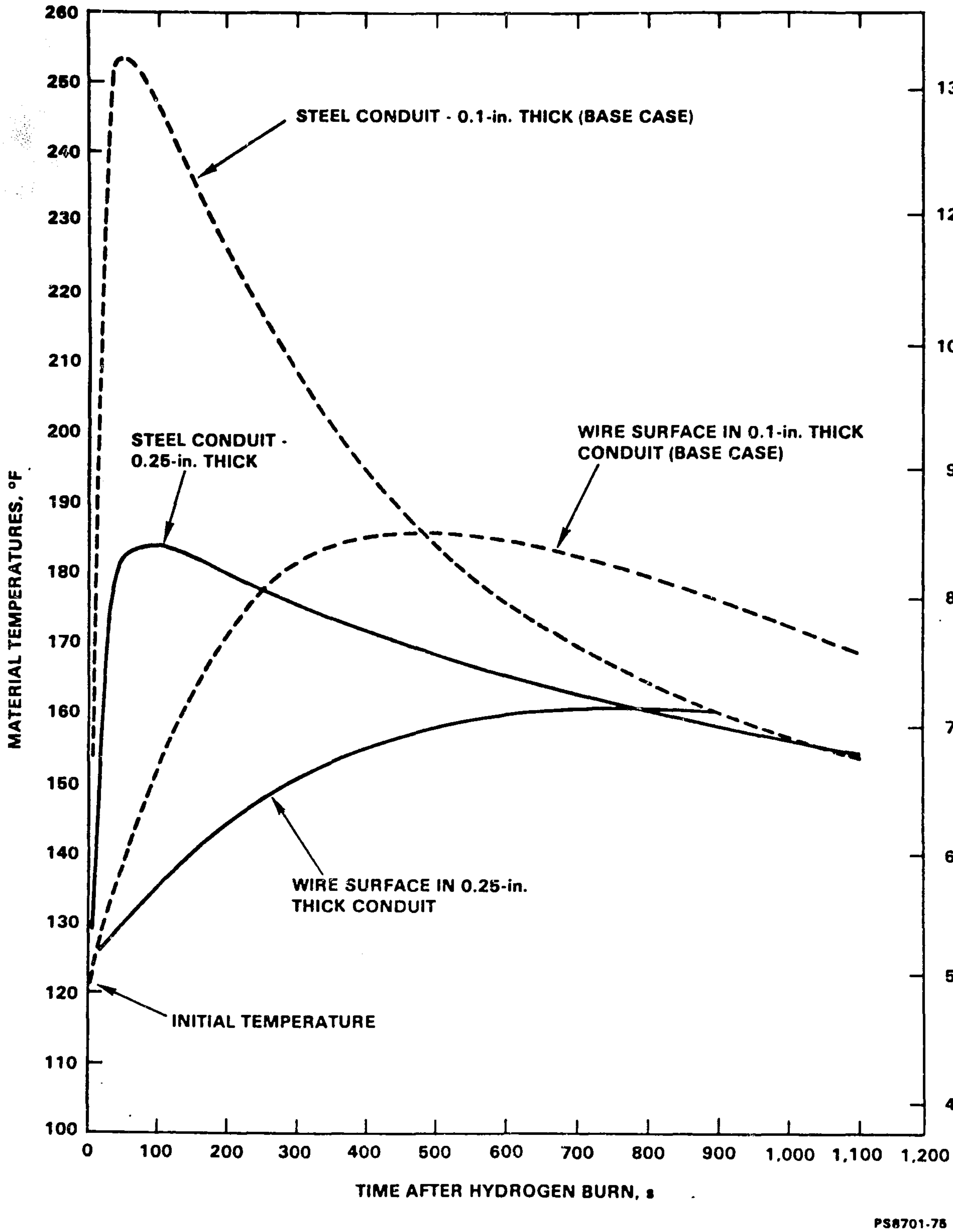

Figure D-4. Effect of Conduit Thickness on Conduit and Wire Temperatures.

Calculations for a thin tube in place of a normal conduit were also performed. The thin tube would serve as a radiation shield and as a convection suppressor, but would not be as effective in storing heat as the normal conduit. Results obtained for the thin tube are shown in figure D-5. From the curves of figure D-5, it is apparent that the 0.01-in. thick tube reaches a peak temperature of 640 °F (338 °C) compared to 254 °F (123 °C) for the base case. The wire-surface temperature peaks at 267 °F (131 °C) for the thin tube case, significantly higher than the 186 °F (86 °C) peak surface temperature reached for the base case.

D.2.4 Effect of External Insulation

An effective design method for limiting the temperature rise of equipment exposed to a burn transient is to provide a thermal insulation barrier between the heat source and the receptor. The base case was modified by applying 1 in. of magnesia insulation to the outside of the conduit. This analysis was based on steady state conduction through the insulation, and therefore, will overpredict the temperature rise of the receptor as compared to a model that would account for the time delay for conduction through the insulation.

For 1 in. of magnesia, the insulation parameter (thickness/conductivity) was computed to be 8570-s/°F-ft^2/Btu. Results obtained for this case are shown graphically in figure D-6. The insulation has a dramatic effect on limiting the temperature rise of the conduit and its contents. As shown by the curves of figure D-6, the steel conduit temperature peaks at 134 °F (57 °C) compared to a peak of 254 °F (123 °C) for the noninsulated case. Likewise, the wire surface temperature increases to only 131 °F (55 °C), which is substantially less than the peak of 180 °F (82 °C) when the conduit was not insulated.

For most cases, it is anticipated that the use of insulation would not be required because temperature peaks reached without insulation would still be below the failure threshold. However, the results shown in this section illustrate the significant effect of insulation on limiting the heatup of receptors in a hydrogen burn event.

D.2.5 Effect of Containment Building Spray Operation

As shown by the curves of figure 5-1, the operation of containment sprays at 32 s after the hydrogen burn causes a rapid reduction in containment gas temperature. In order to illustrate the relative importance of spray operation, analyses were performed for a case in which it was assumed that containment sprays did not operate. The cooldown of the containment atmosphere for this case would be controlled by heat transfer to building surfaces and by operation of the containment air coolers. Results of the analysis for this case are shown in figure D-7.

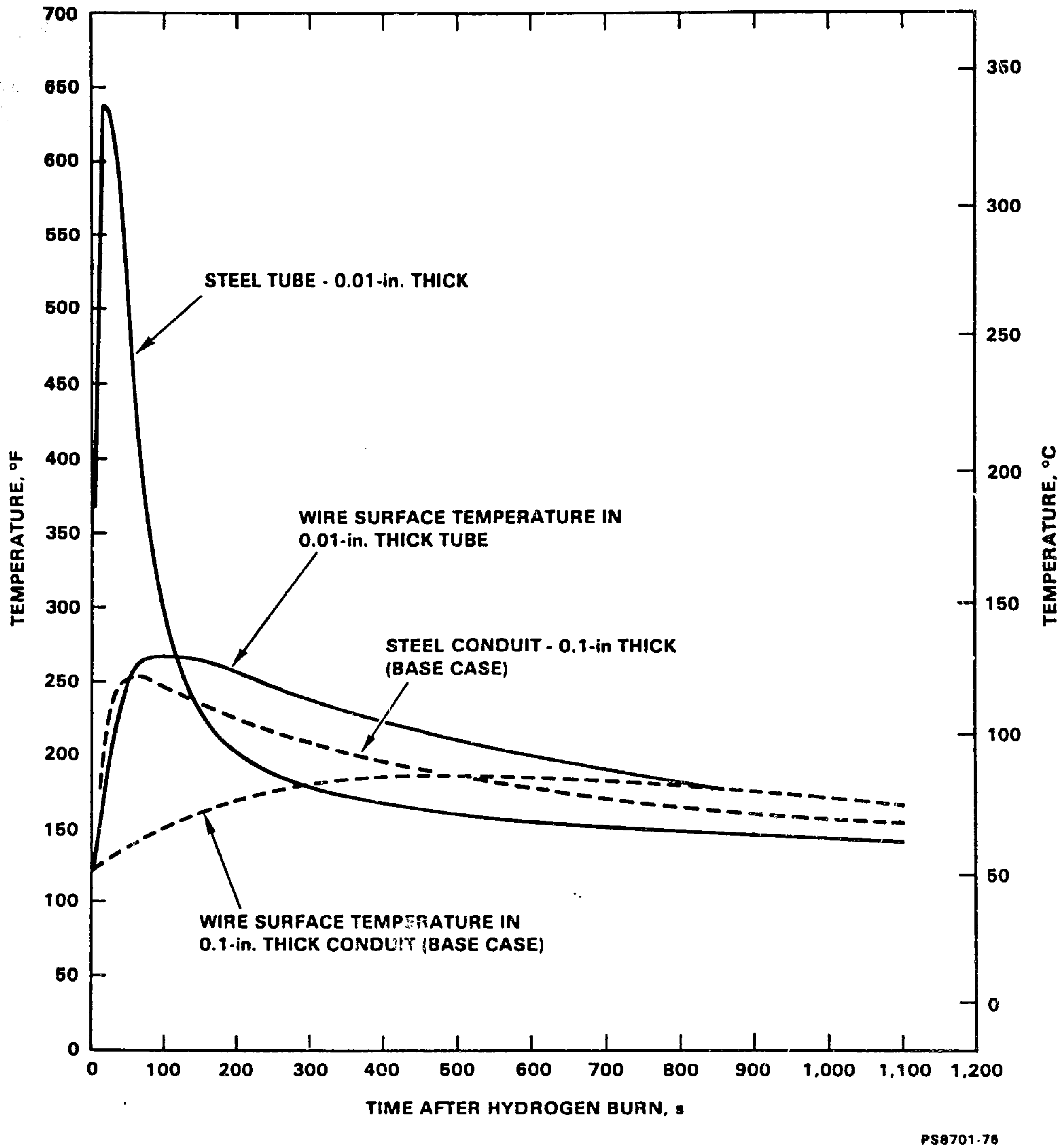

Figure D-5. Heatup of Wires in a Thin Steel Tube Compared With Heatup in a Conduit.

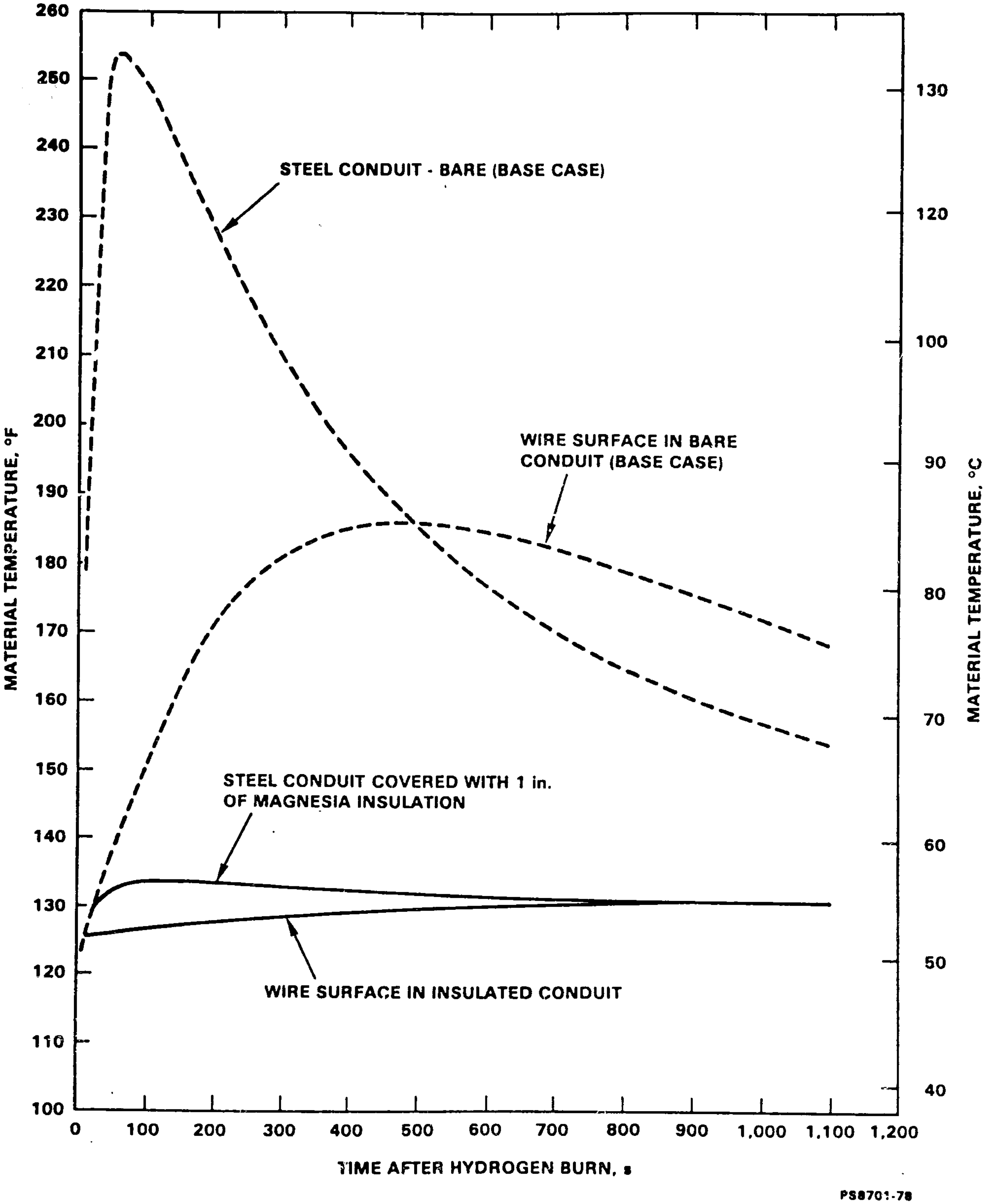

Figure D-6. Effect of Insulation on Heatup of Conduit and Internal Wires.

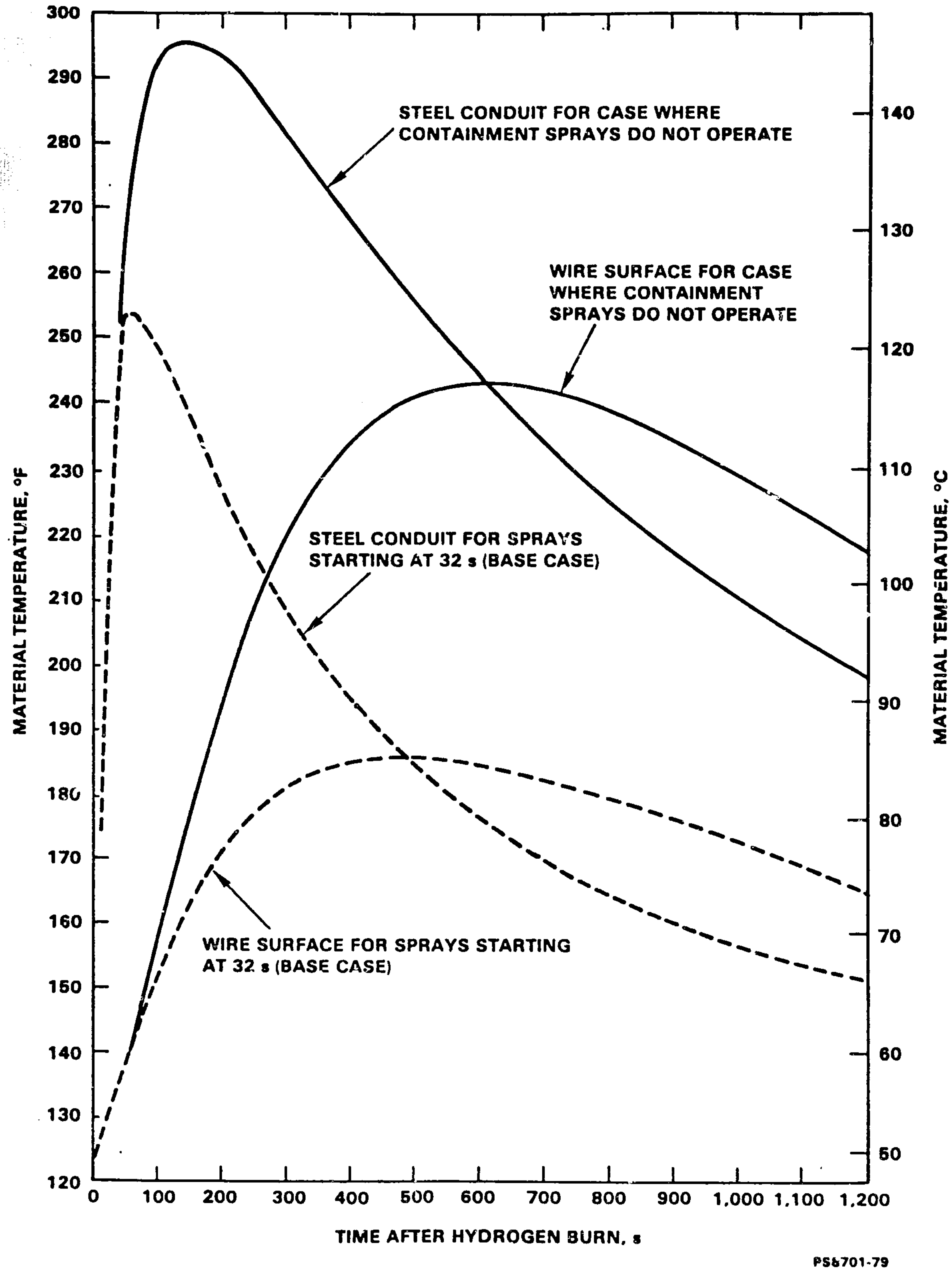

Figure D-7. Effect of Containment Spray Operation on Component Temperatures.

The curves of figure D-7 show that the steel conduit temperature reaches a peak temperature of 295 °F (146 °C) at 150 s. This peak is some 41 °F (23 °C) higher than the peak attained for the spray-on case. Also, the wire surface temperature peaks out at 243 °F (117 °C) for the no-spray case, which is 57 °F (32 °C) higher than for the case where spray starts at 32 s. While the peak wire temperatures reached for the no-spray case are probably well below a failure threshold, the temperature rise is significantly higher than for the spray-on case, showing that spray operation is a significant factor in limiting the thermal load imposed on equipment inside containment under conditions of an assumed hydrogen burn.

D.2.6 Effect of Internal Wire Mass

The wires located inside the conduit serve as energy absorbers and, therefore, the mass of the wires would be expected to affect the degree of heatup in a hydrogen burn. The volume of the wires displaces gas volume inside the conduit and reduces the mass of internal gas that can burn, which in turn reduces the energy evolved by an internal burn as compared to an empty conduit. Since both mass and volume increase with the number of wires in a conduit, wires in a full conduit would be heated less than those in a nearly empty conduit. This effect was illustrated by analyzing a case in which it was assumed that only one wire was present. Results are shown in figure D-8.

An examination of the curves of figure D-8 shows that the peak steel conduit temperature is increased only approximately 4 °F (2 °C) when 19 of 20 wires are removed. Wire-surface temperature is more affected by the number of wires, but peaks at approximately 204 °F (96 °C) when only one wire is present. This is approximately 18 °F (10 °C) difference, a relatively minor influence. It is concluded that the wire load in a conduit has a measurable, but not dramatic, effect on the time-temperature history of the conduit and internal wires.

D.3 PARAMETRIC ANALYSIS FOR WIRES IN PANEL BOX GEOMETRY

The heatup model used for the conduit geometry was modified to permit the steel enclosure to have the geometry of a rectangular-shaped box like ordinary electrical panel boxes. Model parameters are those listed earlier in table D-1. Differences in wire heatup can be expected for the panel box, as compared to a conduit, because the internal gas volume of the panel box is much larger than for a conduit and because the larger size of a panel box means that its surface-to-volume ratio would be smaller than for a conduit.

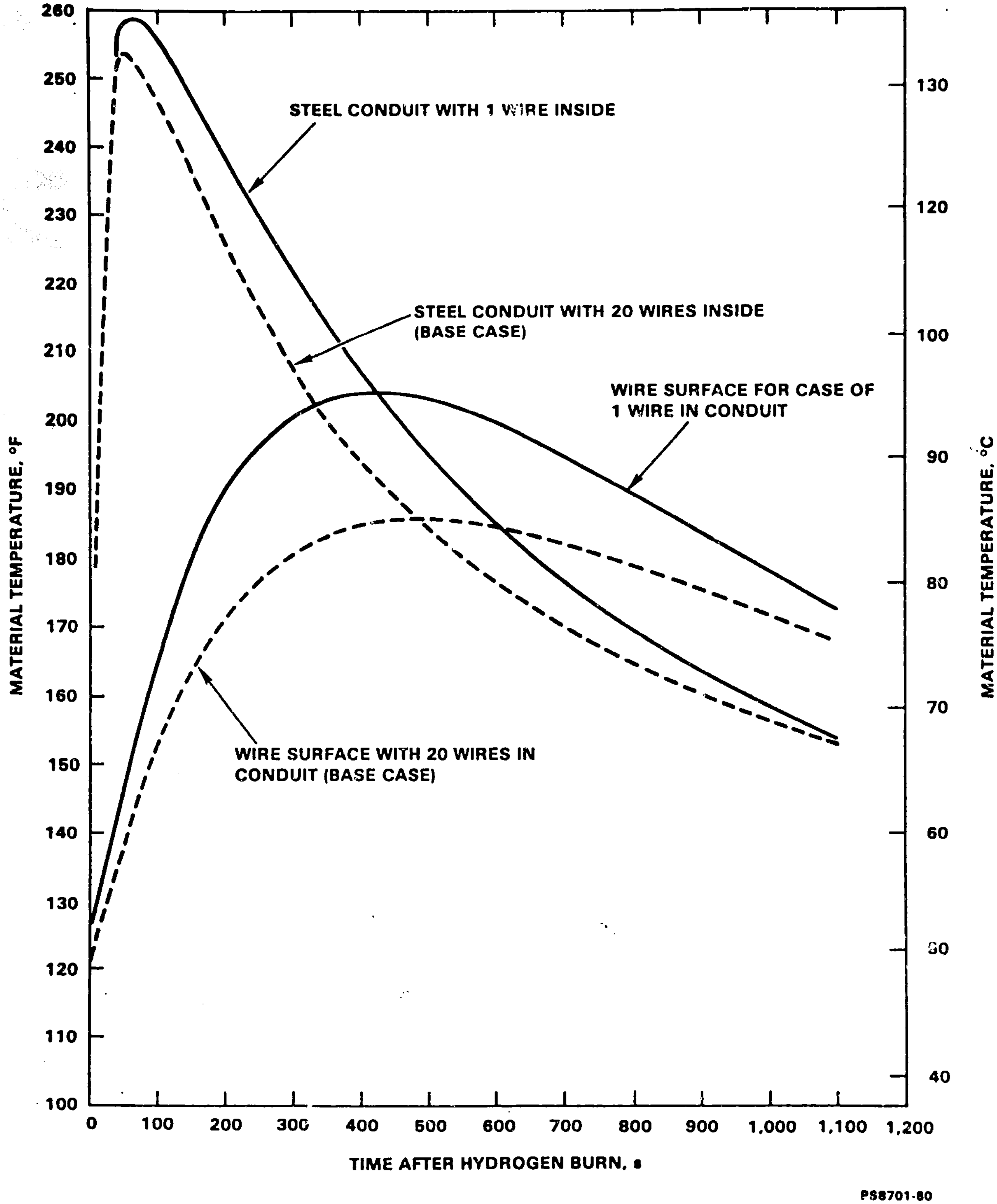

Figure D-8. Effect of Number of Wires in Conduit on Temperatures Reached.

D.3.1 Base-Case Parameters

Parameters for the base case were the same as those used for the conduit geometry (see table D-2) except for the surface area and volume of the box and the quantity of wire inside the enclosure. Values for these parameters for a 2 ft by 4 ft by 6 in. deep box are listed in table D-3.

Table D-3. Base-Case Parameters For Panel Box Geometry.

Parameter	Value
Surface area (with internal panel)	26 ft^2
Fraction exposed	0.54
Internal volume	4 ft^3
Length of wire	100 ft
All others	Table D-2 values

Results of calculations for the base case are shown in figure D-9. The curves of figure D-9 show that the exposed steel temperature peaks out at 260 °F (127 °C), which is some 25 °F (14 °C) higher than the peak seen in the conduit. These differences are attributable mainly to the bigger impact of the internal hydrogen burn in the panel box. The relatively larger internal volume of the panel box means that the internal burn produces relatively more energy to heat the internals and the steel enclosure.

D.3.2 Effect of Panel Box Wall Thickness

In order to illustrate the effect of thickness of the steel walls of the panel box, a test was performed for a wall thickness of 0.25 in. All other parameters were the same as for the base case. Results obtained for the thick-walled box are compared to results for the base case (1-in. thick walls) in figure D-10. Inspection of the curves of figure D-10 show that exposed steel temperature peaks at 211 °F (99 °C) for the thicker wall case. This peak is some 50 °F (28 °C) lower than for the base case. The curves for wire-surface temperature indicate that a peak of 188 °F (87 °C) is reached in the thicker walled box, which is 23 °F (13 °C) cooler than in the base case.

While the effect of the thicker-walled panel box is similar to the results obtained for the conduit geometry case (see fig. D-4) the temperature peaks are higher for the panel box geometry. The higher wire temperatures in the panel box result from the larger volume-to-surface ratio for the box geometry as compared to the geometry. The use of thicker steel could be used to limit component heatup in both enclosure geometries.

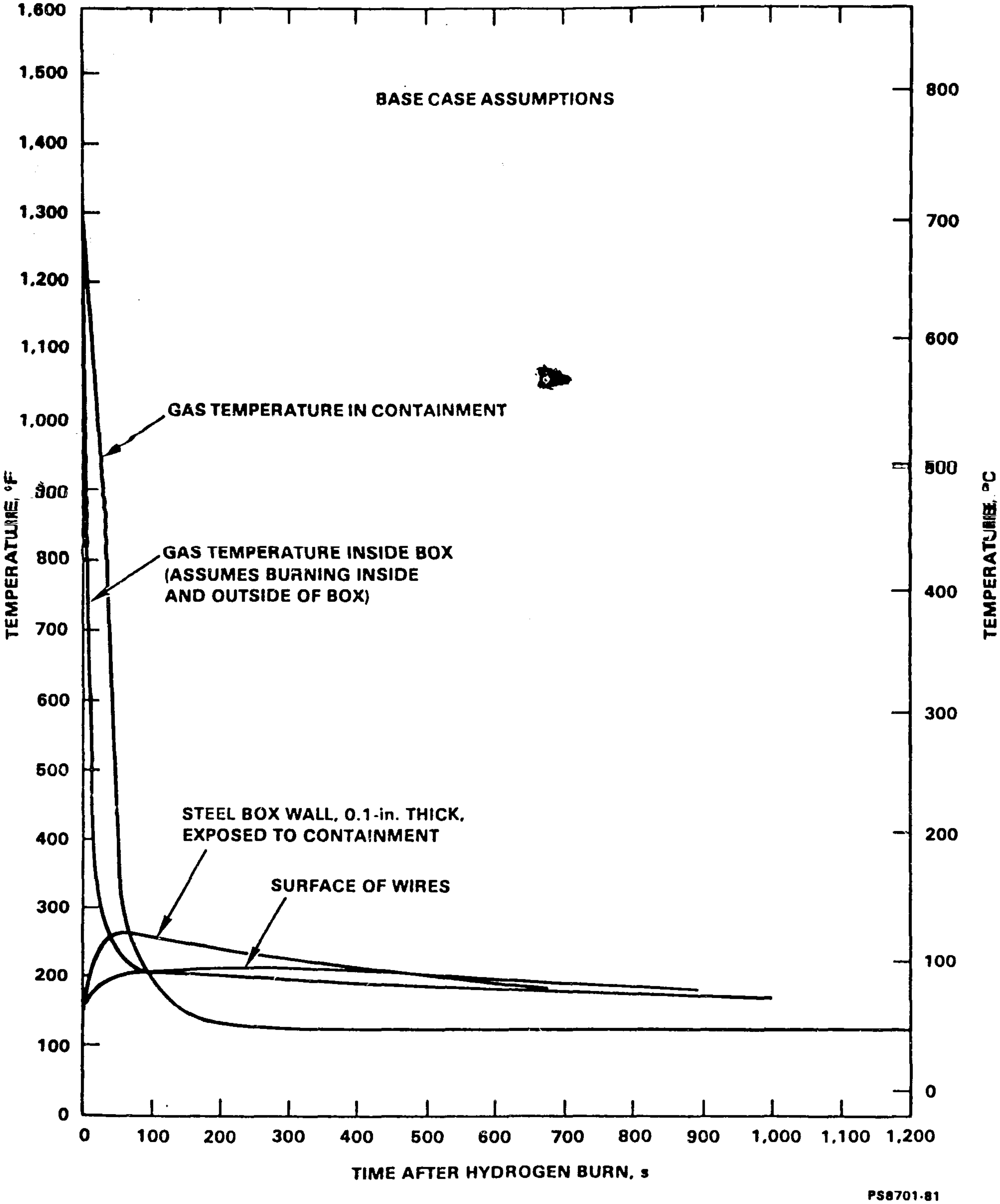

Figure D-9. Gas and Solid Temperatures for an Electrical Panel Box Following a Hydrogen Burn.

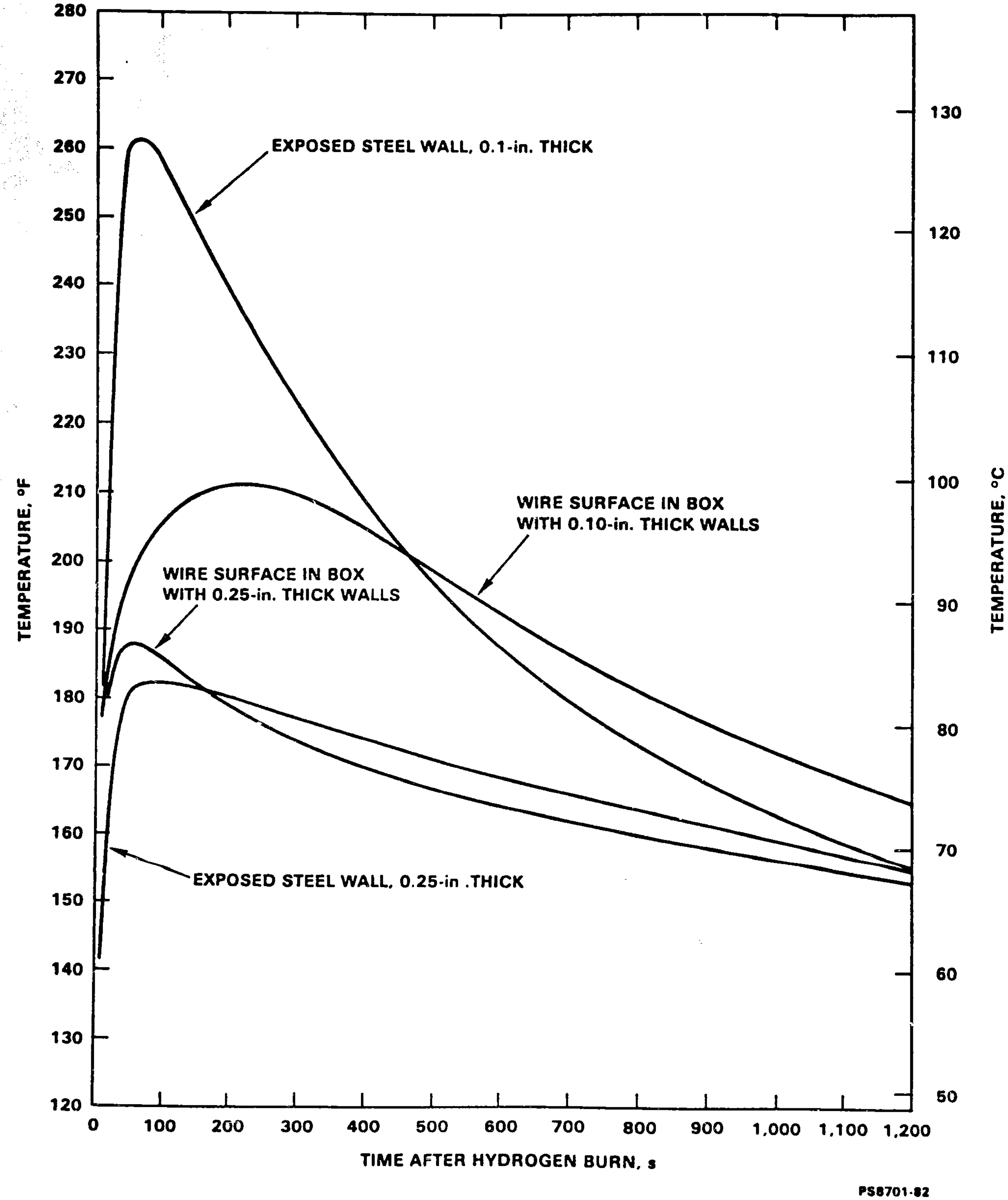

Figure D-10. Effect of Panel Box Wall Thickness on Heatup of Components.

D.3.3 Effect of Internal Hydrogen Burn

The large volume-to-surface ratio for the panel box geometry as compared to a conduit is expected to cause an internal hydrogen burn to be relatively more important. This was found to be true, as shown by the results of calculations presented in figure D-11, which are based on a run where it was assumed that no hydrogen burned inside the enclosure.

As shown by the data of figure D-11, the exposed steel attains a peak temperature of 247 °F (119 °C) compared to the peak of 261 °F (127 °C) reached for the base case where an internal hydrogen burn was assumed to occur. The difference attributable to the internal burn, 14 °F (8 °C), though minor on an absolute scale, is significantly higher than the 3 °F (2 °C) effect noted for the conduit geometry (see fig. D-3).

The wire-surface temperature peaks at 191 °F (88 °C) for the no-burn case, which is roughly 21 °F (112 °C) lower than for the burn-assumed case. Again this difference is significantly greater than the 3 °F (2 °C) effect that was indicated for the conduit geometry (see fig. D-3).

In summary, the effect of an internal hydrogen burn is greater for the panel box geometry than for a conduit, but still has a limited effect on the heatup of equipment protected by the steel enclosure.

D.3.4 Effect of Containment Spray Operation

As described in section D.2.5, the operation of containment sprays has a significant impact in limiting the heat up of a conduit and its internal wires. A similar effect is expected for the panel box geometry.

Results from a calculational case in which containment building sprays did not operate are presented in comparison with the base case in figure D-12. As shown by the plots of figure D-12, the exposed steel reaches a peak temperature of 303 °F (151 °C), which is 41 °F (23 °C) higher than attained when sprays operated at 32 s. Likewise, the wire temperature peaks at 250 °F (121 °C) for the no-spray case, which is approximately 39 °F (22 °C) higher than for the case where sprays started at 32 s. It is apparent from these results that the early operation of containment sprays decreases heat pressure (temperature-time integral) and limits the heatup of equipment located inside an enclosure in containment. Thus, the operability of containment sprays is a factor that needs to be accounted for when analyzing the thermal cycle endured by equipment in a hydrogen burn.

D.3.5 Effect of External Insulation

As was illustrated in section D.2.4, the application of 1 in. of magnesia insulation to the outside of a conduit has a very significant impact on the heatup of both the conduit and its wire load. For the panel

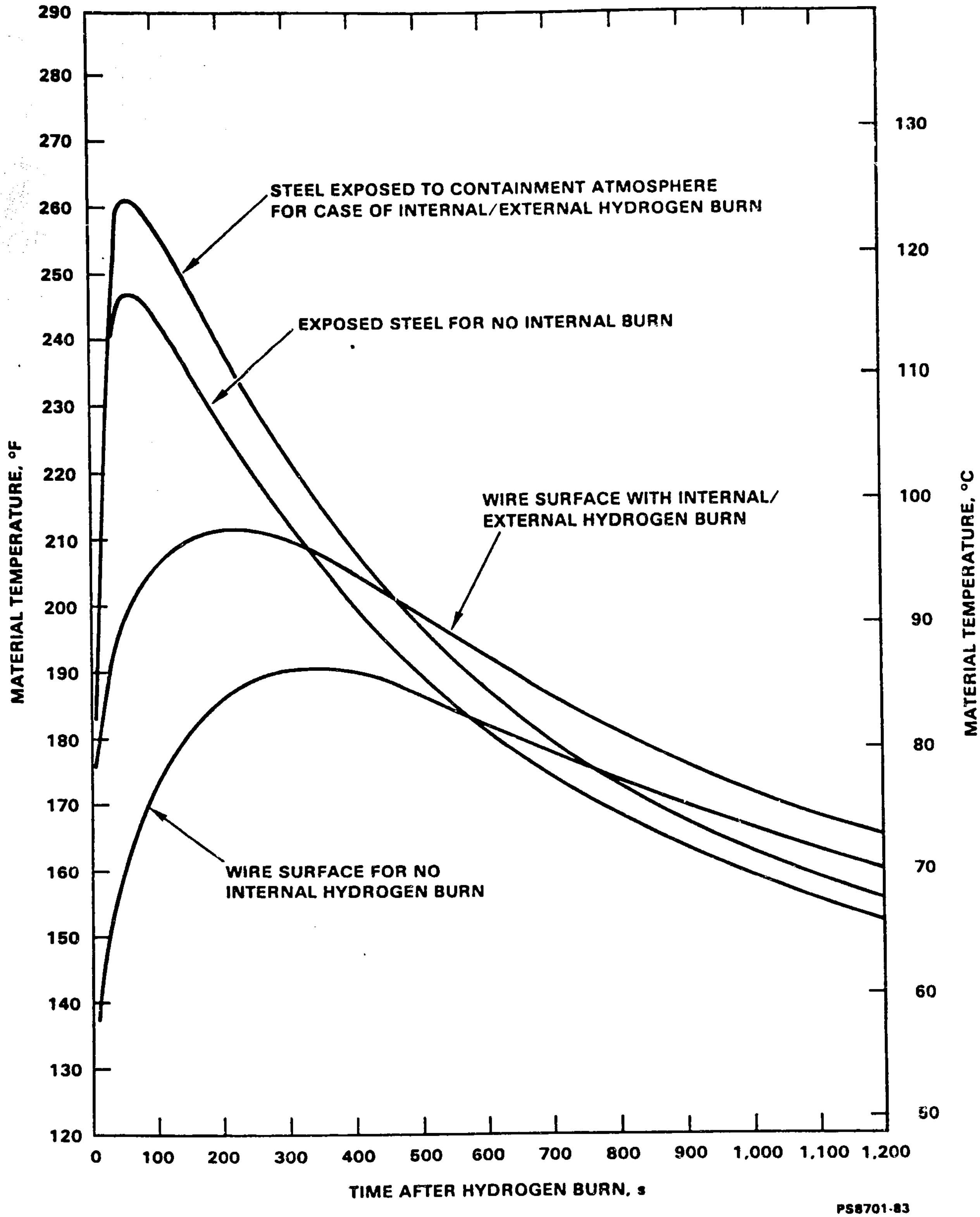

Figure D-11. Effect of Internal Hydrogen Burn on Temperatures in an Electrical Panel Box.

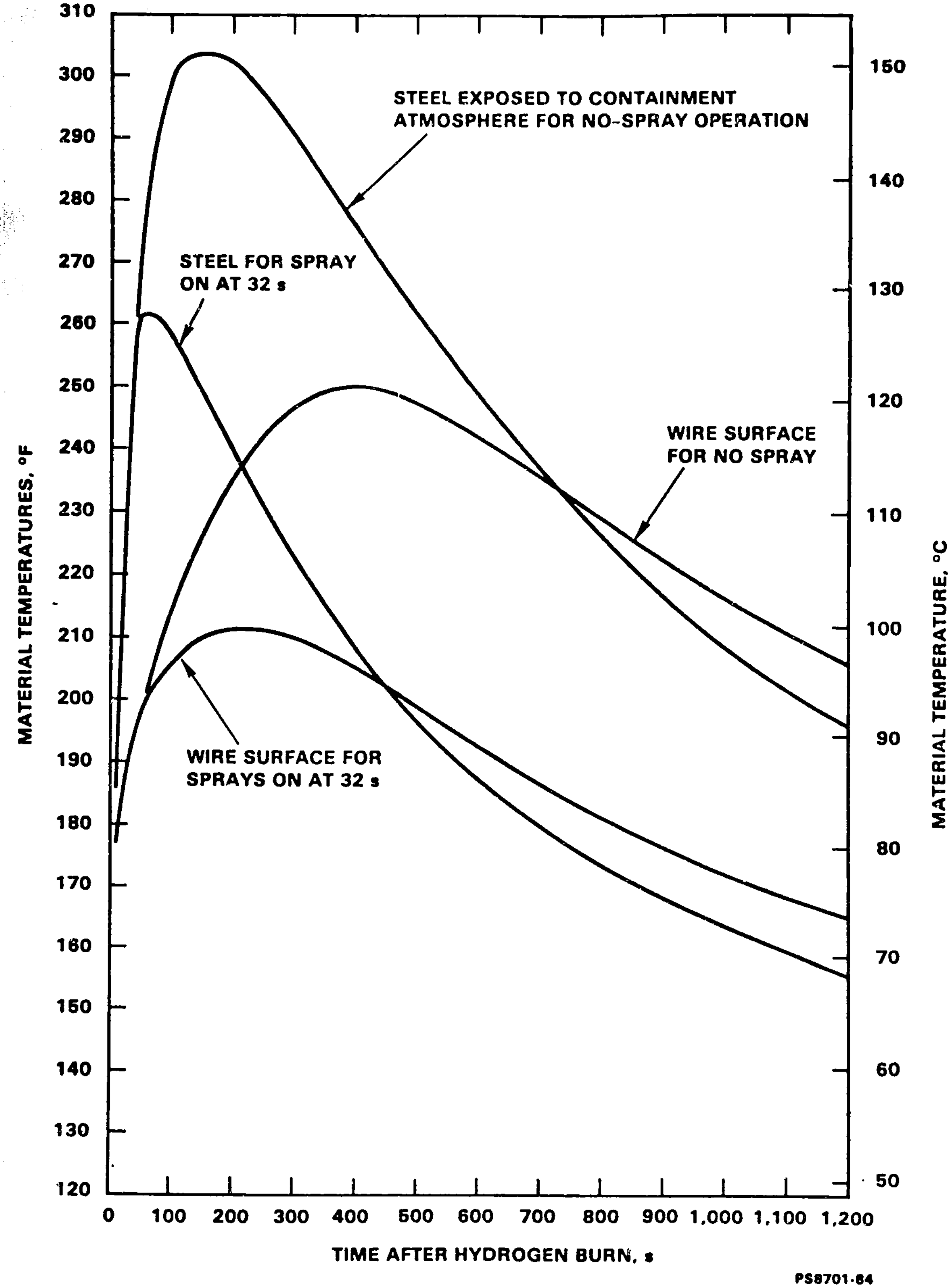

Figure D-12. Effect of Spray Operations and Temperatures in an Electrical Panel Box.

box geometry, the higher volume-to-surface ratio is expected to make external insulation less important for cases where an internal hydrogen burn is assumed; the internal hydrogen burn is relatively more important for geometries that have higher volume-to-surface ratios.

Results from an analysis made for the case where the panel box was covered externally with 1 in. of magnesia insulation (thickness/conductivity ratio of 8570-s/°F-ft^2/Btu) are shown in figure D-13. As indicated by the curves of figure D-13, the external insulation has a dramatic effect on limiting the temperature rise of the steel walls of the panel box. Peak steel temperatures are only 148 °F (64 °C) compared to the peak of 261 °F (127 °C) for the noninsulated case. The outer insulation decreases the peak wire temperature but the effect is less dramatic. Peak wire surface temperatures are 185 °F (85 °C) with insulation, compared to 211 °F (99 °C) for the noninsulated case. The relatively lower impact of insulation on the wires as compared to the steel walls is as expected because most of the heating energy is supplied by the internal hydrogen burn. The hot gas inside the box is able to heat the wires more rapidly than the steel walls of the enclosure.

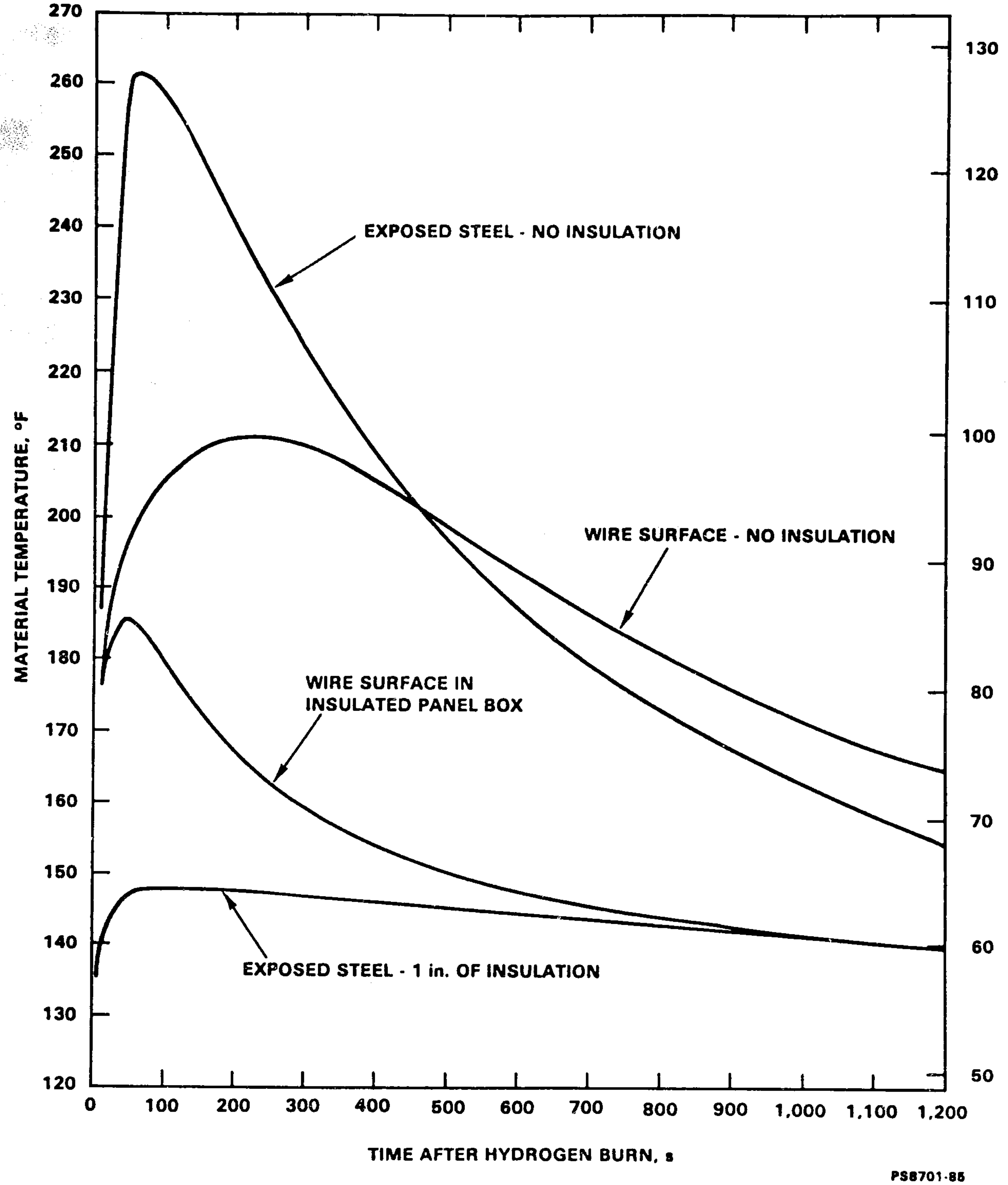

Figure D-13. Effects of External Insulation on Heatup of a Panel Box and Interior Wires.